Copper Isotope Fractionation and the Evolution of Sulfide Alteration in a Sudbury Tailings Impoundment

by

Justin Robert Buis

A thesis

presented to the University of Waterloo

in fulfilment of the

thesis requirement for the degree of

Master of Science

in

Earth Sciences

Waterloo, Ontario, Canada, 2016

Author's Declaration

I hereby declare that I am the sole author of this thesis. This is a true copy of the thesis, including any required final revisions, as accepted by my examiners.

I understand that my thesis may be made electronically available to the public.

Abstract

The fate of dissolved Cu in the Copper Cliff Central Tailings Impoundment was investigated to better understand the extent of Cu stable isotope fractionation accompanying the oxidation of Cu-bearing sulfide minerals and the retention of Cu through secondary mineral formation. Stable isotope ratios ($\delta^{65}Cu$) were measured in samples of pore water extracted from the oxidized zone of the tailings. Samples of the tailings solids were analyzed using a wide range of analytical techniques including transmitted and reflected microscopy, X-ray fluorescence, selective extractions and synchrotron based X-ray absorption spectroscopy (XAS). Observations were compared to the results from a study conducted at the same location on the tailings at the Copper Cliff Central tailings area, which was completed in 1990, allowing for an evaluation of the physical and chemical effects of sulfide alteration over a prolonged period.

Prolonged sulfide alteration has led to an expansion in the depth of oxidation from 0.8 m below the ground surface (m bgs) in the previous study to a depth of 1.6 m bgs in the current study, sulfide oxidation was modelled using PYROX and results were compared to measurements of gas-phase O_2. Analysis of current pore-water chemistry shows the maximum concentration of dissolved Cu (700 mg L^{-1}) occurs near the boundary between the oxidized and unoxidized zones at 1.6 m bgs, with a sharp decline to lower Cu concentrations at greater depths. Analysis of the tailings solids shows an accumulation of Cu (3,000 ppm) at 1.8 m bgs immediately below this sharp decrease in aqueous Cu. Comparison of the aqueous and solid phase concentrations, selective extraction measurements and mineralogical observations indicate that formation and dissolution of covellite (CuS) at the base of the oxidized zone is the main geochemical control on the mobility of Cu.

The dissolution of previously precipitated covellite has led to depletion of aqueous phase ^{65}Cu (-3.93±0.03‰) above a zone of declining Cu concentrations and an enrichment of ^{65}Cu (12.01 ±0.50‰) that is attributed to the precipitation of covellite. These observations demonstrate the value of integrating aqueous water chemistry and isotope measurements of field samples to assess the oxidation of Cu-rich sulfide tailings. The Cu isotope fraction observed during covellite formation has the potential for use as an indicator of the natural attenuation of dissolved Cu concentrations by sulfide precipitation as a result of changing redox conditions.

Acknowledgements

I would like to acknowledge my supervisor, Dr. David Blowes for his guidance and advice readily given. To my committee members Dr. Carol Ptacek for her support and critical commentary; Dr. Dogan Packtunc for his always helpful and constructive advice; and Dr. Richard Amos for his support and encouragement.

Funding for this project was provided by the Natural Sciences and Engineering Research Council of Canada Strategic Project Grant program (STPGP 413161 - 11). Synchrotron-based techniques were performed at Sector 13 GSECARS and Sector 20 PNC/XSD at the Advanced Photon Source (APS) and at SXRMB of the Canadian Light Source (CLS). GSECARS is supported by the National Science Foundation—Earth Sciences (EAR-1128799) and Department of Energy—GeoSciences (DE-FG02-94ER14466). PNC/XSD is supported by the US Department of Energy—Basic Energy Sciences, the CLS and its funding partners, the University of Washington, and the Advanced Photon Source. This research used resources of the APS, a U.S. Department of Energy (DOE) Office of Science User Facility operated for the DOE Office of Science by Argonne National Laboratory. The CLS is supported by the Canada Foundation for Innovation, NSERC, the University of Saskatchewan, the Government of Saskatchewan, Western Economic Diversification Canada, the National Research Council Canada, and the Canadian Institutes of Health Research.

I would like to thank Dr. Jane Eagling for her almost constant support throughout the course of the project. I would like to thank current graduate student Roberta Parigi for her help in the field and in processing our many samples. Thanks to Jeff Bain for his help navigating the Sudbury area and knowledge regarding everything related to mine waste. I would also like to

thank a list of current graduate students for an assortment of reasons: Filip Budimir, Jeffery Leon, Lingyi Kong, Heather Shrimpton, Colleen Atherton and Sara Fellin. Thanks to Joy Hu, Laura Groza and Julia Jamieson-Hanes for their hard work analyzing samples in the laboratory.

Dedication

With all my gratitude I would like to dedicate this thesis to my always supportive parents Bob and Ruth. For their endless help throughout all aspects of my life.

Table of Contents

List of Figures

List of Tables

Chapter 1. Introduction

1.1. Background

1.1.1. Mine Tailings

Mine tailings are a by-product of the milling process used to extract the economically valuable minerals from ore deposits. This process involves crushing and milling the ore which creates clay-to-silt sized particles (<0.002 – 0.05 mm). The milled rock is combined with water and surfactant chemicals that promote the separation of sulfide minerals by floatation and decantation. Contains both gangue minerals and residual sulfide minerals. Exposure of tailings can produce acidic drainage through the oxidation of sulfide minerals by O_2 and water (Blowes et al., 2003).

Pyrrhotite ($Fe_{1-x}S$) is the principal sulfide mineral present in the tailings within the Copper Cliff Central Tailings Impoundment. The crystal structure of pyrrhotite has vacancies related to Fe(II) deficiency, which can be charge compensated for by Fe(III) (Jambor, 2003). Pyrrhotite commonly hosts trace elements including Ni and Co (McGregor et al., 1998; Gunsinger et al., 2006). The oxidation of pyrrhotite by O_2 is described by Nicholson and Scharer (1994) as:

$$(1.1)\ Fe_{(1-x)}S_{(s)} + \left(2 - \frac{1}{2}x\right)O_2 + xH_2O \rightarrow (1-x)Fe^{2+} + SO_4^{2-} + 2xH^+$$

The amount of Fe(II) and H^+ released during pyrrhotite oxidation is dependent on the initial mass of pyrrhotite and the extent of O_2 ingress into the tailings impoundment. The partial oxidation of pyrrhotite to form marcasite (FeS_2) and elemental sulfur (S^0) has been observed in pyrrhotite-rich

tailings (McGregor et al., 1998; Johnson et al., 2000; Moncur et al., 2005). The partial oxidation of pyrrhotite with O_2 proceeds as follows (Nicholson and Scharer, 1994; Gunsinger et al., 2006)

$$(1.2)\ Fe_{(1-x)}S_{(s)} + \left(\frac{1}{2} - x\right)O_2 + 2(1-2x)H^+ \rightarrow FeS_{2(s)} + (1-2x)Fe^{2+} + (1-2x)H_2O$$

$$(1.3)\ Fe_{(1-x)}S_{(s)} + \left(\frac{1-x}{2}\right)O_2 + 2(1-x)H^+ \rightarrow (1-x)Fe^{2+} + S^0 + (1-x)H_2O$$

The formation of secondary alteration rims of marcasite and elemental sulfur limit the formation of sulfate as a product of sulfide oxidation reactions (Moncur et al., 2009; Blowes et al., 2014). In the presence of O_2, Fe (II) oxidizes to Fe(III), consuming H^+ and hydrolysing Fe(III) at pH values greater than ~4 followed by precipitation of Fe(III) hydroxides and generation of H^+:

$$(1.4)\ Fe^{2+} + \frac{1}{4}O_2 + H^+ \rightarrow Fe^{3+} + \frac{1}{2}H_2O$$

$$(1.5)\ Fe^{3+} + 3H_2O \leftrightarrow Fe(OH)_{3(s)} + 3H^+$$

Oxidation of Fe(II) to Fe(III) and precipitation of Fe(III) (oxy)hydroxide generates additional H^+ (Nicholson and Scharer, 1994; Thomas et al., 1998; Janzen et al., 2000). Pyrrhotite can also undergo oxidation with dissolved Fe(III):

$$(1.6)\ Fe_{(1-x)}S_{(s)} + (8-2x)Fe^{3+} + 4H_2O \rightarrow (9-3x)Fe^{2+} + SO_4^{2-} + 8H^+$$

The oxidation of pyrrhotite by Fe(III) has been observed to be more rapid than atmospheric O_2 and the presence of Fe(III) in pyrrhotite may also increase the overall rate of pyrrhotite oxidation (Nordstrom and others, 1982; McGregor et al., 1998; Moncur et al., 2009). Pyrrhotite also can undergo non-oxidative dissolution under acidic conditions generating Fe(II), H_2S and elemental S (Chiriţă and Rimstidt, 2014):

$$(1.7)\ Fe_{(1-x)}S_{(s)} + 2(1-x)H^+ \rightarrow (1-x)Fe^{2+} + (1-x)H_2S + xS^0$$

Other iron-bearing sulfide minerals of interest at the Copper Cliff site include chalcopyrite ($CuFeS_2$), sphalerite ((Zn,Fe)S) and pentlandite ($(Fe,Ni)_9S_8$); oxidation of chalcopyrite, pentlandite and sphalerite are important sources of dissolved metals, including Fe, Cu, Ni, Zn and Co. Chalcopyrite oxidation by O_2 proceeds as follows:

$$(1.8)\ CuFeS_{2(s)} + O_2 + 4H^+ \rightarrow Fe^{2+} + S^0 + 2H_2O$$

The dissolution of chalcopyrite results in the release of Cu, Fe and in the consumption of H^+. However subsequent oxidation of Fe(II) and S^0 generates H^+:

$$(1.9)\ S^0 + \frac{3}{2}O_2 + H_2O \rightarrow 2H^+ + SO_4^{2-}$$

Similar to pyrrhotite, chalcopyrite can be oxidized by Fe(III) as shown by (Rimstidt et al., 1994):

$$(1.10)\ CuFeS_{2(s)} + Fe^{3+} + H_2O \rightarrow Cu^{2+} + 17Fe^{2+} + 16H^+ + 2SO_4^{2-}$$

Both pentlandite and sphalerite are susceptible to oxidation by $O_{2(g)}$ and Fe(III) although less abundant than pyrrhotite and chalcopyrite at the Copper Cliff site.

The formation of secondary minerals provides a control on metal mobility (McGregor et al., 1998; Lindsay et al., 2015). Secondary minerals commonly found in sulfide mine tailings include goethite, gypsum, jarosite, covellite, marcasite and sulfur (Blowes et al., 2013; Lindsay et al., 2015). Extensive secondary mineral precipitation and cementation can lead to the formation of a hard pan layer (Blowes et al., 1990). The hard pan layer can potentially limit the downward migration of pore water and O_2. The acid generated by sulfide oxidation is neutralized by the successive dissolution of carbonate, Fe and Al (oxy)hydroxide, and silicate minerals

present in the sulfide tailings deposit. Both acidic and neutral mine drainage can potentially contain dissolved metals (Lindsay et al., 2009). The mobility of the released cations depends not only on pore-water pH but also biogeochemical processes that influence the redox state of dissolved metals (Lindsay et al., 2009; Pérez Rodríguez et al., 2013). Mine impacted water with declining pH and elevated concentrations of sulfate and metals can be detrimental to the environment and to local water resources (Blowes et al., 2003).

1.1.2. Mining in Sudbury

Mining in the Sudbury Region is associated with an igneous rock assemblage known as the Sudbury Igneous Complex. The Complex is elliptical in shape, and approximately 60 by 27 km (Pye et al., 1984). The Sudbury Igneous Complex consists of a basal norite which grades upwards through a quartz gabbro unit which gradually becomes a granophyre. At the contact between the Complex and the surrounding host Archean and Proterozoic bedrock is a discontinuous layer called the Sublayer. The Sudbury Igneous Complex is host to of one of the largest Ni and Cu sulfide-ore regions in the world. Many of the ore deposits are associated with the Sublayer and occur as lenses of massive sulfide which contains between 5 and 60 wt. % sulfide minerals. Predominant sulfide minerals found in Sudbury ore bodies include pyrrhotite ($Fe_{(1-x)}S$), pentlandite ($(Fe,Ni)_9S_8$), chalcopyrite ($CuFeS_2$) and pyrite (FeS_2) (Naldrett, 1984). Minor amounts of galena (PbS), sphalerite (ZnS), and cobaltite (CoAsS) also occur. Platinum group elements (PGE) are associated with the deposits of Sudbury and may occur in economic concentrations. Mining in Sudbury was first started in 1886 by the Canadian Copper Company. Copper was the first metal to be extracted and it was not until 1887 that economic quantities of nickel were detected (Pye et al., 1984).

The Copper Cliff Central Tailings Impoundment near the City of Sudbury, Ontario was the focus of this study. The impoundment covers an approximate area of 22 km^2 (Coggans et al., 1999). The tailings facility consists of several valleys filled to depths of up to 45 m with silty sand tailings above lacustrine and glacial sediments, bounded by bedrock.

1.1.3. Cu Isotope Measurement and Fractionation

Copper has two oxidation states: +1, present in minerals such as chalcopyrite, covellite and chalcocite and +2 which is highly soluble and present in aqueous solutions. Copper has two stable isotopes: Cu^{65} and Cu^{63} with global relative abundances of 30.85% and 69.15% respectively (de Laeter et al., 2003). Copper isotope ratios are expressed using δ notation, with values reported in ‰ units according to the equation:

$$(1.11)\ \delta^{\frac{65}{63}}Cu = \left[\frac{\left({}^{65}Cu/{}^{63}Cu\right)_{sample}}{\left({}^{65}Cu/{}^{63}Cu\right)_{standard}} - 1\right] \times 1000$$

The isotopic composition of the primary Cu sulfide mineral chalcopyrite is generally 0±1‰ (Maréchal et al., 1999; Zhu et al., 2000; Larson et al., 2003; Graham et al., 2004; Mathur et al., 2005; Rouxel et al., 2005; Mason et al., 2005; Markl et al., 2006; Asael et al., 2007). A laboratory study on the oxidative dissolution of chalcocite and chalcopyrite with and without bacteria reported isotopically heavy results in the leach solution for abiotic oxidation (δ^{65}Cu =5.34±0.16‰ and 1.90±0.16‰, respectively) and values similar to the starting material (δ^{65}Cu =2.60±0.16‰ and 0.58±0.16‰) prior to oxidation in the presence of *Thiobacillus ferrooxidans* (Mathur et al., 2005). Understanding the isotopic ratio of Cu when it is released into the environment is important to understanding the effects of the various reaction mechanisms controlling Cu mobility.

Copper isotope ratios have been successfully measured for a range of reaction mechanisms and environmental settings. Several reaction mechanisms have been shown to cause isotope fractionation including dissolution and precipitation. Oxidation reduction reactions have also been shown to affect Cu isotope fractionation (Ehrlich et al., 2004). The reduction of aqueous Cu(II) to Cu(I) is the main factor affecting the fractionation during covellite formation

in low temperature geological environments (Ehrlich et al., 2004; Pérez Rodríguez et al., 2013). Fractionation between aqueous Cu(II) and covellite (CuS) during abiotic precipitation experiments reported an isotope separation $\Delta^{65}Cu$ ($\delta^{65}Cu(II)_{aq}$-$\delta^{65}CuS$) value of 3.06±0.14‰ (Ehrlich et al., 2004). Iron (oxy)hydroxides are common in mine tailings and are able to retain trace elements such as Cu by adsorption or co-precipitation. Several studies have shown adsorbed Cu on ferrihydrite and goethite is more enriched in Cu^{65} relative to aqueous Cu (Balistrieri et al., 2008; Pokrovsky et al., 2008). Under acidic conditions and in the presence of Fe oxidizing (*Adicithiobaccilius ferrooxidans*) bacteria an isotopically light solution was observed due to the uptake of Cu^{65} on oxide surfaces formed on cell walls (Mathur et al., 2005; Pokrovsky et al., 2008). Understanding how different reaction mechanisms alter the Cu isotope ratio in isolation can aid in identifying the dominant reactions in different environmental settings.

A variety of reactions can simultaneously affect Cu isotope ratio trends at mine-waste sites. Pérez Rodríguez et al. (2013) digested solid mine tailings from an abandoned Cu mine site in northern Sweden and measured Cu isotope ratios along depth profiles with changing redox conditions. In a secondary Cu enrichment zone at the Laver mine $\delta^{65}Cu$ values of -4.35±0.02‰ and a $\Delta^{65}Cu$ ($_{\text{fresh tailings – oxidation front}}$) value of 5.66‰ were observed. Kimball et al. (2009) measured the Cu isotopic composition during leaching of primary minerals and in mine-impacted stream water in Colorado, USA.

1.2. Research Objectives

The research studies detailed in this thesis present a multi-disciplinary approach to understanding copper (Cu) isotope fractionation and the geochemical and mineralogical evolution of Ni-Cu mine tailings. The studies focus on the following research questions: i) What changes have occurred in the Copper Cliff tailings since the previous study that ended in 1993? ii) Can Cu isotope analysis be used to better understand the fate of Cu in mining impacted groundwater? iii) Is there potential for the analysis of Cu isotope ratios to provide insight into the prevailing reaction mechanisms and the progression of oxidation in sulfidic mine tailings?

1.3. Organization of Thesis

The contents of this thesis are presented in four chapters. Chapter one consists of an introduction including a background on sulfidic mine tailings with a special focus on the Sudbury area and research on the measurement and analysis of Cu isotopes. Chapters two and three were prepared as standalone articles for submittal to peer-reviewed journals.

The goal of Chapter two is to characterize the evolution of sulfide oxidation and observed changes to the aqueous and solid-phase geochemistry as a function of depth at the Copper Cliff Central Tailings impoundment. Parameters are measured along a depth profile at the study location. Modelling of O_2 depletion and sulfide oxidation, mineralogical observations of sulfide alteration, concentrations of dissolved constituents and results of selective extractions are compared to results of a study completed in 1990. The comparison of results over a 25 year period provide an understanding of sulfide oxidation and the long-term geochemical evolution of sulfidic mine tailings.

The purpose of Chapter three is to link changes in the Cu isotope ratio with prevailing reaction mechanisms and sulfide oxidation in sulfidic mine waste. The aqueous- and solid-phase geochemistry of the study profile at the Copper Cliff Central Tailings Impoundment are analysed to provide an understanding of prevailing reaction mechanisms and sulfide oxidation.

Chapter four presents a global conclusion and discusses the broader implications of the measurement of Cu isotope ratios.

Chapter 2. Geochemical and Mineralogical Evolution of Cu Attenuation in the Copper Cliff Tailings Impoundment

2.1. Overview

Oxidation of sulfide-rich tailings in Sudbury, Ontario at the Copper Cliff tailings impoundment has resulted in the degradation of tailings pore-water over time. This study focused on an area of tailings where deposition of fresh tailings ceased in 1960. Oxidation of sulfide tailings has resulted in the advance of low pH pore-water and increased concentrations of dissolved constituents at greater depths in the tailings profile. Numerical modelling of sulfide oxidation and gas-phase O_2 depletion using PYROX show the advance of the oxidation front. Elevated concentrations of dissolved metals (up to 2000 mg L^{-1} Fe, 600 mg L^{-1} Cu, 400 mg L^{-1} Ni, 25 mg L^{-1} Co and 15 mg L^{-1} Zn) were observed in the tailings profile. Oxidation of the predominant sulfide minerals, pyrrhotite, pentlandite, chalcopyrite, pyrite and sphalerite to a depth of 1.7 m has resulted in depletion of S, Fe, Ni, Co, Cu, and Zn near the ground surface. Results of selective extractions identified considerable masses of metals associated with reducible iron phases in the oxidized zone and considerable masses of metals in the oxidizable fraction in the transition and unoxidized zones. Copper was observed in the weathered rims of pyrrhotite grains in the transition zone as predominantly covellite. Covellite formation is linked to the sharp decrease in the dissolved Cu concentration at the base of the transition between the oxidized tailings and the underlying unaltered tailings. Previous research of the Copper Cliff tailings impoundment between 1990 and 1994 identified an oxidation front at a depth of 1 m and the current in the depth of oxidation of 1.7m is associated with further increase in dissolved metal concentrations and the continued degradation of pore-water quality.

2.2. Introduction

The oxidation of sulfide rich tailings can cause the release of high concentrations of dissolved metals and low pH pore-water into surrounding aquifers and surface water bodies. The occurrence of elevated concentrations of dissolved Fe, Ni, Cu and Zn in tailings pore waters are expected based on the known sulfide ore assemblage and on previous studies at this site (Coggans et al., 1999; McGregor et al., 1995). This study focuses on the evolution of Cu-Ni mine tailings at the Copper Cliff Central Tailings facility in Sudbury, ON. The oxidation of sulfide minerals in Copper Cliff tailings impoundments has been the focus of previous studies of mine waste (McGregor et al., 1998; Coggans et al., 1999; Brookfield et al., 2006). Pyrrhotite ($Fe_{(1-x)}S$), pentlandite ($(Fe, Ni)_9S_8$) and chalcopyrite ($CuFeS_2$) are the principal sulfide minerals present in the Copper Cliff tailings impoundment (Naldrett, 1984). Pyrrhotite commonly hosts trace elements including Ni and Co (McGregor et al., 1998; Gunsinger et al., 2006). Minor amounts of pyrite (FeS_2), and sphalerite (ZnS) are also present in the tailings (Naldrett, 1984). The oxidation of the most abundant sulfide mineral, pyrrhotite, by O_2 and Fe (III) is the main cause of elevated concentrations of Fe and SO_4^{2-} in the groundwater, and is described by Nicholson and Scharer (1994) as :

$$(2.1)\ Fe_{(1-x)}S_{(s)} + \left(2 - \frac{1}{2}x\right)O_2 + xH_2O \rightarrow (1-x)Fe^{2+} + SO_4^{2-} + 2xH^+$$

$$(2.2)\ Fe_{(1-x)}S_{(s)} + (8-2x)Fe^{3+} + 4H_2O \rightarrow (9-3x)Fe^{2+} + SO_4^{2-} + 8H^+$$

Oxidation of pentlandite and pyrrhotite release Ni into the pore-water while chalcopyrite oxidation is the source of Cu in the tailings. The oxidation and dissolution of chalcopyrite by O_2 results in the release of Cu, Fe and in the consumption of H^+. However subsequent oxidation of Fe(II) and S^0 generates H^+:

$$(2.3)\ CuFeS_{2(s)} + O_2 + 4H^+ \rightarrow Fe^{2+} + S^0 + 2H_2O$$

The formation of secondary alteration rims during pyrrhotite oxidation include marcasite (FeS_2) and elemental sulfur (S^0) that limit the formation and release of sulfate (Moncur et al., 2009; Blowes et al., 2014). Under oxidative conditions secondary Fe(III) (oxy) hydroxides such as, goethite (α-FeOOH), ferrihydrite ($Fe_2O_3 \cdot 0.5H_2O$), lepidocrocite (γ-FeOOH) and jarosite ($KFe^{3+}_3(OH)_6(SO_4)_2$) can provide an additional boundary to the oxidation of sulfides. Fe (oxy) hydroxides are also an important for the attenuation by co-precipitation or adsorption of metals including Cu, Ni and Zn.

Extensive secondary mineral precipitation and cementation can lead to the formation of hard pan layers consisting of Fe (oxy) hydroxides and or (hydroxy) sulfates, commonly observed in a variety of sulfide tailings impoundments (McGregor and Blowes, 2002). The precipitation of gypsum ($CaSO_4 \cdot 2H_2O$) in hard pan layers is linked to the attenuation of SO_4^{2-}. Hard pan layers have the potential to limit the downward migration of pore water and O_2, impeding the progress of oxidation reactions.

The secondary mineral covellite (CuS) has been observed in weathered tailings and is related to the attenuation of dissolved Cu in mine impacted groundwater ((Lindsay et al., 2015)). Various pathways for the formation of covellite exist and included Cu(II) replacement of Fe(II) and Zn within sphalerite (Blowes and Jambor, 1990), reaction with pyrrhotite (Wang et al., 1989) and during Fe(III) leaching of chalcopyrite (Córdoba et al., 2008).

A previous geochemical study of the Copper Cliff tailings impoundment in 1990 investigated the ongoing sulfide oxidation. The tailings were estimated to continue to oxidize for 300 years (Coggans et al., 1999). The estimation was based on oxygen diffusion and the

shrinking core model developed by (Davis and Ritchie, 1986) and the water table in 1990. The purpose of this study is to compare the current geochemical conditions to previous geochemical studies of the Copper Cliff tailings impoundment, to better understand sulfide oxidation and the attenuation of pore-water contaminants over the 25 year period. Understanding the advance of sulfide oxidation and the availability of metals in tailings impoundments is important to better understand the geochemical environment within the mine tailings impoundment and the groundwater that flows out of the mine tailings impoundment.

2.3. Site Description

The Copper Cliff Central Tailings Facility is located near the communities of Copper Cliff and Lively, Ontario (Figure 2-1). The tailings impoundment is currently operated by Vale Canada Limited, has been used continuously since 1936. The impoundments cover an area of 22 km^2. The tailings disposal area includes several impoundments which received tailings sequentially since production started. The Copper Cliff tailings facility encompasses several valleys, bounded by bedrock ridges, filled to depths of up to 45 m with silty sand tailings, overlying the natural lacustrine and glacial sediments.

The tailings impoundment is a local groundwater recharge area with a water table elevated 20-30 m relative to the surrounding area (Coggans et al., 1999). The elevated water table is maintained by continued pumping of water into ponds within the impoundment. A previous study focused on the hydrogeochemistry along a cross section of the tailings in the direction of one of the major flow paths (Coggans et al., 1999). Groundwater recharge rates were estimated at 0.24 to 0.28 m/a. Seepage from the tailings disposal area recharges the underlying unconsolidated sediment aquifer and travels laterally towards Finlander Creek, adjacent to the tailings impoundment. In 1957 a revegetation program was initiated to stabilize the tailings surface and prevent air pollution. The program involved spreading limestone, seeding with a variety of vegetation types and application of fertilizer (Peters, 1995). During field visits it was noted that ample vegetation was covering the study location.

This study focused on samples collected from a location adjacent to a piezometer nest (IN13) in the M1 impoundment of the tailings disposal area (Figure 2-1), previously sampled by McGregor et al. (1995), Coggans et al. (1999), and Brookfield et al. (2006). Tailings deposition in the M and M1 impoundments of the tailings disposal area, which covers an area of 2.8 km^2

commenced in 1945 and ended in 1960. The average sulfide content of the tailings varied over time as a result of modifications to the milling process. The sulfide content of the tailings in the M area is 6 wt.% S (Coggans et al., 1999). At IN13, a zone of complete sulfide oxidation was observed in the upper 0.3 m and a zone of active oxidation extended to a depth of 1 m bgs. The pore-water pH values ranged from 3.6 to 4.2. Concentrations of dissolved metals and sulfate were elevated, with maximum concentrations of dissolved Fe (1060 mg L^{-1}), SO_4 (8700 mg L^{-1}), Ni (641 mg L^{-1}), Cu (12.5 mg L^{-1}), Co (23.3 mg L^{-1}) and Zn (13.2 mg L^{-1}) observed in the pore water. Mineralogical analysis identified jarosite, goethite, covellite and gypsum as major secondary precipitates in the tailings and these minerals were inferred to control the mobility of Fe, Cu, SO_4, K and Ca. A hardpan layer consisting of jarosite, gypsum and goethite was identified within the oxidation zone. This study area was selected for further study due to the extensive information obtained in previous years.

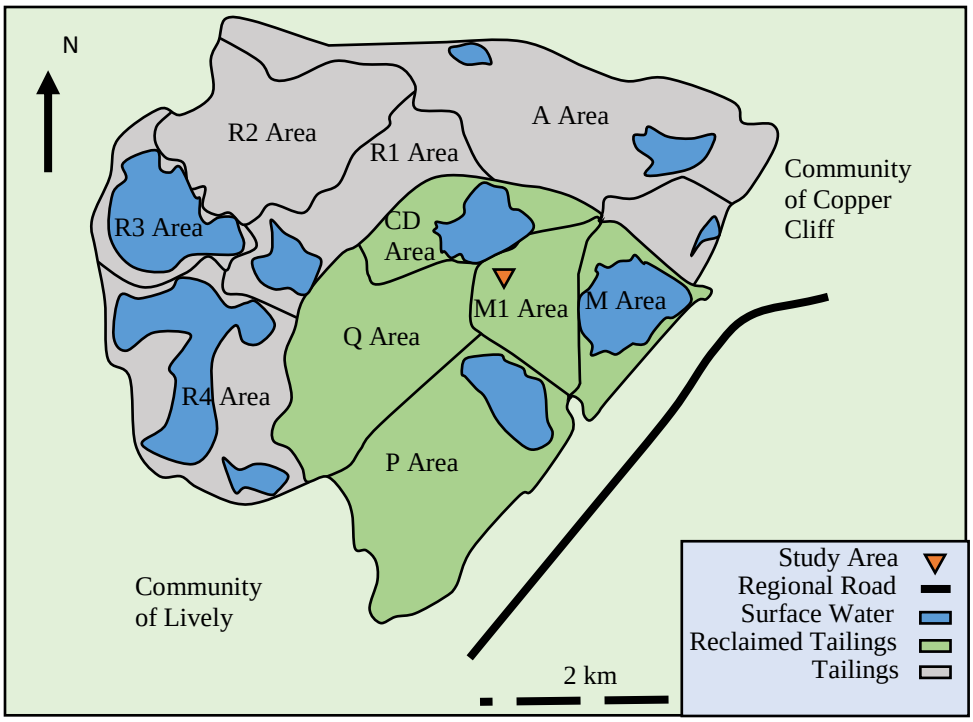

Figure 2-1 Location map showing the Copper Cliff Central Tailings Impoundment and the communities of Copper Cliff and Lively.

2.4. Materials and Methods

2.4.1. Geochemical Sampling

During the summers of 2012, 2014 and 2015 pore-water samples were collected from a piezometer nest at IN13 containing nine drive-point piezometer and three soil water suction samplers (SWSS) (.

Table 2-1). Drive-point piezometers were constructed of stainless steel or PVC drive-point tips that were machined to fit onto threaded 1.27 cm steel pipe or 3.17 cm schedule 80 PVC pipe. The SWSS were installed at 0.2 m depth intervals above the 2014 water table. Pore-water was collected from the SWSS into disposable 60 mL polyethylene syringes by applying a vacuum of approximately 70 kPa. Samples of tailings water were collected from piezometers using a peristaltic pump.

Continuous core samples were collected in 2012 and 2014 for pore-water extraction, geochemical analysis and mineralogical study (Table 2-2). Core samples were collected in 5.08 cm and 7.62 cm diameter thin-walled aluminum tubing sealed with low-density polyethylene caps, and transported to the University of Waterloo where cores for mineralogical analysis were frozen and cores for pore-water extraction were refrigerated.

In 2015, samples for pore gas O_2 concentration determinations were collected using thin walled 0.64 m diameter stainless steel tubing installed into the tailings at 10 cm intervals to a depth of 1.4m. Samples were collected by connecting glass syringes to the stainless steel tubing and transferred to glass bottles submerged in DI water. These samples were transported to the University of Waterloo for analysis by gas chromatography (GC; SRI 8610a Gas Chromatograph).

Table 2-1. Summary of groundwater samples collected in 2014 at the IN13 nest location. GPS coordinates reported in UTM Zone 17N Nad83

Location	**Date**	**Piezometer Type**	**Screen Depth (m bgs)**	**GPS Coordinates**	
				Easting	Northing
VL101-1.8sws	09/2014	SWSS Suction Lysimeter	1.78	491823.5	5146266
VL101-2.0sws	09/2014	SWSS Suction Lysimeter	1.97	491823.5	5146266
VL101-2.2sws	09/2014	SWSS Suction Lysimeter	2.20	491823.5	5146266
VL101-2.5	09/2014	Vyon tip drive point	2.44	491823.5	5146266
VL101-2.6	09/2014	Vyon tip drive point	2.58	491823.5	5146266
VL101-3.2	09/2014	Steel drive point	3.27	491823.5	5146266
VL101-3.9	09/2014	Steel drive point	3.91	491823.5	5146266
IN13-B	1990	PVC tip drive point	5.88	491823.5	5146262
IN13-C	1990	PVC tip drive point	8.88	491823.5	5146262
IN13-D	1990	PVC tip drive point	10.53	491823.5	5146262
IN13-E	1990	PVC tip drive point	22.42	491823.5	5146262
IN13-NA	1990	Unknown	2.53	491828	5146232
IN13-ND	1990	Unknown	2.95	491828	5146232
IN13-NB	1990	Unknown	5.07	491828	5146232

Table 2-2. Summary of tailings samples collected in 2012 and 2014 at the IN13 nest location.

Location	Date	Diameter (cm)	Depth (m bgs)	GPS Coordinates	
IN13	2012	7.62	4.11	491823.5	5146262
IN13	2012	5.08	2.44	491823.5	5146262
IN13A	2014	7.62	2.65	491823.5	5146266
IN13B	2014	5.08	2.62	491823.5	5146266
IN13C	2014	7.62	2.46	491823.5	5146266

2.4.2. Pore-water Analysis

Pore-water was collected from piezometers in the field and from core samples cut into approximately 25 cm sections using the pore-water extraction technique described by Moncur et al. (2013). All samples were filtered through 0.45 µm cellulose acetate membranes, then split into two subsamples. Chemical analyses were conducted to determine the concentrations of major and minor cations passed through a 0.45 µm cellulose acetate filter and preserved at a pH < 2 with Omni Trace metal grade nitric acid (HNO_3). Major cations (Ca, K, Mg, Mn, Na, Si) and minor and trace elements (Al, Be, B, P, Ti, V, Cr, Fe, Co, Ni, Cu, Zn, As, Se, Sr, Mo, Ag, Cd, Sn, Sb, Hg, Tl, Pb, U) were analysed at the University of Waterloo by Inductively Coupled Plasma Atomic Emission Spectrometry (ICP-OES; iCAP 6000, Thermo Scientific, USA), and Inductively Coupled Plasma Mass Spectrometry (ICP-MS; XSeries 2, Thermo Scientific, USA). Anion (F^-, Cl^-, NO_3^-, NO_2^-, Br^-, SO_4^{2-}, PO_4^{3-}) samples were filtered through a 0.45µm cellulose acetate filter and analysed at the University of Waterloo by ion chromatography (IC; DX6000, Dionex, USA). Readings of pH, Eh, electrical conductivity and alkalinity were made at the time of sample collection at the piezometer nests and following pore water extraction in the laboratory. The calibration of the pH electrode (Orion 8156BNUWP, Thermo Scientific, USA) was confirmed between measurements using pH 1.68, 4.0 and 7.0 standards traceable to NIST. The performance of the Eh electrode (Orion 9678BNWP, Thermo Scientific, USA) was assessed using Zobell's solution (ZoBell, 1946; Nordstrom, 1977) and Light's solution (Light, 1972). Determinations of alkalinity were made when sufficient sample volume was available with bromcresol green-methyl red indicator using a Hach digital titrator containing 0.16 N H_2SO_4 (Hach method 8203).

2.4.3. Geochemical Modelling

The aqueous geochemical measurements were used to model geochemical speciation and the degree of saturation with respect to various minerals, represented as the saturation index (SI). Geochemical modelling of speciation and saturation index (SI) were calculated in PHREEQC (Parkhurst and Appelo, 2013) using the WATEQ4F geochemical database modified to include the mineral phases siderite, lepidocrocite and schwermannite. The distribution of redox species and saturation indices are based on element concentrations in solution and the geochemical parameters pH, pe, and temperature. Based on input conditions, SI modelling helps predict which phases are thermodynamically favourable.

2.4.4. Tailings Solids

Core samples of the tailings solids were collected in 2012 and 2014 and the geochemistry and mineralogy examined. The core sections were cut into 0.1 m sections while frozen and transferred to an anaerobic chamber to minimize alteration due to contact with atmospheric $O_{2(g)}$. Samples were collected for mineralogical analysis, X-ray fluorescence (XRF) analysis, X-ray absorption spectroscopy (XAS), determinations of the total carbon and sulfur content bulk density, gravimetric and volumetric moisture content. Subsamples were collected for synchrotron-based. Bulk density and moisture content were measured gravimetrically using samples of a known volume collected from the 5.08 cm core, and oven-dried at 100˚C. Porosity and volumetric moisture content were calculated from measured values of bulk density, gravimetric moisture content and previously reported particle density (McGregor, 1994). Carbon and sulfur contents were measured using an ELTRA CS 2000 induction and resistance furnace. Samples were combusted at 1350˚C, and evolved $CO_{2(g)}$ and $SO_{2(g)}$ was measured by infrared (IR) detection. Sample splits were pulverized in a rock mill and an 8 g sample was used for bulk powder XRF analysis (PANalytical MiniPal4 XRF). Samples for bulk mineralogy, selective extractions and XAS analysis were collected in glass vials in the glovebox and immediately frozen in liquid N_2. Subsamples for mineralogical characterization were freeze dried and sent to Vancouver Petrographics Ltd., where they were prepared with non-aqueous epoxy, double polished to 60 µm thickness, and mounted on glass slides. Polished thin sections were examined under reflected and transmitted light (Nikon Eclipse LV100N-POL) and with scanning electron microscopy with energy dispersive spectrometry (SEM-EDS; Hitachi TM3000, QUANTAX 70 EDS) at the University of Waterloo. Qualitative observations of sulfide alteration were based on the sulfide alteration index (SAI) developed for Copper Cliff (Table 2-3, Jambor, 1994)

Table 2-3. Sulfide Alteration Index (SAI) developed by and modified to reflect Sudbury ore mineralogy (Jambor, 1987; Blowes and Jambor, 1990; Coggans et al., 1999)**.**

Numerical Scale	Description
10	Pyrrhotite and pyrite completely altered, chalcopyrite shows evidence of alteration in fractures and at rims, magnetite only metallic mineral present.
9	Similar to 10, some remnant grains of pyrite, chalcopyrite shows no too little evidence of alteration.
8-7	Cores of some (10%) pyrrhotite present with thick alteration rims, no alteration of chalcopyrite.
6-2	At 6, pyrrhotite has thick alteration rims but most (80%) pyrrhotite grains have a core of unaltered material, marcasite is present as alteration rims around pyrrhotite. At 2, a thin rim of alteration exists, marcasite exists as separate grains.
1-0	Most pyrrhotite grains (90%) are unaltered; at a scale of 1 some may contain fractures with alteration products associated with them.

2.4.5. Sulfide Oxidation Modelling

Sulfide oxidation was modelled to confirm measured O_2 concentrations and mineralogical observation using an O_2 diffusion model (PYROX) for non-homogenous media (Wunderly et al., 1996). PYROX couples O_2 diffusion within the tailings with a shrinking-core model to simulate O_2transport through media with variable bulk-diffusion coefficients. The model used in PYROX was originally developed by Davis and Ritchie (1986) and used to predict rates of sulfide mineral oxidation in the Copper Cliff tailings impoundment (McGregor, 1994; Coggans et al., 1999). The oxidation rate in PYROX is assumed to be limited by two diffusive parameters. The first parameter, D_1 (m^2s^{-1}) is referred to as the bulk diffusion coefficient and represents the rate that O_2 diffuses from the tailings surface downward through the pore-space. The bulk diffusion coefficient is controlled by the tailings matrix and is dependent on the water content. The second diffusive term, D_2 (m^2s^{-1}) is referred to as the intraparticle O_2 diffusion coefficient and represents the rate that O_2 diffuses through secondary alteration rims on sulfide grains.

The parameters used in the PYROX model are summarized in Table 2-4. Several of the parameters including, the grain radius (m), diffusion coefficient for oxidized coatings (m^2s^{-1}), depth of the unsaturated zone (m), fraction of the bulk density that consists of sulfides (kg kg^{-1}), porosity (m^3m^{-3}), temperature (˚C) and bulk density (kg m^{-3}) were assumed to be constant for the IN13 depth profile. The bulk diffusion coefficients are dependent on the volumetric water content of the unsaturated tailings. Volumetric moisture contents for October 2014 can be found in the appendix. The D_2 used for this study was based on the D_2 used in the previous study of Copper Cliff tailings (Coggans et al., 1999). The time step (d*t*) used was 0.01 years. Nodes were distributed evenly across the unsaturated zone at 0.01 m intervals. The grain size was assumed to

be the same as previous studies of the Copper Cliff tailings (McGregor, 1994; Coggans et al., 1999). The depth of the unsaturated zone was assumed to be the depth from the tailings surface to the water table. The fraction of the tailings consisting of sulfide minerals was assumed to be the average of the measured sulfide content in the unoxidized tailings. Porosity and bulk density were assumed to be the average of calculated values. Sulfide oxidation was assumed to only occur during 6 months of the year.

Table 2-4 Parameters used to model sulfide oxidation in PYROX. Parameters used to model sulfide oxidation in previous studies included for comparison.

Parameters	**This Study**	**Coggans et al., (1999)**	**McGregor, (1994)**	**Units**	**Source**
D_2 (for oxidized coatings)	$2.6x10^{-12}$	$2.6x10^{-12}$	$2.6x10^{-10}$	m^2s^{-1}	estimated
D_1 (modelled)	$2.6x10^{-6} – 2.6x10^{-8}$	$4.0x10^{-6}$	$7.70x10^{-7}$	m^2s^{-1}	calculated
Depth of unsaturated zone	2.3	2.92	2.42	m	measured
Thickness of oxidized tailings	1.6	0.92	1.10	m	-
Grain radius	0.045	0.045	0.45	mm	measured
Bulk density	1550	-	1508	kg m^{-3}	measured
Porosity	0.47	0.48	0.48	N/A	measured

2.4.6. Selective Extractions

A six step selective extraction procedure was used to identify availability of metals of interest (*e.g.*, Cu, Fe, Ni and Zn) in response to changing groundwater conditions and oxidative weathering. Samples were taken from the mineralogy core samples at approximately 10-15 cm intervals. The extraction steps are summarized in Table 2-5. Deionized (DI) water purged with Ar was used to target water soluble phases and weakly adsorbed SO_4 and metals (Ribet et al., 1995; Dold, 2003; Gunsinger et al., 2006; Parviainen, 2009). 1.0 M $MgCl_2$ was used to target strongly adsorbed ions and is referred to as the exchangeable fraction (Tessier et al., 1979). A weakly acidic solution of NH_4OAc adjusted to a pH of 4.5 with 17 M HOAc was used to target carbonate minerals and associated adsorbed ions (Dold, 2003; Hayes et al., 2014). A weak acid extraction using 0.5 M HCl was used to target amorphous and poorly crystalline Fe phases, (Heron and Crouzet, 1994; Gunsinger et al., 2006). Whereas a strong acid extraction using 6.0 M HCl was used to target amorphous and crystalline Fe oxyhydroxide phases (Heron and Crouzet, 1994; Silveira et al., 2006). Oxidizable phases including primary and secondary sulfides and organics were targeted using 15 mL of 30% wt. H_2O_2 and 1.0 M NH_4OAc adjusted to a pH of 2.0 with HNO_3. The first three steps were completed in an anaerobic glove box and the extractant solutions were argon purged. After the specified reaction time, the extractant solutions were centrifuged and decanted. Results were compared to powder XRF results and an aqua regia extraction completed in 2012 (Fellin, 2013).

Table 2-5. Summary of extraction steps used to evaluate metal availability in mine tailings.

Step	Fraction	Target phase(s)	Solution	Application
1	Water soluble	Soluble species	40 ml Millipore water, CO_2 equilibrium (Dold, 2003)	1hr, Ar purged, agitation, RT
2	Exchangeable	Adsorbed ions	40 ml 1M $MgCl_2$ (pH 7) (Gibbs, 1977; Tessier et al., 1979; Elliott, 1990)	2hr, Ar purged, agitation, RT
3	Carbonates, less-readily exchangeable	Adsorbed species and carbonates	40 ml 1M NH_4OAc (acidified to pH 4.5 with acetic acid) (Zeien and Bruemmer, 1991; Gómez Ariza et al., 2000)	2hr, Ar purged, agitation, RT
4	Reducible	Poorly crystalline Fe phases	40 ml 0.5 M HCl (Heron and Crouzet, 1994; Silveira et al., 2006)	Overnight (24 hr) agitation, room temp
5	Reducible	Amorphous and crystalline Fe phases	6M HCl (Heron and Crouzet, 1994; Silveira et al., 2006)	Overnight (24 hr) agitation, room temp
6	Oxidizable	Sulfides	30% w/v H_2O_2 (pH 2 with HNO_3) and 1M NH_4OAc (Rauret et al., 1999; Dold and Fontboté, 2001)	1-hr slight agitation, then heat at 85ºC for 1-hr, repeat, add 1M NH_4OAc and agitate overnight

2.4.7. Synchrotron Analysis

Sulfide minerals mounted on thin sections were examined using XAS analysis on beamline 13 ID-E (microprobe) at the Advanced Photon Source (APS) at Argonne National Laboratory in Argonne, Illinois, USA. Beamline 13-ID-E uses a Si (111) crystal monochromator to deliver an incident beam energy between 2.4-28 keV. Data acquisition was performed using a four element, Hitachi Vortex, silicon drift detector and a focused beam measuring approximately 2 x 2 μm. Micro x-ray fluorescence (μ-XRF) maps of sulfide minerals examined for XAS analysis were collected at 18 keV for Fe and Cu distribution maps with a dwell time of 30 ms per pixel. Micro-XRF elemental distribution maps of sulfide grains were used to locate areas of interest to collect Cu micro X-ray absorption near edge spectra (μ-XANES).

Data processing and analysis were completed using ATHENA which is part of the IFEFFIT software package (Ravel and Newville, 2005). All XAS data was calibrated using either Cu foil or elemental S based on the maxima of the first derivative. Least squares linear combination fitting (LCF) of normalized spectra using relevant mineral standards was completed to gain an understanding of the mineral species present in the tailings samples.

2.5. Results and Discussion

2.5.1. Sulfide Oxidation

Sulfide oxidation has been ongoing since tailings deposition stopped in 1960 and has resulted in the release of contaminants into the groundwater. Qualitative observations of sulfide oxidation based on the sulfide alteration indices (SAI) were determined for thin sections as a function of depth according to the scheme developed by Jambor (1994). Examples of sulfides with different levels of alteration from different depths is provided in Figure 2-2. Values from 2012 and 2014 for the location IN13 are compared to SAI values from 1990 presented by Coggans et al. (1999) (Figure 2-4). Sulfide minerals in the top 1.6 m were heavily weathered. Pyrrhotite was not observed in the top 1.5 m and chalcopyrite showed signs of weathering. Sulfide minerals in the transition zone approximately 1.6 m to 2.0 m ranged from pyrrhotite grains with thick rims of secondary weathering products to very thin rims along grain boundaries. Based on SAI values, the active oxidation front was estimated to be at a depth of approximately 0.9 m in 1990 whereas the current oxidation front is approximately 1.6 m bgs. The results show the alteration of sulfide minerals between the depths of 0.5 and 1.3 m bgs has progressed dramatically since 1990.

Sulfide minerals were observed to be extensively weathered and total S contents measured on tailings solids indicate depletion of S in the upper 1.6 m of the tailings (Figure 2-4The sulfide content of the unoxidized tailings was determined to be 4.5 wt. % S in the unoxidized zone and 1.0 wt. % in the oxidized zone. Whereas the results presented by Coggans et al. (1999) show the sulfur content is depleted in the upper 0.8 m with similar values for the oxidized and unoxidized zone. The increased depth of sulfur depletion can be used as an indicator of the extent of oxidation that has occurred over the last 25 years.

Sulfide oxidation and oxygen depletion at IN13 was modelled using PYROX and compared to data from 1990, 1992 and 2015 (McGregor, 1994; Coggans et al., 1999). Measured and calculated gas-phase O_2 and total S profiles are presented in Figure 2-4. Modelled O_2 using 2015 conditions are in agreement with field data collected in 1990 and 1992. The modelled sulfur oxidation is in agreement with the measured sulfur depletion observed in the analysis of total sulfur in 2014. The time until complete oxidation of sulfides at the profile location based on the current depth to the water table is an additional 70 years from 2014 compared to the 300 year estimate from 1990 by Coggans et al., 1999. Whereas (McGregor, 1994) estimated a total time of 153 years from 1992 using a D_2 value that was two orders of magnitude greater. Variations in the depth to the water table may be linked to the difference between estimated times to complete oxidation of sulfides at IN13. The models run with the parameters used in 1990 and 1992 are included in the appendix.

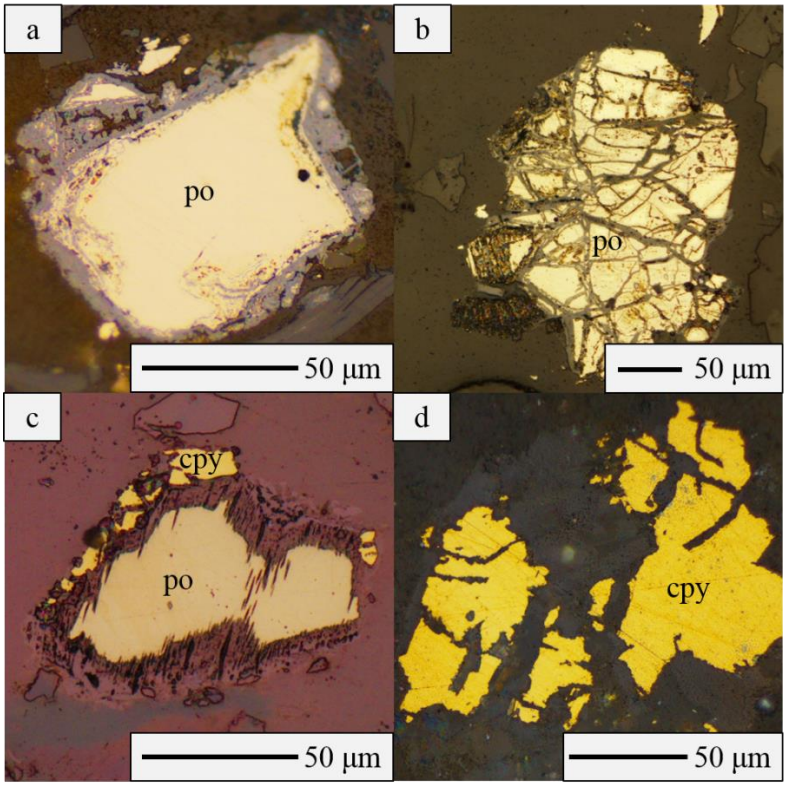

Figure 2-2. Examples of pyrrhotite (a, b and c) and chalcopyrite grains (d) from the tailings profile undergoing oxidation. Reflected light images are organized in order (a, b, c, d) from least weathered (a) in the upper left hand corner to most weathered in the bottom right hand corner (d).

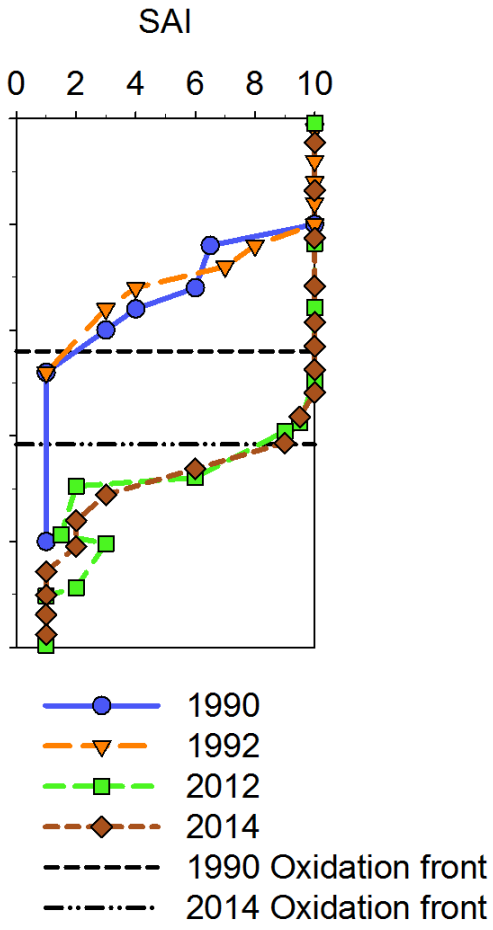

Figure 2-3. Sulfide alteration index (SAI) depth profile of the IN13 location for multiple years including, 1990, 1992, 2012 and 2014 (Coggans, 1992; McGregor, 1994). SAI values are based on qualatative observations made under reflected light and Table 2-3.

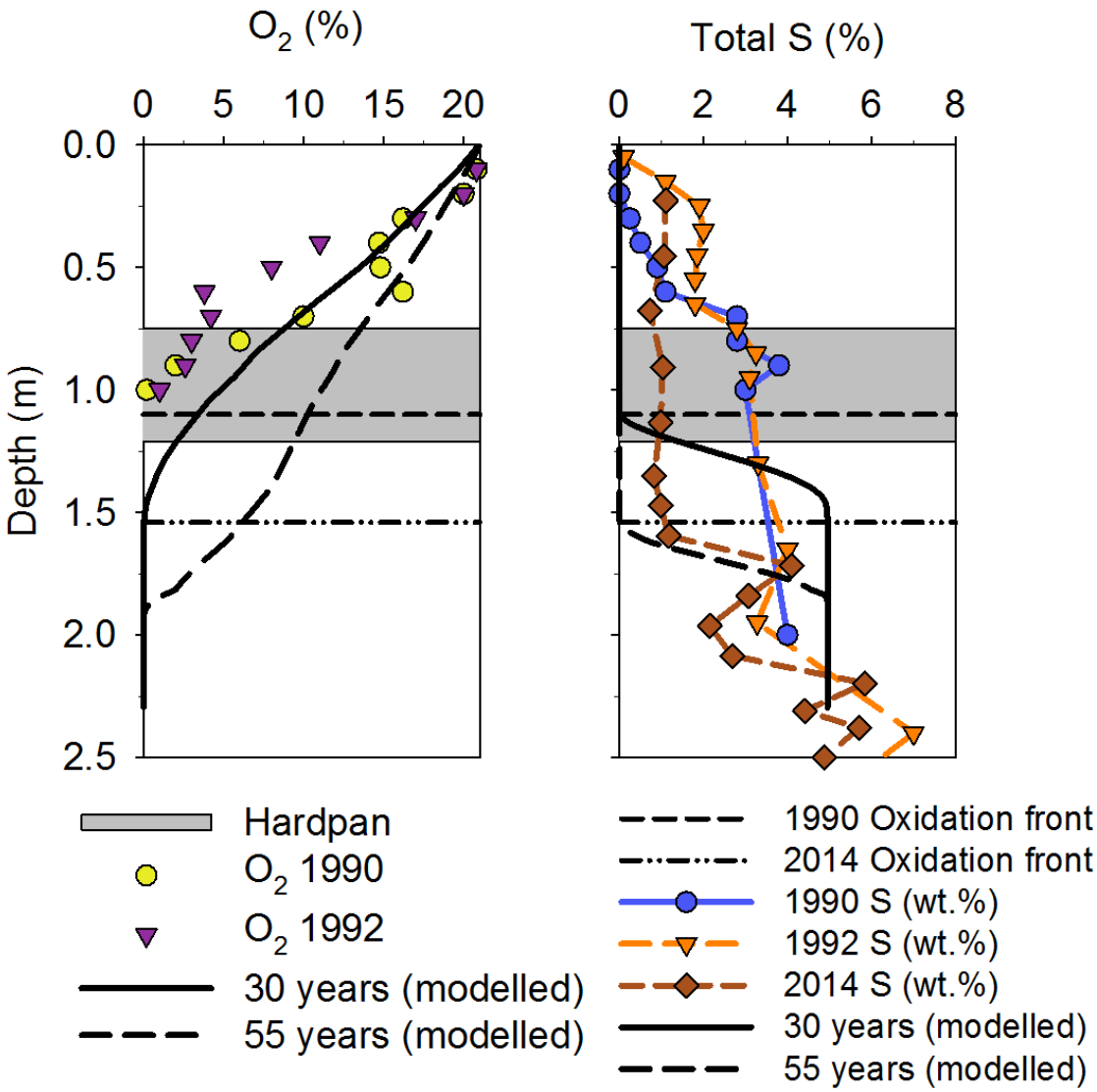

Figure 2-4 Left: Measured concentrations of gas-phase O_2 for 1990 and 1992. O_2 depletion was modelled for 1990 (30 years) and 2015 (55 years) using PYROX. Right: Total sulfur content of samples collected in 1990, 1992 and 2014. The amount of sulfides remaining was modelled for 1990 (30 years) and 2015 (55 years) using PYROX. The oxidation fronts are based on the PYROX model output.

2.5.2. Solid-Phase Geochemistry

The abundance of elements in the tailings based on powder XRF analysis follows the order Si > Al > Fe > Mg > Ca > K > Na = Mn. Results of the powder XRF analysis from 2014 can be found in Appendix A (**Error! Reference source not found.**). The order of abundance is consistent with the mineralogy of the tailings, which includes quartz, augite, plagioclase, hypersthene, pyrrhotite, and chalcopyrite comprising the bulk of the host rock and ore. The abundance of trace metals follows the order Cu > Ni > Cr > Zn > Co > Pb. Copper and Ni were both found in concentrations greater than 1000 mg/kg and represent the contribution of the predominant ore minerals pyrrhotite, pentlandite, and chalcopyrite. Sphalerite can be found with chalcopyrite and acts as the main source of Zn in the tailings. Pyrrhotite at Copper Cliff contains trace amounts of Co (Jambor, 1994). Depth dependent trends were observed for Cu, Ni, and Zn (Figure 2-5). These concentration trends are consistent with observations of sulfide-mineral occurrence and alteration during the mineralogical study. Nickel, Cu and Zn were relatively depleted in the oxidized zone due to the oxidation of sulfide minerals. Data from 2012 was previously described and was used here to better delineate the concentration of solid phase metals to a depth of 4 m bgs (Fellin, 2013). A zone of relative Cu enrichment was observed between the depths of 1.9 m and 2.5 m. Covellite was observed at a depth of 1.9 m bgs and had been previously observed and suggested to control Cu attenuation (Coggans et al., 1999). Covellite was observed as small (0.01 mm) isolated anhedral grains and in the weathered rims of pyrrhotite grains.

Results from a whole-rock extraction completed on samples collected in 1992 are included in Figure 2-5 (McGregor et al., 1998). The advance of the oxidation front can be seen by comparing the depths where Cu, Ni and Zn are depleted, 0.8 m bgs in 1992 compared to 1.7

m bgs in 2014. An enriched Cu zone can be seen in the 1992 data between a depth of 0.8 and 1.4 m bgs.

Sulfide grains from varying depths were analysed using scanning electron microscopy with energy-dispersive spectroscopy (SEM-EDS) and synchrotron-based µ-XRF elemental mapping to better understand the release and attenuation of metals (Figure 2-6). Iron and Cu µ-XRF elemental distribution maps show irregular Fe intensities related to weathering and secondary mineral precipitation. Increased Cu intensities observed in fractures and on grain boundaries related to Cu attenuation. Whereas chalcopyrite inclusions in pyrrhotite grains contribute to elevated Cu intensities The formation of secondary Fe minerals goethite, lepidocrocite, and ferrihydrite were expected based on previous studies; detection of these phases in the weathered rims of pyrrhotite grains using µ-XRD was unsuccessful, likely due to lack of sample crystallinity. Copper was observed in the alteration rims and micro-fractures of sulfide grains in the secondary enrichment zone whereas Ni and Zn were less abundant.

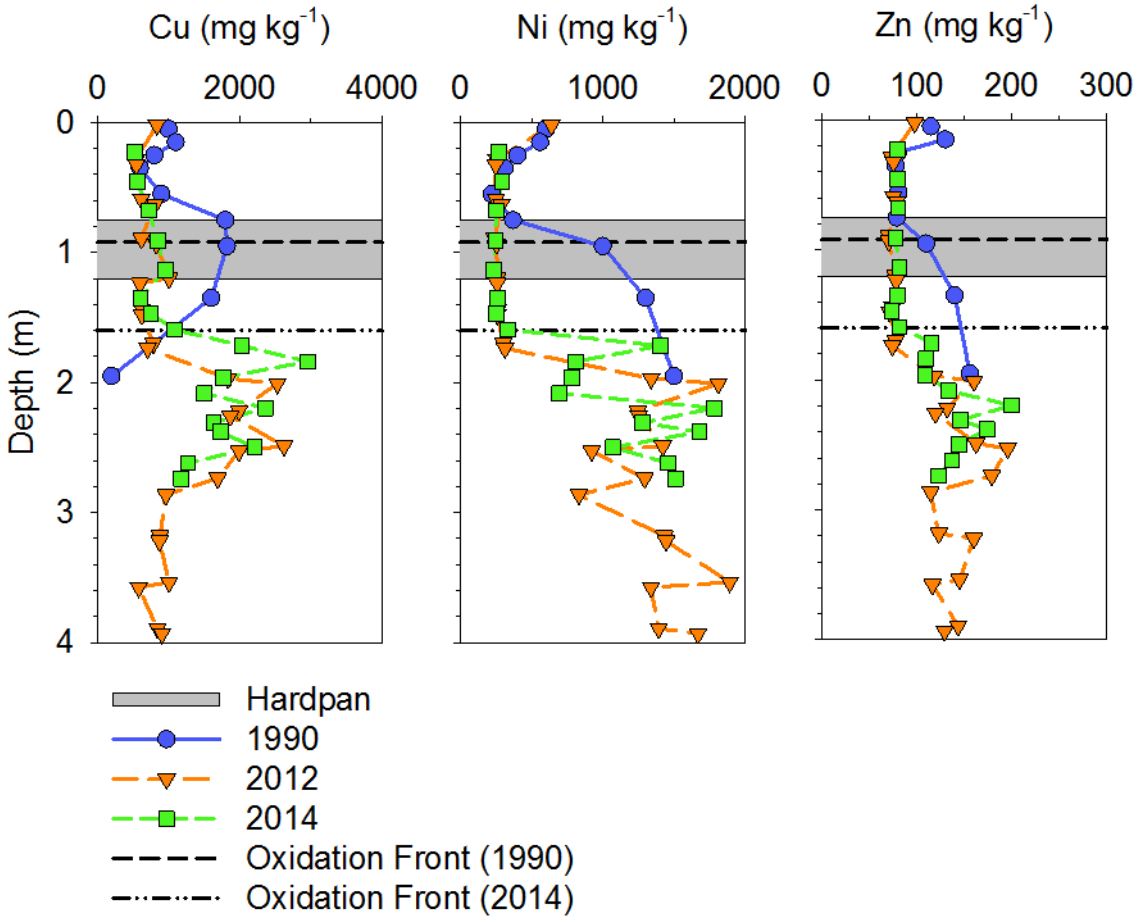

Figure 2-5 Depth profiles of Cu, Ni and Zn from the IN13 location for 2012 (Fellin, 2013) and 2014. The shaded grey area represents the hardpan and the dashed line indicates the water table.

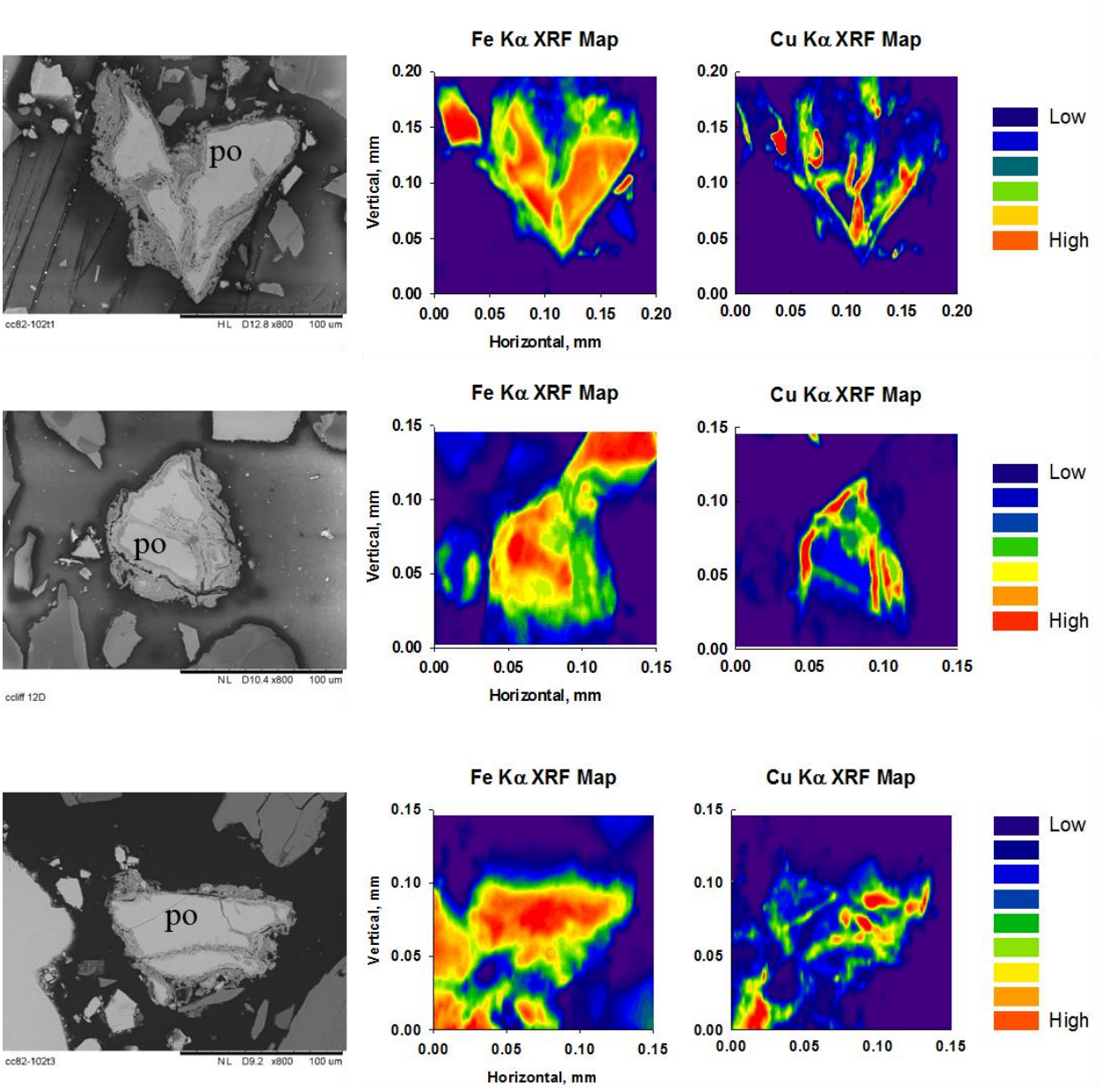

Figure 2-6. SEM images of the pyrrhotite ($Fe_{(1-x)}S$) sulfide minerals from a depth of 1.9 m bgs in the tailings profile with visible weathered rims (dark grey) of Fe (oxy) hydroxides. Iron and Cu µ-XRF elemental distribution maps show irregular Fe intensities related to weathering. Increased Cu intensities observed in fractures and on grain boundaries related to Cu attenuation and possible chalcopyrite inclusions in pyrrhotite grains.

2.5.3. Aqueous Geochemistry

The long-term oxidation of sulfide minerals present within the tailings impoundment has resulted in low pH groundwater (3.0-4.4) that increases (5.5-6) at a depth of 6 m bgs. Sulfide oxidation has led to elevated concentrations of SO_4 (up to 28,000 mg L^{-1}), Fe (up to 2,000 mg L^{-1}) and trace metals that peak in the transition zone and decrease in the unoxidized zone in 2014 (Figure 2-7). The pore-water chemistry for 2012 and 2015 are located in Appendix A.

The pH values recorded were fairly constant between values of 3.5 and 4.5 until a depth of approximately 5 m bgs. The lowest pH values were observed between a depth of 1.6 and 2.5 m. The H^+ generated by sulfide oxidation in mine tailings is consumed by reactions involving calcite, dolomite, siderite, Al-silicates, Al-hydroxides, and Fe-hydroxides (McGregor et al., 1998; Coggans et al., 1999; Lindsay et al., 2015). Results from a previous study of the Copper Cliff tailings pore-water are shown in Figure 2-7. Reported pH values less than 4.0 are seen at a depth of 1.5 m, increasing to 5.99 at a depth of 4.0 m (Coggans et al. 1999). Low pH pore-water has advanced an additional 1.5 m into the tailings deposit. Measurable alkalinity detected below the zone of low-pH pore water was slightly less than the alkalinity measurements reported in 1990. Saturation indices were calculated for pore-water samples with pH values greater than 4 and measureable alkalinity (Figure 2-8). Geochemical modelling indicates that the pore-water is saturated with respect to calcite and siderite below a depth of 5.9 m bgs.

Sulfate is the major anion in the groundwater with values as high as 15,000 mg L^{-1} measured in 2014. Sulfate concentrations greater than 3,000 mgL^{-1} persist to a depth 10.6 m. Maximum SO_4 concentrations have increased since 1990 (8,000 mg L^{-1}) at a depth of 0.9 m (Coggans et al., 1999). Geochemical modelling indicates all pore-water samples in the depth profile are saturated with respect to gypsum.

Major cations in the Copper Cliff tailings include Ca, Mg, K, Fe, Cu, Ni, and Zn. The concentration of Ca decreased near the hardpan layer but was constant below the water table. A maximum concentration of Ca (600 mg L^{-1}) was detected near the hardpan in 2014 (Figure 2-7). Hardpan layers generally contain gypsum (Blowes et al., 1990; Moncur et al., 2005; Lindsay et al., 2015). The dissolution or precipitation of gypsum could act as a source or sink of Ca. Other sources of Ca at Copper Cliff include the milling reagents and Ca derived from the dissolution of carbonate and alumino-silicate minerals (Coggans et al., 1999). Concentrations of Mg in the unsaturated zone reached a maximum concentration (675 mg L^{-1}) at a depth of 1.6 m bgs. The concentration of Mg has decreased from a 1990 values (1000 mg L^{-1}) measured at a depth between 4.5 m bgs and 6.5 m bgs.. Sources of Mg may include the dissolution of aluminosilicates.

A maximum Fe concentration of 1800 mg L^{-1} was measured at 3.0 m bgs and 5.1 m in 2014. The maximum concentration of 900 mg L^{-1} Fe in the unsaturated zone was observed at a depth of 1.6 m bgs and coincides with the pH value of 3.4. Dissolved Fe concentrations decreased rapidly below a depth of 6 m. The solubility of Fe is controlled by pH, changing redox conditions and the precipitation of Fe(III) oxyhydroxides and hydroxysulfates (Lindsay et al., 2015). Geochemical modelling of the groundwater suggests that precipitation of secondary Fe(III) oxyhydroxides and hydroxysulfates control the concentrations of dissolved Fe. The pH increases to approximately 6.2 at a depth of 6 m bgs and the concentration of dissolved Fe decreases. In 1990, the peak Fe concentration (1060 mg L^{-1}) was measured at a depth of 0.7 m bgs and elevated Fe concentrations persist to a depth of 2 m bgs. The slight increase in the aqueous Fe concentration between 1990 and 2014 and increased depth of elevated Fe

concentrations is due to the ongoing oxidation of pyrrhotite and the advance of low pH pore-water.

Copper was the second most abundant dissolved metal in the pore water in 2014. A maximum concentration of 600 mg L^{-1} was observed at a depth of 1.7 m bgs in 2014 (Figure 2-7). The concentration of Cu rapidly decreased to values less than 10 mg L^{-1} below the water table. The concentration of Cu has increased greatly since 1990 when a maximum concentration of 10 mg L^{-1} was detected at a depth of 0.42 m bgs. The increase in the maximum dissolved Cu concentration can be linked to the slow rate of oxidation of chalcopyrite relative to the other sulfides (Lindsay et al., 2015). Secondary covellite was observed as small anhedral grains and incorporated in weathered pyrrhotite rims in tailings samples collected in 2012 and 2014, and in previous studies of the Copper Cliff tailings impoundment (MacGregor et al., 1998; Coggans et al., 1999). Secondary covellite precipitation was observed to limit Cu concentrations in other tailings impoundments (Boorman and Watson, 1975; Blowes and Jambor, 1990; Pérez Rodríguez et al., 2013; Moncur et al., 2015).

Nickel and Zn exhibit maximum concentrations below the hardpan and near oxidation front, and then decrease deeper into the tailings. Maximum concentrations of Ni, 350 mg L^{-1} and Zn, 30 mg L^{-1} were observed at depths of 1.6 and 3.0 m bgs respectively (Figure 2-7). Ni and Zn concentrations decrease below a depth of 6 m. Secondary Ni or Zn minerals were not observed in the tailings. In 1990, maximum concentration of Ni (200 mg L^{-1}) and Zn (9 mg L^{-1}) were observed at a depth of 2.1 m bgs. Adsorption of Ni on Fe(III) oxyhydroxides is enhanced in the near neutral pH observed at a depth of 5.8 m bgs (Langman et al., 2015). The advance of low pore-water pH is likely related to differences observed in the Zn concentrations. Attenuation of Cu, Ni, and Zn by sorption and co-precipitation with secondary Fe(III) (oxyhydr)oxides have

been observed in other tailings impoundments (Moncur et al., 2005; Gunsinger et al., 2006; Lindsay et al., 2009).

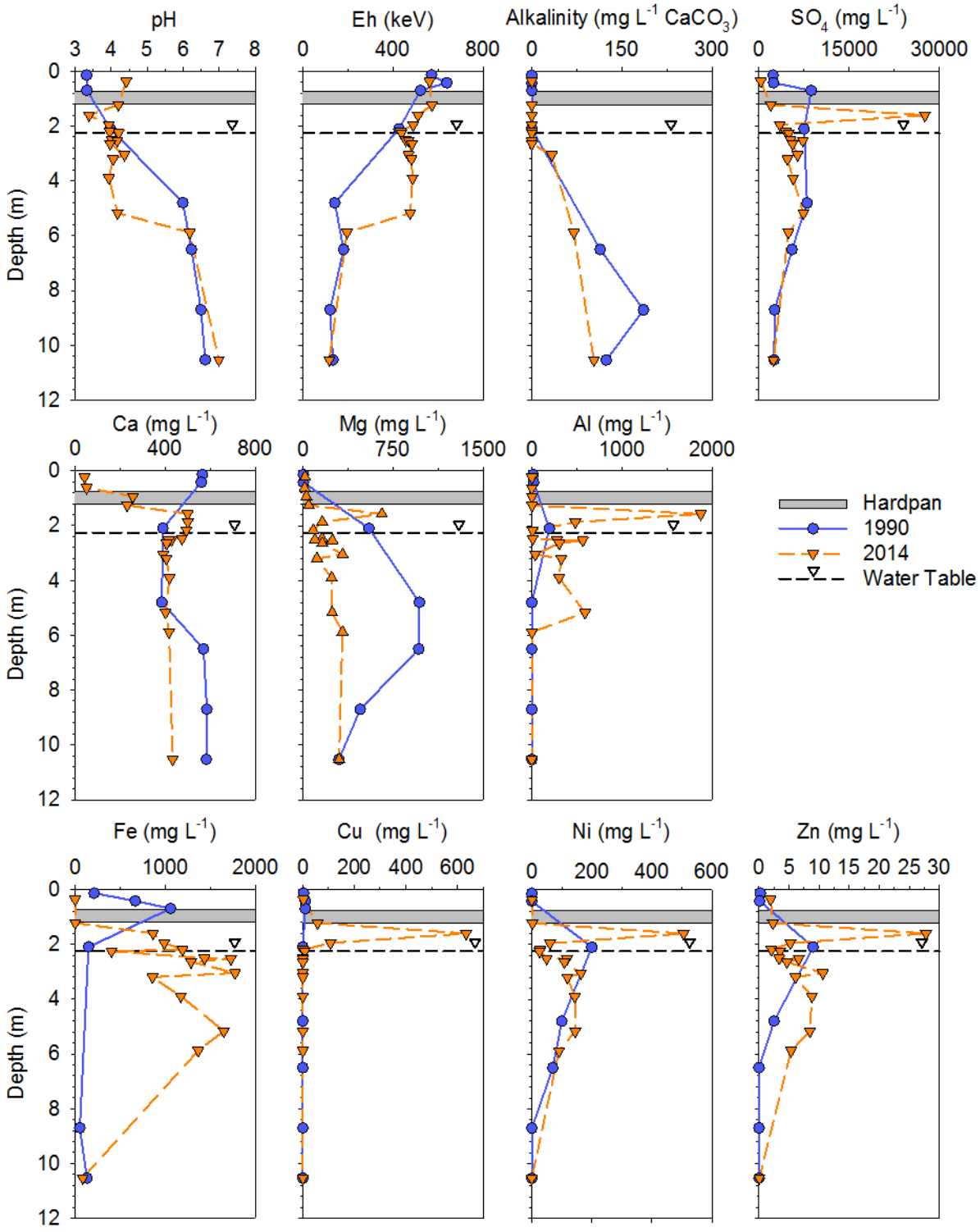

Figure 2-7. Geochemical depth profiles of pH, Eh, Alklainity, SO_4, Ca, Mg, Al, Fe, Cu, Ni and Zn of the IN13 location for 1990 (Coggans et al., 1999) and 2014 profile A. Geochemical data for profile B collected in 2014 are located in the appendix. The shaded grey area represents the hardpan and the dashed line indicates the water table.

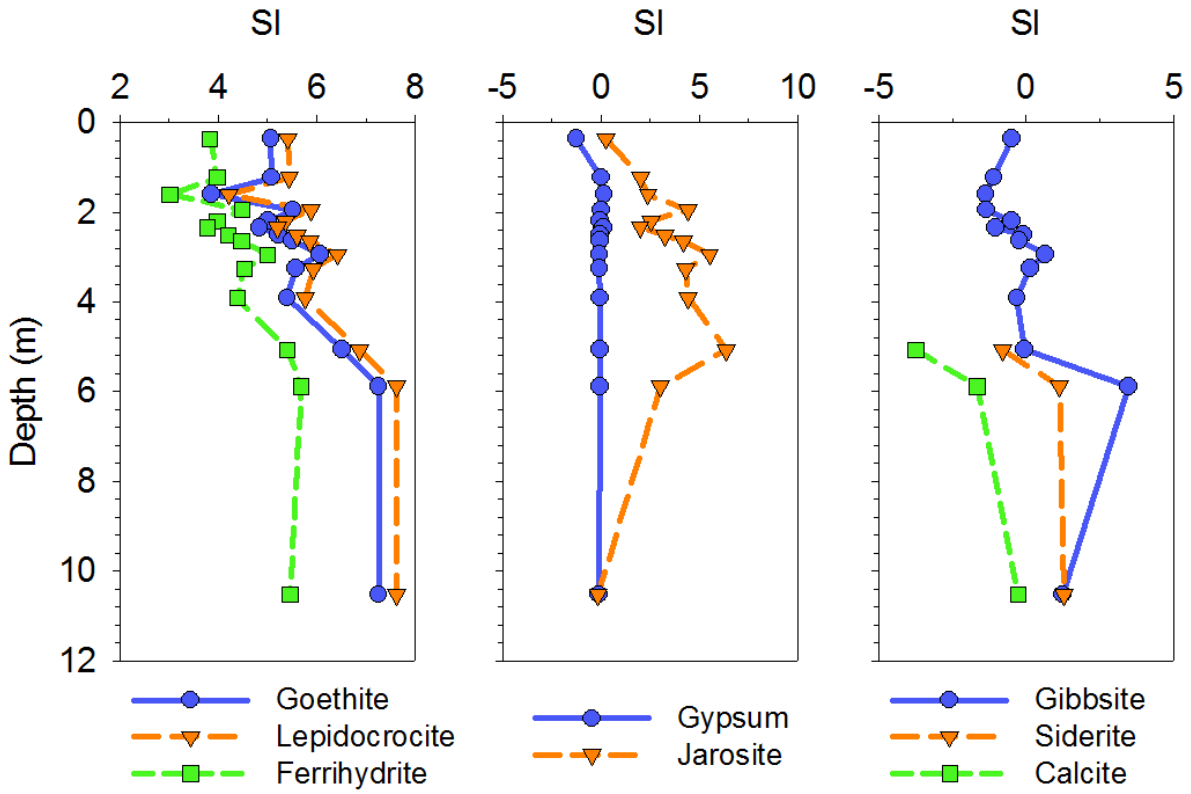

Figure 2-8. Geochemical modelling of saturation indices of mineral phases which potentially control precipitation-dissolution reactions in the Copper Cliff tailings.

2.5.4. Selective Extractions

A series of selective extractions was completed to assess the availability of Fe, Cu, Ni and Zn in the tailings (Figure 2-9, Figure 2-10). The extractions targeted water soluble, exchangeable cations, carbonate minerals, reducible and acid leachable Fe-phases and oxidizable mineral phases. The water soluble and carbonate phases account for relatively less metals in the tailings solids. The majority of available metals in the tailings profile are associated with the exchangeable, reducible and oxidizable extractions. There are observable differences in the metal availability between the different zones that have developed in the tailings profile. The oxidation of sulfide minerals in the oxidized zone and transition zone has resulted in the release of metals into the groundwater.

Results of the water soluble fraction indicate that only Ca and SO_4 had significant soluble components. Water-soluble ferrous sulfate minerals, *e.g.*, melanterite ($FeSO_4 \cdot 7H_2O$), could be the host for Fe associated with the peak in water soluble metals observed between the water table and the oxidation front (Blowes et al., 1991; Moncur et al., 2005).

Exchangeable metals are available in the hardpan, the transition and unoxidized zones. The majority of the exchangeable Fe, Ni and Zn was observed in the transition zone and increasing into the unoxidized zone. The exchangeable fraction contained the largest concentration of Ni compared to the other extractions. Copper in the exchangeable extraction was more abundant in the transition zone where Cu released by oxidation is being attenuated and the concentration of Cu in the pore-water is decreasing. Sorption onto the secondary Fe(III) phases ferrihydrite, jarosite, goethite and on to the unaltered sulfide minerals has the potential to attenuate dissolved metals (Lindsay et al., 2015).

Iron and a small amount of Cu were detected in the carbonate fraction. Iron associated with the carbonate fraction was detected in the hardpan and in the transition and unoxidized zones. Copper was detected in the carbonate fraction in the hardpan and transition zones. Ni and Zn do not have significant soluble components associated with the carbonate fraction. The occurrence of siderite ($FeCO_3$) in the tailings can be linked to the Fe in the carbonate fraction (Blowes et al., 1990; Dold, 2003).

The extractions utilizing 0.5 M and 6 M HCl targeted reducible and acid leachable Fe phases such as Fe (III) (oxy)hydroxides, ferrihydrite, goethite (α-FeOOH) and jarosite ($KFe_4(OH)_6(SO_4)_2$). The contribution of exchangeable metals was accounted for based on results of the $MgCl_2$ extraction. The 6 M HCl extraction was adjusted to account for the contribution of the 0.5 M HCl extraction and gain a better understanding of the contribution of my crystalline Fe oxides to the attenuation of metals in the tailings profile. The 6 M HCl is extraction is sufficiently strong that partially weathered sulfides like pyrrhotite may have been dissolved as well. Large masses of Fe in the extractions were observed in tailings samples from the hardpan and at the base of the oxidized zone in the 0.5 M HCl step. The mass of Fe released in 6 M HCl extractable step was relatively high in the oxidized zone and decreased sharply at the base of the oxidized zone.

Relatively large concentrations of Cu and Zn were retained in the 0.5 M HCl extractable fraction in the transition zone. A larger amount of Cu and Zn were detected in the 6M HCl extraction step in the oxidized zone, similar to the trend seen in the Fe concentrations. Copper and Zn extracted from samples collected from the oxidized zone were likely adsorbed to or co-precipitated with Fe(III) (oxy)hydroxides, whereas Cu and Zn in the transition between oxidized and unoxidized tailings were more likely associated with less crystalline Fe(III) (oxy)hydroxides.

A small amount of Ni was detected in the oxidized and transition zones in the 0.5 M and 6 M HCl extractable fractions. Pore-water in the tailings profile is acidic (pH ~ 4) and Ni solubility increases below near-neutral pH (pH ~ 5.5) (Stumm, 1992; Langman et al., 2015).The adsorption and co-precipitation of Ni with Fe(III) oxyhydroxides is likely enhanced in near neutral pH pore-water (Sidenko et al., 2005; Langman et al., 2015).

Results from the oxidizable extraction indicate that oxidizable metals are depleted in the oxidized zone. The greatest depletion was observed for Fe and Ni, both of which are associated with pyrrhotite, the most abundant sulfide. Nickel-bearing pyrrhotite ($Fe_{1-x}S$) and pentlandite (Fe_7S_8) are the principal sources of Ni in the tailings. The depletion of Cu and Zn are more gradual from the oxidized to unoxidized zones. There is a pronounced increase in the amount of oxidizable Cu in the transition zone where secondary copper sulfides have been observed. Chalcopyrite and sphalerite are the main sources of Cu and Zn in the tailings and both are more resistant to weathering than pyrrhotite (Lindsay et al., 2015).

A previous study of sulfide mine tailings at the Copper Cliff Tailings Impoundment utilized a series of three extractions (Ribeta et al., 1995; McGregor et al., 1998). The three steps included a water-soluble fraction targeting metals derived from the dissolution of phases such as gypsum ($CaSO_4 \cdot 2H_2O$). Similar results for the water soluble fraction were observed in both studies, water soluble metals accounted for less than 3% of the total.

Next, an acid-leachable step that targeted water-insoluble sulfates such as jarosite, carbonate minerals such as calcite and dolomite and poorly crystalline Fe(III) (oxy)hydroxides. In the acid-leachable extraction the maximum concentration of Fe, the predominant cation in jarosite and poorly crystalline Fe (oxy) hydroxides, was observed at the base of the oxidized zone and in the hardpan. The distribution of trace metals Cu, Ni and Zn was observed to follow

the Fe trend, suggesting that they are co-precipitated with jarosite and poorly crystalline Fe (oxy) hydroxides. The acid-leachable extraction and the 0.5 M HCl extraction step used in this study showed similar results for trace metals and Fe. The oxidized zone was depleted in Ni for acid-leachable and 0.5 M extraction of both studies.

The final extraction was adapted from Ribet et al. (1995) and targeted reducible Fe (oxy) hydroxides. Results of the reducible step indicated that Fe concentrations were at their highest in the oxidized zone in which pyrrhotite has been replaced by goethite, sulfur and jarosite. Iron concentrations decrease at the base of the oxidized zone. A similar trend in the Fe distribution was observed in the 6 M HCl extraction step used in this study. Trace metals Cu, and Zn followed trends similar to Fe in both the previous and current studies. Elevated Cu was observed at the base of the oxidized zone and in the hardpan in the reducible fraction and was thought to be associated with covellite (CuS) whereas there was no elevated Cu in the reducible extraction of this study relative to the oxidizable extraction. Differences were observed in regards to the amount of Ni in the reducible steps of this study and the studies by McGregor et al., (1995);and Ribeta et al., (1995). The McGregor extraction reported a larger percentage of Ni in the reducible phase and the use of different reagents and extraction procedures could be related to the observed differences.

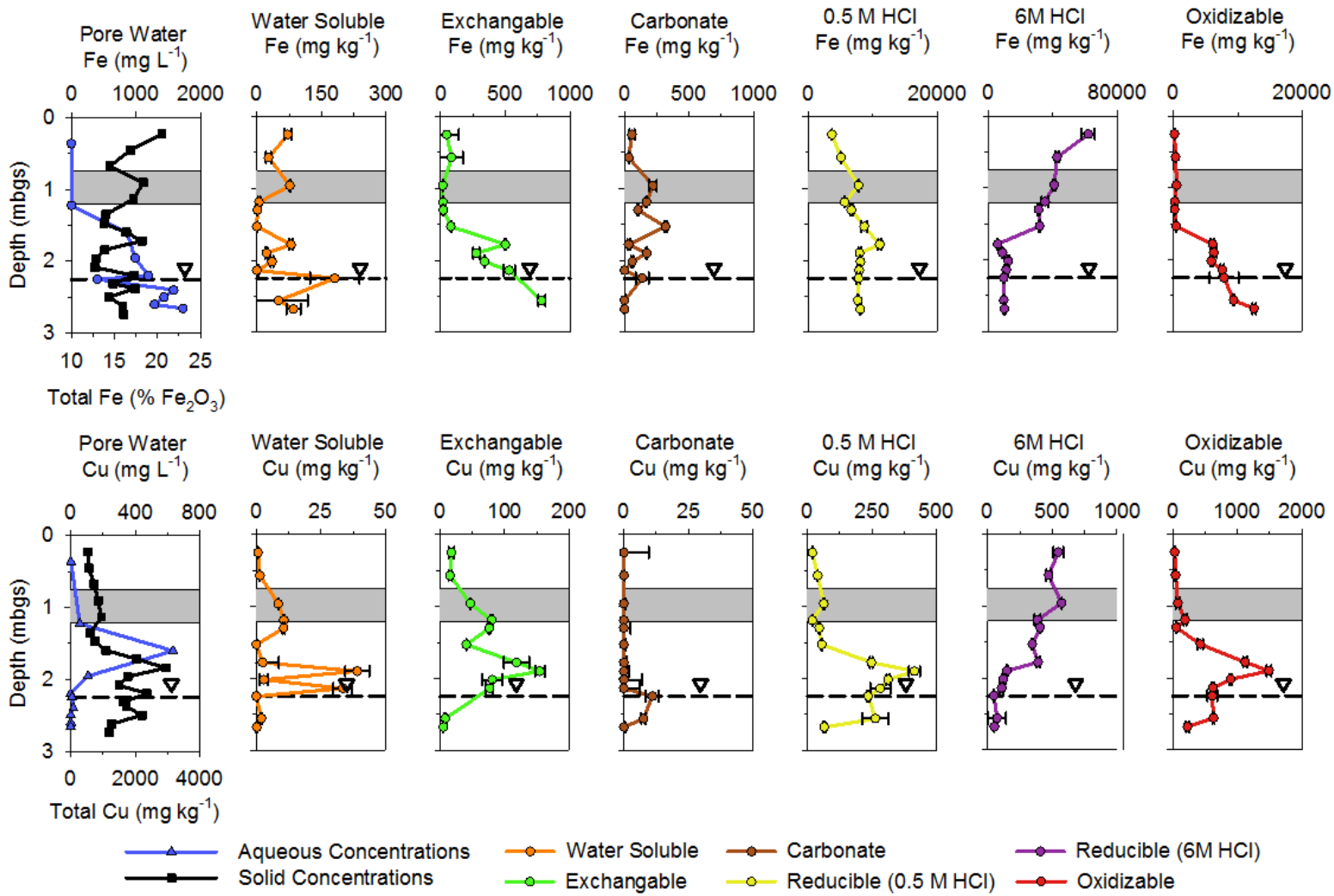

Figure 2-9. Results from selective extractions plotted against depth and geochemical profiles of Fe (top) and Cu (bottom). The shaded grey area represents the hardpan and the dashed line indicates the water table.

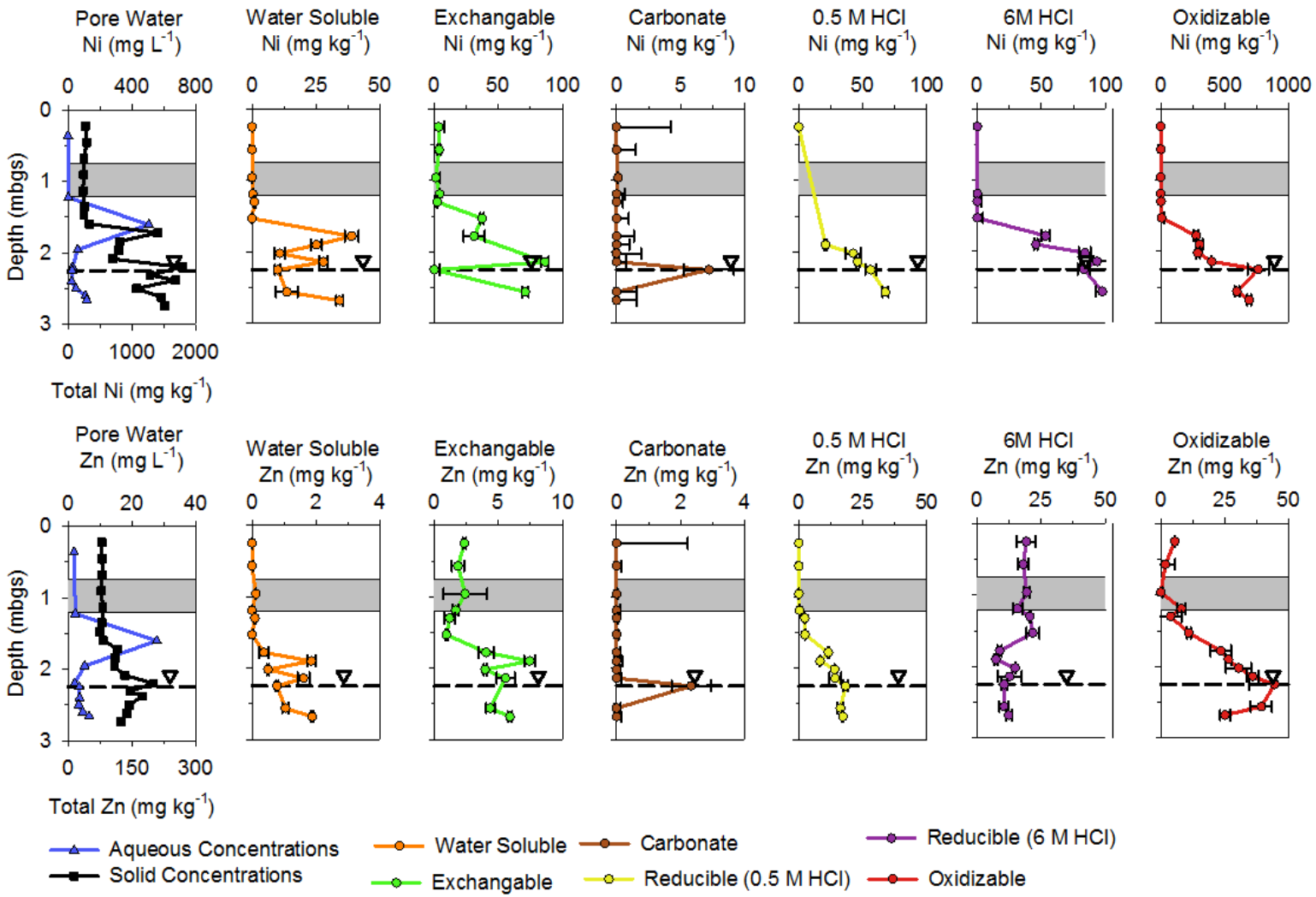

Figure 2-10. Results from selective extractions plotted against depth and geochemical profiles of Ni and Zn. The shaded grey area represents the hardpan and the dashed line indicates the water table.

2.5.5. Micro X-ray Absorption Spectroscopy

Synchrotron-based spectroscopic studies of selected mineral grains were utilized to better characterize the micro-scale geochemical conditions in the mine tailings profile. Detailed Cu and Fe µ-XRF elemental distribution maps were collected of pyrrhotite grains with signs of alteration and weathered rims (Figure 2-11). The elemental maps of Cu and Fe indicate the centers of the sulfide grains contain large masses of Fe, whereas the rims contain relatively less Fe compared to the unaltered core. Copper was abundant in the rims and micro fractures within the core of the sulfide grains. The XRF maps show that Cu is incorporated in the rims that surround the unaltered cores of sulfide grains but do not provide information on the chemical speciation.

Discrete locations were chosen for µ-XAS analysis based on the elemental distribution maps and sample depth. Cu XANES spectra were collected in sulfide rims from different depths and at different locations within the grains to determine the speciation of Cu (A1-3, D1-2; Figure 2-11, Figure 2-12). Linear Combination Fitting (LCF) analysis of Cu XANES spectra was completed to determine the Cu speciation on two sulfide grains from depths of 1.7 m and 2.0 m (Figure 2-12). Results and goodness of fit parameters can be found in Table 2-6. Standards of Cu-bearing minerals likely to be found in the tailings, including covellite (CuS), chalcocite (Cu_2S) and chalcopyrite ($CuFeS_2$) were used as standards. $Cu(OH)_2$ and $CuSO_4$ were also used as standards. Cu adsorption onto secondary Fe(oxy)hydroxides forms complexes with OH^- and is enhanced in the presence of SO_4^{2-}. Copper hydroxide and $CuSO_4$ are not expected to form at pore water pH values present in the unsaturated zone (Webster et al., 1998; Swedlund and Webster, 2001; Peacock and Sherman, 2004). The results of the LCF analysis for all five spectra (A1-3, B1-2) indicate that the secondary minerals covellite (CuS) and chalcocite (Cu_2S) were present at all locations, but dominated the spectra in samples collected from a depth of 2.0 m. Copper

species containing SO_4^{2-} and OH^- were significant components in the sample from a depth of 1.7 m bgs at all three spectra locations (A1-3).

The purpose of the micro-scale synchrotron analysis was to better understand the geochemical environment on the grain scale. Iron, Cu and S were the most abundant elements present on the analysed sulfide grains. Other trace metals Ni and Zn were less commonly observed in µ-XRF maps targeting weathered pyrrhotite rims. Both Ni and Zn are more mobile than Cu in the Copper Cliff tailings (McGregor et al., 1998). Copper adsorption and co-precipitation with Fe (oxy)hydroxides accounted for a greater percentage of the Cu spectra in the first sample, at the base of the oxidized zone. Adsorbed Cu(II) in the oxidized zone occurred as complexes with OH^- and SO_4^{2-}anions, in agreement with previous XAFS studies of Cu adsorption onto Fe (oxy)hydroxides (Webster et al., 1998; Swedlund and Webster, 2001). The sample from the bottom of the transition zone immediately above the water table was dominated by the secondary Cu precipitates covellite (CuS), chalcocite (Cu_2S) and chalcopyrite ($CuFeS_2$). Covellite and chalcopyrite are end members of the Cu-S system that includes multiple stable, metastable and intermediary compositions that exist between the two end members (Pattrick et al., 1997). Cu and S in the covellite structure exist as alternating CuS_3-Cu_3S-layers and S_2-layers, with 4 Cu atoms in tetrahedral coordination and two in triangular coordination. The precipitation of Cu^{2+} as covellite involves the reduction of Cu from Cu (II) to Cu (I) (Luther et al., 2002). Copper sulfide precipitation at the grain scale occurs on grain boundaries and in fractures and can be linked to the attenuation of aqueous Cu below the zone of oxidation.

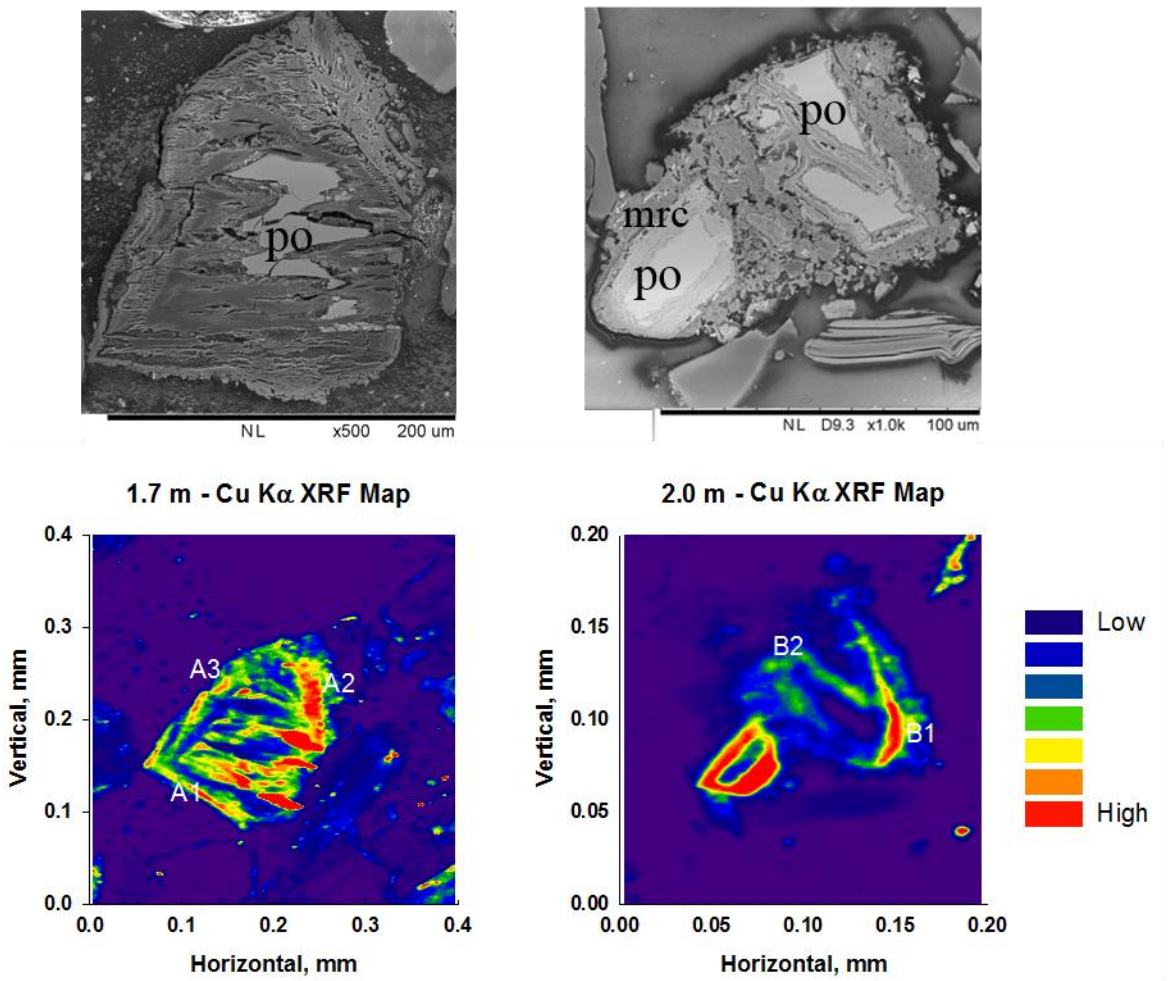

Figure 2-11. Left: sample is from a depth of 1.7 m. Right: sample is from a depth of 2.0 m. Top: BSE images of pyrrhotite grains with different amounts of alteration. Bottom: Locations of Cu spectra are marked on the Cu µ-XRF maps.

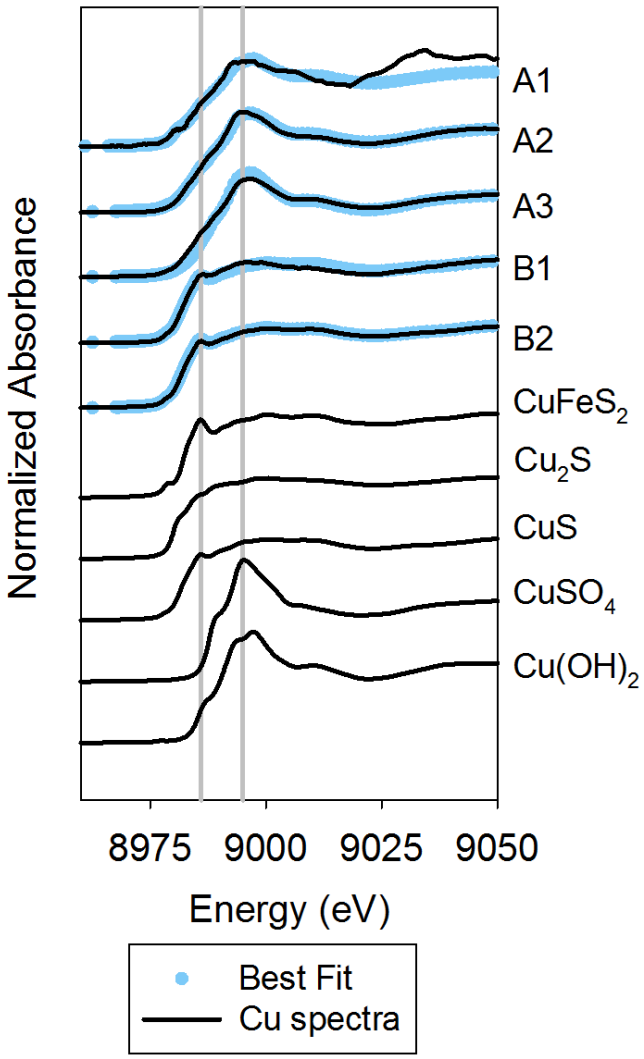

Figure 2-12. Normalized absorbance spectra from locations (A1-3, D1-3) across two weathered sulfide grains from the transition zone collected at APS beamline 13 ID-E (Figure 2-11). Solid lines and blue circles represent experimental and fitted spectra, respectively. Shaded vertical lines represent the energies of defining Cu features.

Table 2-6. Results of least squares linear combination fit for the corresponding Cu spectra from the IN13 depth profile and goodness of fit parameters.

	A1	A2	A3	B1	B2
Chalcopyrite	0.05	0.265	0.105	0.236	0.352
Covellite	-	0.025	0.03	0.576	0.39
Chalcocite	0.376	0.133	0.085	0.157	0.232
CuSO4	0.099	0.281	0.322	-	-
Cu(OH)2	0.373	0.285	0.441	-	-
Sum	0.897	0.989	0.983	0.969	0.973
Chi-square	0.08676	0.06418	0.03542	0.07868	0.05711

2.6. Conclusions

Hydrogeochemical investigations conducted at the Copper Cliff tailings impoundment reveal the advance of sulfide oxidation from 0.5 m in 1990 to 1.5 m in 2014. Depletion of S and metals (*e.g.*, Fe, Cu, Ni, and Zn) in the oxidized zone of the solid tailings profile are indicative of the sulfide oxidation of the most abundant sulfide minerals, pyrrhotite, chalcopyrite, pentlandite and sphalerite.

Measured and modelled gas-phase O_2 values are in agreement and show the advance of the oxidation front from 1990 to 2015. The oxygen diffusion model also accurately describes the observed sulfur depletion in the oxidized zone. The oxidation of sulfide minerals can be linked to the changes observed in solid concentrations between 1990 and 2014.

Several different trends are apparent in the concentrations of dissolved metals in the pore-water. Dissolved Cu, Ni and Zn concentrations peak at the base of the oxidized zone. Copper concentrations decrease rapidly with depth whereas Ni and Zn concentrations decrease gradually. Dissolved Fe peaks near the water table and decreases gradually with increasing depth. Dissolved Cu concentrations have increase drastically since 1990, whereas maximum concentrations of Fe, Ni and Zn show only a slight increase at the oxidation front. Elevated concentrations of Fe, and Zn have followed the advance of low pH pore-water and now extend to depths of 6 m.

Geochemical modelling indicates that the tailings profile is saturated with secondary Fe(III) (oxy)hydroxides, hydroxysulfates and gypsum. Geochemical extractions reveal that co-precipitation and adsorption with and on crystalline Fe(III) (oxy)hydroxides are important to the mobility of metals in the tailings profile.

An increased concentration of solid phase Cu was observed between the transition zone and the unoxidized tailings at a depth between 1.9 and 2.0 m bgs. Copper was present on grain boundaries, in the weathered rims and micro-fractures of pyrrhotite grains. Covellite was observed under reflected light microscopy and detected at a depth of 2.0 m using µ-XRF and µ-XAS synchrotron techniques. Geochemical extractions identified a significant amount of oxidizable Cu in the transition zone of the tailings. There is a noticeable drop in the amount of Cu in the oxidizable fraction at greater depths in the unoxidized tailings. The advancing oxidation front observed by comparing the sulfide alteration index and the modelling of O_2 diffusion of studies of the same tailings profile 25 years apart can be linked to the increase in dissolved Cu concentrations and for the accumulation of Cu at the leading edge of the oxidation front as covellite.

Chapter 3. Copper Isotope fractionation in the Unsaturated Zone of a Sudbury Tailings Impoundment

3.1. Overview

Oxidation of a sulfide-rich tailings impoundment at the Copper Cliff mine site has resulted in the release of dissolved metals into the tailings pore water. The fractionation of stable Cu isotopes and the fate of dissolved Cu at the Copper Cliff Central Tailings impoundment was investigated to better understand the extent of fractionation accompanying the oxidation of Cu-bearing sulfide minerals and the retention of Cu through secondary mineral formation. Stable isotope ratios ($\delta^{65}Cu$) were measured in samples of pore water extracted from the unsaturated zone of the tailings. Solid tailings samples were analyzed using a range of analytical techniques including transmitted and reflected microscopy, X-ray fluorescence and synchrotron based X-ray absorption spectroscopy (XAS). Analysis of pore-water chemistry shows high concentrations of dissolved Cu (700 mg L^{-1}) at the base of the oxidized zone at 1.6 m below the ground surface (m bgs). Analysis of the tailings solids shows an accumulation of Cu (3,000 ppm) immediately below the sharp decrease in aqueous Cu in the transition zone at 1.8 m bgs. Comparison of the aqueous and solid phase concentrations, measurements and mineralogical observations indicate that formation of covellite (CuS) in the transition zone is the main geochemical control on the mobility of Cu. The dissolution of previously precipitated covellite has led to depletion of aqueous phase ^{65}Cu (-3.93±0.03‰) at the base of the oxidized zone and an enrichment of aqueous phase ^{65}Cu (12.01 ±0.50‰) related to the precipitation of covellite in the transition zone. These observations demonstrate the application of aqueous analysis coupled with isotope measurements of field samples to monitor the oxidation and reduction of Cu sulfide-rich mine tailings.

3.2. Introduction

Mining wastes are significant and potentially harmful to the environment. Exposure of mine tailings can produce acidic drainage through the oxidation of residual sulfide minerals by O_2 or dissolved Fe(III) (Blowes et al., 2003). Copper is a common constituent in sulfide-rich mine wastes. Oxidation of sulfide minerals can release high concentrations of Cu, which can lead to contamination of surface water and groundwater (Blowes and Jambor, 1990; Holmstrom et al., 1999; Pérez Rodríguez et al., 2013; Moncur et al., 2015). Precipitation of secondary Cu bearing minerals in mine wastes and in water-treatment systems can potentially attenuate dissolved Cu, mitigating some of the potential environmental impacts associated with mine-waste disposal sites. Fractionation of Cu isotopes during dissolution, precipitation and oxidation reduction reactions has been shown to affect Cu stable isotope ratios in transitionary environments (Mathur et al., 2005; Pokrovsky et al., 2008; Kimball et al., 2009; Pérez Rodríguez et al., 2013).

Samples from the Copper Cliff Central Tailings Area, Copper Cliff, ON were examined during this study. Chalcopyrite is one of the principal sulfide minerals present in the Copper Cliff tailings impoundment and is the source of dissolved Cu in the pore-water. Oxidation of chalcopyrite by O_2 and Fe(III) proceeds as follows (Rimstidt et al., 1994):

$$CuFeS_{2(s)} + O_2 + 4H^+ \rightarrow Cu^{2+} + Fe^{2+} + 2S^0 + 2H_2O \quad (3.1)$$

$$CuFeS_{2(s)} + 16Fe^{3+} + H_2O \rightarrow Cu^{2+} + 17Fe^{2+} + 16H^+ + 2SO_4^{2-} \quad (3.2)$$

The precipitation of secondary minerals in addition to the adsorption of dissolved metals onto the tailings solids are important mechanisms affecting the fate of dissolved metals released by the oxidation of sulfide minerals. Covellite (CuS) is a common secondary Cu sulfide mineral that

has been found in low temperature mine waste environments (Rickard, 1973; Boorman and Watson, 1975; Blowes and Jambor, 1990a; McGregor et al., 1998; Coggans et al., 1999; Lindsay et al., 2015).

The study of copper isotopes in mine tailings systems have focused on the solid phases. Analysing the Cu isotope ratios in solution can provide additional insight into the geochemical environment. Copper has two oxidation states Cu (I) and Cu (II) as well as two stable isotopes: Cu^{65} and Cu^{63} with global relative abundances of 30.85% and 69.15%, respectively (de Laeter et al., 2003). The oxidation states of Cu within minerals such as chalcopyrite and covellite is Cu(I), whereas Cu(II) is highly soluble and present in aqueous solutions (Rickard, 1973; Pattrick et al., 1997). The isotopic composition of chalcopyrite in igneous rocks from different locations is typically 0±1‰ (Maréchal et al., 1999; Zhu et al., 2000; Larson et al., 2003; Graham et al., 2004; Mathur et al., 2005; Rouxel et al., 2005; Mason et al., 2005; Markl et al., 2006; Asael et al., 2007). The leaching of chalcopyrite a primary mineral in mine waste resulted in isotopic values of $\delta^{65}Cu$ that ranged between 0.16±0.16‰ and -0.94±0.1‰ in biotic and abiotic experiments (Kimball et al., 2009). Understanding the initial Cu isotope ratio can provide information on observable fractionation.

The measurement of stable Cu isotope ratios for a range of reaction mechanisms, including dissolution, precipitation, adsorption and oxidation reduction have been shown to cause isotope fractionation in different environmental settings (Ehrlich et al., 2004; Balistrieri et al., 2008; Pokrovsky et al., 2008; Kimball et al., 2009; Pérez Rodríguez et al., 2013). Isotopic fractionation was observed during abiotic precipitation experiments with Cu. A $\Delta^{65}Cu$ ($\delta^{65}Cu(II)_{aq}$-$\delta^{65}CuS$) value of 3.06±0.14‰ was reported for the precipitation of CuS (Ehrlich et

al., 2004). Experiments focusing on the measurement of the Cu isotope ratios for specific reactions can provide insight into more complex systems with multiple reaction mechanisms.

Solid samples of tailings from a Cu mine tailings impoundment located at the Laver Cu Mine in northern Sweden were analyzed and changes in the Cu isotope ratios were observed versus depth in profiles with changing redox conditions. A δ^{65}Cu values of -4.35±0.02‰ and a Δ^{65}Cu ($_{\text{fresh tailings – oxidation front}}$) value of 5.66‰ were observed in a zone of secondary Cu enrichment at the Laver Cu mine (Pérez Rodríguez et al., 2013). Several studies have shown that Cu adsorbed on Fe (oxy) hydroxides such as ferrihydrite and goethite is enriched in Cu^{65} relative to aqueous Cu (Balistrieri et al., 2008; Pokrovsky et al., 2008). Analysis of stable Cu isotopes in mine waste has the potential to give insight into the prevailing reaction mechanisms.

3.3. Site Description

The Copper Cliff ore body consists of the Cu-Ni bearing sulfide minerals pyrrhotite, pentlandite, and chalcopyrite with lesser amounts of sphalerite and pyrite (Rickard and Watkinson, 2001). The tailings impoundment is currently operated by Vale Canada Limited., is located near the communities of Copper Cliff, Lively and within the Regional Municipality of Sudbury, Ontario (Figure 3-1). The tailings impoundment has been in use since 1936 (McGregor et al., 1998). The Copper Cliff tailings facility consists of several valleys filled to depths of up to 45 m with silty sand tailings above lacustrine and glacial sediments, bounded by bedrock. The tailings impoundment is a local groundwater recharge area with a water table elevated 20-30 m relative to the surrounding area (Coggans et al., 1999). Seepage from the tailings disposal area recharges the underlying unconsolidated sediment aquifers and travels laterally toward Finlander Creek, adjacent to the tailings impoundment.

The objective of this study was to analyse Cu isotope fractionation to better understand the relationship between fractionation and prevailing reaction mechanisms in sulfide-bearing mine tailings. This study focused on samples taken from a location adjacent to a piezometer nest (IN13) previously sampled by Coggans et al. (1999). The IN13 piezometer nest is located in the M1 impoundment of the tailings disposal area, which covers an area of 2.8 km^2. Tailings deposition in the M and M1 impoundments commenced in 1945 ended in 1960 and This location was selected for study due to the extent of sulfide oxidation and the measured aqueous Cu concentrations (McGregor, 1994; Coggans et al., 1999). Visible signs of the boundary between oxidized and reduced tailings were observed at a depth of 0.8 m bgs in previous studies (McGregor et al., 1998; Coggans et al., 1999). A recent investigation (Chapter 2) showed that the oxidation zone currently extends to 1.7 m below the ground surface, and a more extensive zone

of low-pH water containing high concentrations of dissolved metals has developed in the shallow tailings. A series of acid-neutralization reactions and secondary mineral constraints on dissolved metal concentrations were identified. The mechanism limit the migration of low pH water and result in the attenuation of some dissolved elements (Chapter 2). The principal mechanisms affecting the concentration of dissolved Cu were identified to by oxidation of chalcopyrite in the shallow oxidation zone of the tailings, and formation of secondary covellite in the transition zone, and adsorption of Cu onto secondary iron oxyhydroxides and the primary tailings minerals (Chapter 2).

Defining the secondary mineralogy in the oxidized and transition zones is important to understanding the mobility of dissolved metals. The formation of covellite as a secondary copper-sulfide mineral has been previously identified in the tailings and identified as a control the mobility of Cu in the groundwater (Boorman and Watson, 1976; Blowes and Jambor, 1990; McGregor et al., 1998; Coggans et al., 1999; Holmstrom et al., 1999; Dold and Fontboté, 2001; Gunsinger, Ptacek, Blowes and Jambor, 2006; Moncur et al., 2012; Pérez Rodríguez et al., 2013). Additional secondary minerals that influence the geochemistry in the M impoundment include jarosite, ferrihydrite, goethite, marcasite, and elemental sulfur (Jambor, 1994; McGregor et al., 1998; Coggans et al., 1999; Lindsay et al., 2015).

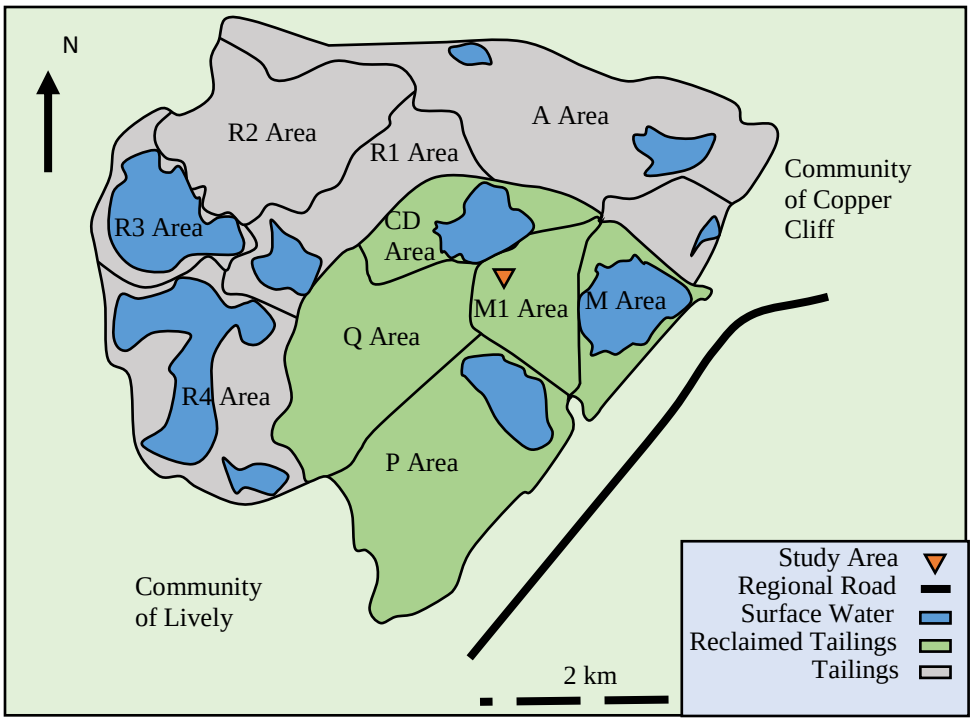

Figure 3-1. Location map showing the Copper Cliff Central Tailings Area and the communities of Copper Cliff and Lively (from Chapter 2).

3.4. Materials and Methods

3.4.1. Geochemical Sampling and Analysis

Continuous core samples for pore-water extraction, isotope and geochemical analysis and mineralogical study were collected in close proximity to the IN13 nest location from tailings surface to a maximum depth of 2.65 m (Table 3-1). Details on collection of pore-water samples and samples of tailings solids for mineralogical and geochemical study are described in Chapter 2.

Table 3-1. Summary of core samples obtained in 2014.

Location	Date	Core ID	Purpose	Diameter (cm)	Depth (m)
IN13	2014	A	Squeeze	7.63	2.63
IN13	2014	B	Mineralogy	5.08	2.62
IN13	2014	C	Squeeze	7.63	2.46

Methods regarding determinations of pore-water pH (Orion 8156BNUWP, Thermo Scientific, USA), Eh (Orion 9678BNWP, Thermo Scientific, USA), cation and anion analysis are described in Chapter 2. Samples for isotope analysis were filtered through cellulose acetate membranes (0.45 µm pore size), and preserved at a pH < 2 with Omni Trace metal grade nitric acid (HNO_3).

Core samples of the tailings solids were subsampled in an anaerobic chamber to prevent contact with atmospheric $O_{2(g)}$. Preparation of tailings solids for powder XRF analysis, and mineralogical investigation are described in Chapter 2.

3.4.2. X-ray Absorption Spectroscopy (XAS)

Bulk tailings samples and sulfide minerals mounted on polished thin sections were examined using synchrotron X-ray absorption spectroscopy (XAS) on beamlines 20 ID and 13 ID-E (microprobe) at the Advanced Photon Source (APS) at Argonne National Laboratory in Argonne, Illinois, USA and SRXMB (06B1-1) at the Canadian Light Source (CLS), Saskatoon, CA. Beamline 13-ID-E uses a Si (111) monochromator to deliver an incident beam energy between 2.4-28 keV. Data acquisition was performed using a four element, Hitachi Vortex, silicon drift detector and a focused beam measuring approximately 2 x 2 μm. The collection of micro x-ray fluorescence (μ-XRF) maps for Fe and Cu are described in Chapter 2. Sulfur μ-XRF distribution maps were collected at 2.52 keV for S and a dwell time of 30 ms per pixel. Micro sulfur XAS data was collected in a helium atmosphere at beamline 13 ID-E and under a vacuum at beamline SXRMB to prevent signal attenuation. μ-XRF elemental distribution maps of sulfide grains were used to locate areas of interest to collect S micro x-ray absorption near edge spectra (μ-XANES).

Additional S XAS data including μ-XRF and μ-XANES was collected at SRXMB. The samples were held in a vacuum at the microprobe end-station during analysis. SRXMB uses a Si(111) crystal monochromator. Spectra were collected using total electron yield (TEY). Samples for bulk Cu EXAFS were collected on beamline 20 ID using a step size of 0.5 and 0.7 eV in the XANES and EXAFS regions respectively. For Cu XANES spectra at beamline 20 ID, spectra for Cu foil was measured continuously to account for beam shift. Data processing and analysis of XAS data is described in Chapter 2.

3.4.3. Copper Isotope Sample Preparation

Purifications of Cu isotope samples was carried out in duplicate using anion exchange chromatography to extract Cu from aqueous pore-water using a procedure described by (Maréchal et al., 1999). Aqueous samples and standards (ERM-AE633; IRMM) containing 10.0 µg of Cu were evaporated, the residue was re-dissolved in 1 mL of 7 M HCl and evaporated to dryness twice.

Samples were then loaded onto the resin in glass anion exchange columns (Bio-rad Glass Econo-Column 0.7 mm ID) filled with pre-cleaned AGMP-1M resin (Bio-Rad) to give a resin bed height of 4 cm. Copper was retained on the resin and unwanted cations and anions (including S, K, Ni, Ca and Na) were washed from the resin in 5 mL of 7 M HCl. Copper was eluted from the resin in 50 mL 7 M HCl which was collected and evaporated to dryness. The residues were dissolved in 5 M HNO_3 and evaporated down twice to convert the chloride species to nitrate prior to MC-ICP-MS analysis.

Incomplete recovery of Cu during ion-exchange chromatography has been shown to result in significant Cu isotope fractionation (Maréchal et al., 1999; Liu et al., 2014). Copper recoveries greater than 92% based on measurements before and after purification were required prior to determinations of isotope ratios. Aliquots of the purified samples and standards were analysed by ICP-OES to ensure possible interferences for Cu isotope analysis including: $^{47}Ti^{16}O$ and $^{23}Na^{40}Ar$ on ^{63}Cu and $^{25}Mg^{40}Ar$, $^{32}S^{33}S$ and $^{47}Ti^{18}O$ on ^{65}Cu were effectively removed during purification.

High concentrations of Fe were measured in the unpurified samples. Iron has been shown to interfere with Cu isotope measurements (Archer and Vance, 2004). Iron concentrations in the

purified samples were monitored to ensure Cu:Fe molar ratios 10:1 were achieved in the purified samples.

3.4.4. Copper Isotope Measurement

Isotope ratios were analysed using a Thermo Fisher Neptune MC-ICP-MS. A sample sample-standard bracketing technique using the reference standard ERM-AE633 (IRMM) was used to correct for analytical isotope fractionation and instrumental mass bias (Zhu et al., 2000). Prior to isotope determination purified samples and standards were diluted to 200 µg L^{-1} and the concentration of Cu measured to ensure that concentrations were within 10 %. One source of 3 % HNO_3 was used for samples, blanks and bracketing standards.

Copper isotopes (^{63}Cu and ^{65}Cu) were measured simultaneously in low resolution mode on the MC-ICP-MS. The samples were introduced via a stable introduction system composed of a PFA nebulizer and a tandem quartz glass chamber (Cyclonic and Scott double pass). Copper was measured over 100 cycles, the ^{63}Cu signal was typically 10 V (200 µg L^{-1} Cu).

Copper fractionation is expressed as δ^{65}Cu relative to the ERM AE 633 Cu standard, where:

$$\delta^{\frac{65}{63}}Cu = \left[\frac{\left(^{65}Cu/^{63}Cu\right)_{sample}}{\left(^{65}Cu/^{63}Cu\right)_{standard}} - 1\right] \times 1000 \quad (3.3)$$

Samples and standards purified in duplicate, with each duplicate being analysed in three analytical events. The average of six duplicate analysis was calculated as the final value. The ERM AE 633 Cu standard was run at the beginning and end of each analytical event to check the efficiency of the sample-standard bracketing approach and the samples were re-run if the δ^{65}Cu was greater than ± 0.05 ‰. The total procedural blanks (incl. chemical purification and mass spectrometry) of Cu contributed in average 1.8 % to the total Cu signal.

3.5. Results

3.5.1. Unsaturated Zone Geochemistry

Water samples were extracted from two core samples and six piezometers providing 19 samples and two geochemical depth profiles, A and B. The water table was 2.25 m bgs during the sample collection period in 2014. Water samples from the unsaturated zone were extracted from 0.25 m long core samples to a depth of 2.5 m. Results described here are of the unsaturated zone and results of the entire profile including samples collected in the saturated zone are described in Chapter 2.

Maximum concentrations of SO_4 (28,000 mg L^{-1}), Fe (1,800 mg L^{-1}), trace metals and low pH groundwater (pH 3.0-4.4) were present in the oxidized zone in both profiles (Figure 3-2). The low pH pore-water (3.4 - 4.4) was present to a depth of 5.0 m. Alkalinity was undetectable in samples collected from depths < 3 m bgs, where the concentration was 50 mg L^{-1} as $CaCO_3$. The maximum concentration of SO_4 (28,000 mg L^{-1}) was observed at a 1.6 m bgs in profile A and the maximum SO_4 concentration observed in profile B was 14,000 mg L^{-1} at 1.6 m bgs.

Maximum dissolved Fe concentrations (1,800 mg L^{-1}) were measured in both profiles at depths between 2.4 to 3.0 m bgs. Maximum observed concentrations of Cu in profiles A and B were 600 mg L^{-1} and 300 mg L^{-1} respectively. While maximum observed concentrations of Ni in profile A and B were 500 mg L^{-1} and 200 mg L^{-1} respectively. Measured concentrations of Zn (30 mg L^{-1}) were significantly lower than both Cu and Ni. Maximum concentrations of Cu, Ni and Zn were found at a depth of 1.6 m in both profiles. Dissolved Cu concentrations decreased rapidly to less than 10 mg L^{-1} below 2.0 m. Dissolved Ni concentrations greater than 100 mg L^{-1}

were still observed at the maximum depth of investigation (3.0 m bgs). A dissolved Zn concentration of 28 mg L^{-1} was measured at a depth of 1.6m.

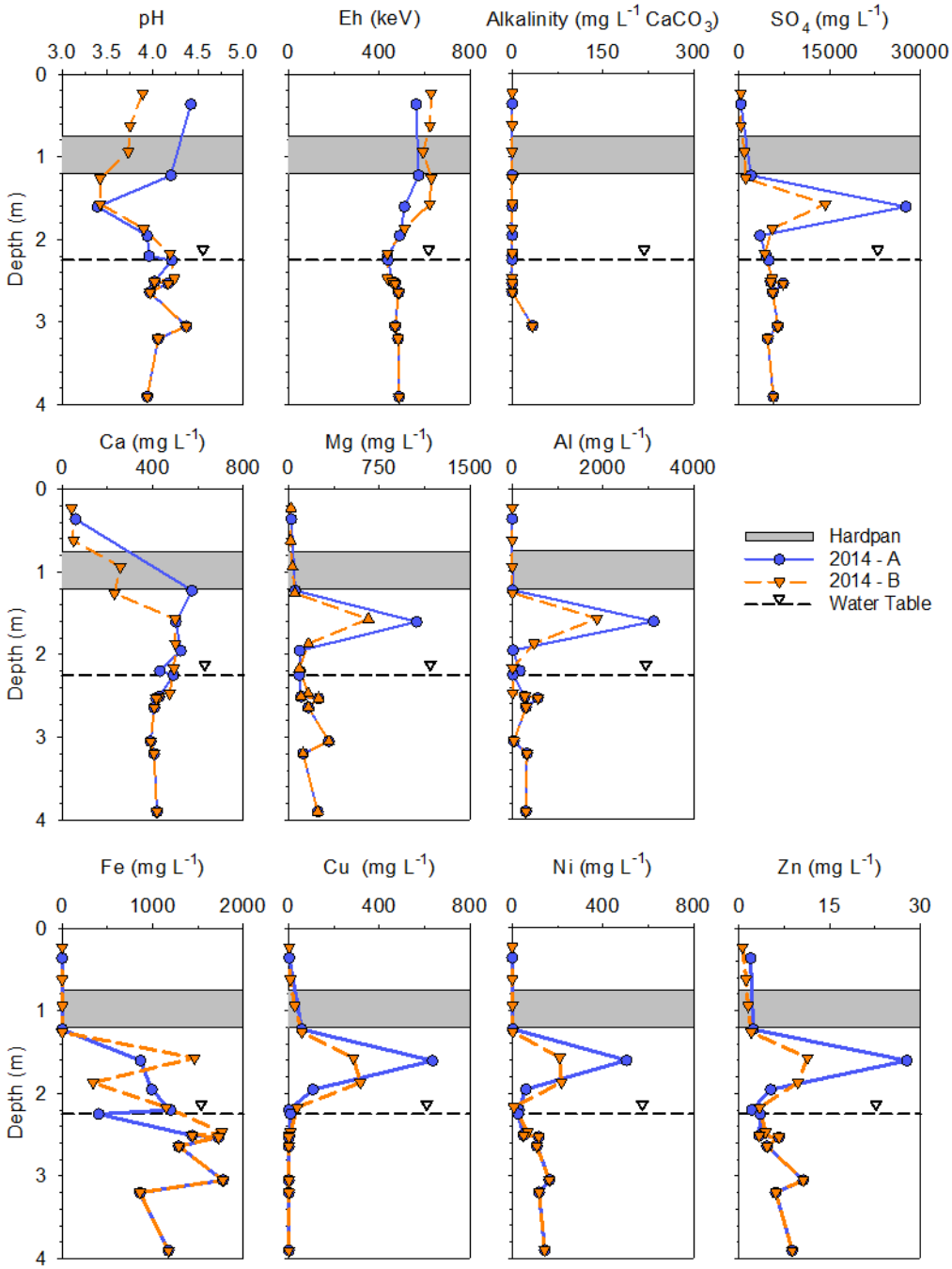

Figure 3-2. Geochemical depth profiles of pH, Eh, alkalinity, SO_4, Ca, Mg, Al, Fe, Cu, Ni and Zn from the IN13 location. Samples were extracted from two cores (A,B) collected side by side and piezometers in 2014. The shaded grey area represents the hardpan and the dashed line indicates the water table (from Chapter 2).

3.5.2. Solid Tailings Characteristics

Sulfide minerals are depleted in the upper 1.5 m of the tailings with remnant chalcopyrite grains persisting. Total sulfur and metal concentrations determined by XRF analysis were analysed throughout the profile and results are reported in Chapter 2. The sulfide alteration index developed for Copper Cliff mine tailings was used to assess the degree of weathering of sulfide minerals (Jambor, 1994). Thin sections of tailings samples from 2014 were inspected under plain reflected light for further mineralogical investigation. Tailings were highly weathered until a depth of approximately 1.7 m, this is observed in measurements of total sulfur and in observations of sulfide alteration with an optical microscope (Figure 3-3). In the transition zone sulfide grains showed alteration on grain boundaries and in micro-fractures. Alteration rims consisting of Fe(III) oxyhydroxides, goethite and Fe(III) hydroxysulfates surrounding and in the micro-fractures of pyrrhotite and chalcopyrite grains were observed using optical microscopy and SEM imaging. The secondary mineral covellite was observed in the transition zone of that tailings. Covellite was observed as isolated anhedral grains with an average grain size of approximately 0.01 mm and in the weathered rims of pyrrhotite grains. Sulfide grains pyrrhotite of a varying size (0.01 mm – 0.05 mm) were found in the vicinity of the covellite grains.

Bulk Cu K-edge spectra were collected to assess the dominant Cu species in the tailings samples, with a focus on the region near the base of the oxidized zone where Cu enrichment is observed. Spectra were collected from five samples of Copper Cliff tailings material, including samples from the oxidized zone at depths of 1.3 and 1.7 m; the transition zone at depths of 1.8 and 2.0 m; and from the unoxidized zone at a depth of 2.25 m (Figure 3-5). Linear combination fitting (LCF) with relevant Cu standards based on expected Cu species in mine tailings was used to assess the relative abundance of phases in the tailings samples. Results of the LCF indicate

that chalcopyrite was present in all samples but made up more of the spectra in the deepest sample (Table 3-2). Covellite (CuS) was a dominant component in transition zone samples with a lesser amount in less altered samples. Covellite was absent from the shallowest sample. Cu adsorbed onto Fe (oxy) hydroxides was present in all samples, with Cu adsorbed onto Fe (oxy) hydroxides and $CuSO_4$ the principal Cu-bearing components in the oxidized samples (Figure 3-5). The χ^2 values as a goodness-of-fit parameter vary between 0.01 and 0.07 indicate a good fit.

Detailed µ-XRF elemental distribution maps were collected for two pyrrhotite grains including their alteration rims from a depth of 1.7 m bgs at the interface between the oxidized and transitionary zones and 2.0 m bgs at the interface between the transitionary and unoxidized zones (Figure 3-6). The elemental maps of Cu, Fe and S indicate the centers of the sulfide grains are composed of a significant amount of Fe and S, whereas the rims contain relatively less Fe compared to the centers. Significant amounts of Cu were detected in the rims and micro fractures of the sulfide grains. The XRF maps show that Cu is incorporated in the rims surrounding sulfide grains but do not indicate the chemical speciation.

Sulfur is an important component to understanding the mine tailings environment. Sulfur K-edge spectra measurements were collected from discrete locations of two weathered sulfide grains. Seven locations were selected from the first sample from a depth of 1.7 m bgs and eight locations on the second sample from a depth of 2.0 m bgs based on S XRF maps (Figure 3-8). Sulfur K-edge spectra of the first grain exhibited a dominant peak at 2472 eV, a shoulder on the dominant peak at 2470 eV and a minor peak at 2482 eV (Figure 3-9). All spectra were consistent, except one of the spectra collected in the center of the visible sulfide grain, which exhibited a peak at 2469 eV and a broad hump at 2478 eV. Sulfur K-edge spectra of the second grain exhibited a peak at 2471 eV, a shoulder at 2469 eV and a minor peak at 2482 eV (Figure

3-8). One of the spectra collected on the boundary of the sulfide grain exhibited a dominant peak at 2482 eV.

Linear combination fitting was performed on spectra to distinguish the dominant sulfur species in the sulfide grain and the surrounding weathered rims (Table 3-3, Table 3-4). Sulfur standards were chosen based on S species previously encountered in mine tailings impoundments. Results of the LCF indicate elemental sulfur was the predominant S species ranging between 36% and 76% throughout the first sample, which was derived from 1.7 m bgs at the start of the transition zone. The S spectra collected in the center of the sulfide grain had a large pyrrhotite contribution (approximately 35%) to the LCF. Elemental sulfur is an intermediary product of pyrrhotite oxidation. Pyrrhotite and marcasite were the dominant S species (24.7% to 63.5%) for the second sample that was derived from 2.0 m bgs at the end of the transition zone. It should be noted that the S spectra of marcasite and covellite are similar and both contribute to the marcasite LCF results. The S spectra collected on the outermost rim of the pyrrhotite grain was predominantly ferrous sulfate (approximately 44%). The χ^2 values as a goodness-of-fit parameter vary from 0.19 to 1.23.

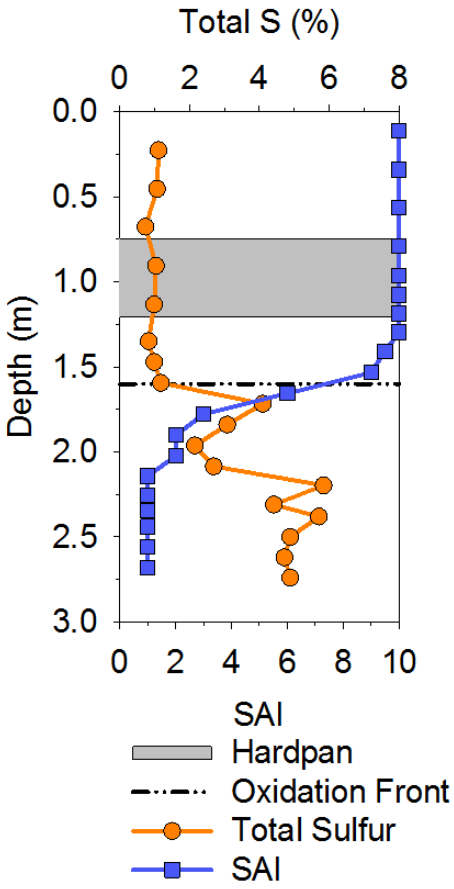

Figure 3-3. Sulfide Alteration Index (SAI) profile and the depth of oxidation for the IN13 depth profile in 2014 (from Chapter 2).

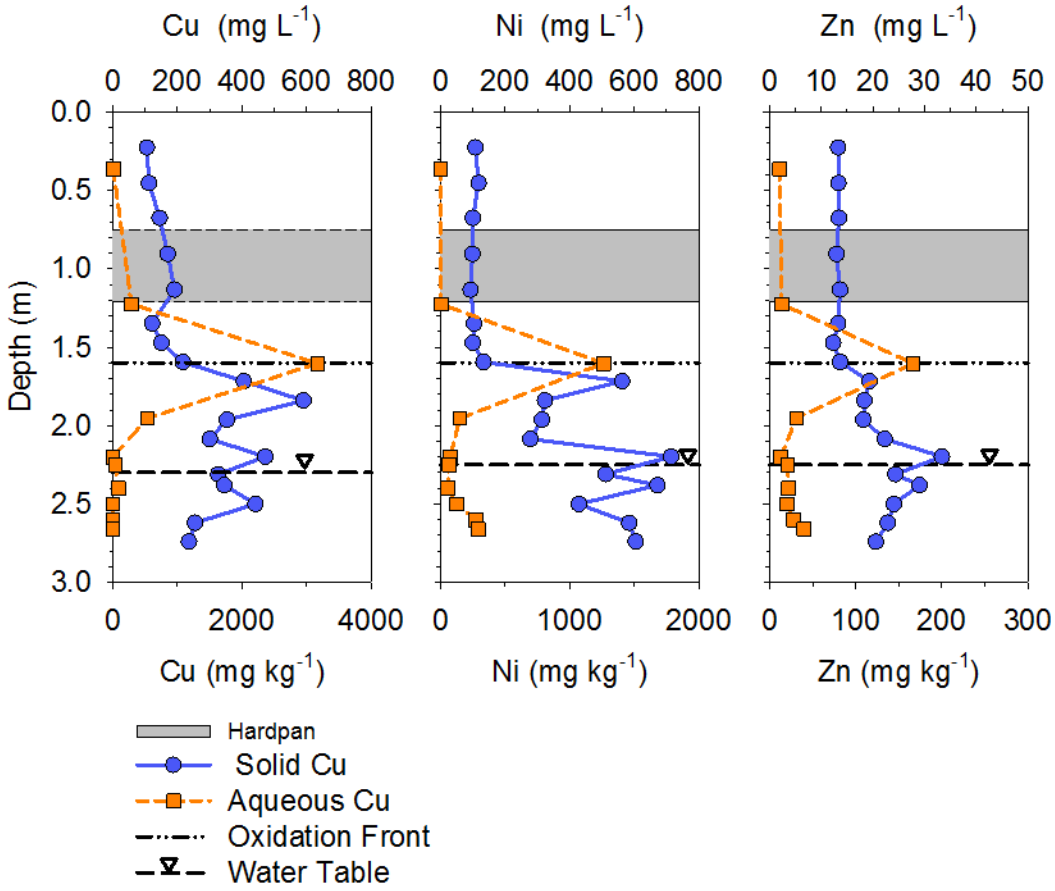

Figure 3-4. Geochemical depth profiles of solid and aqueous Cu, Ni and Zn from the IN13 location. The shaded grey area represents the hardpan, the dashed dotted line represents the oxidation front and the dashed line indicates the water table (from Chapter 2).

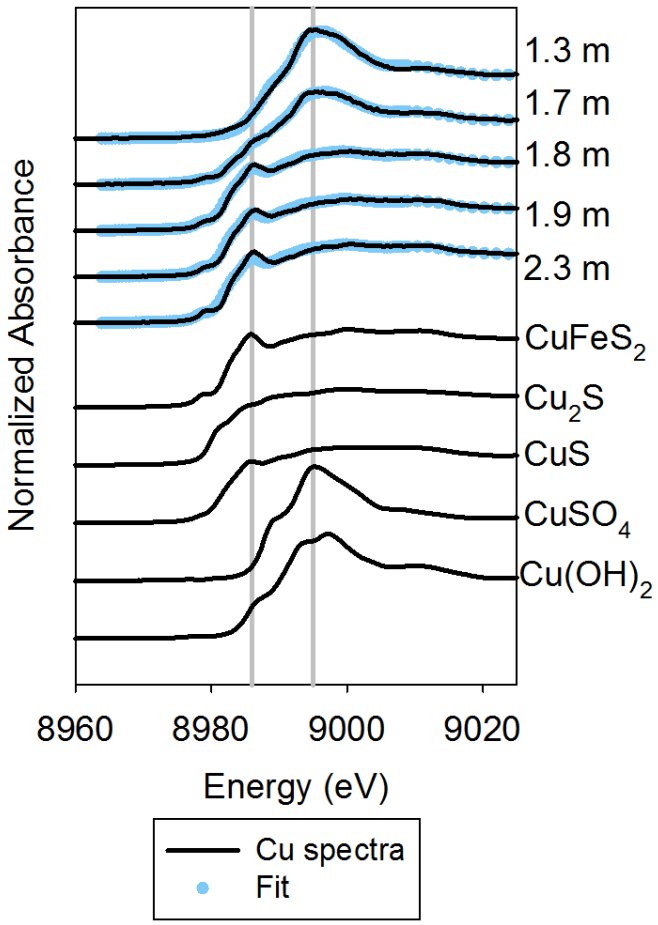

Figure 3-5: Bulk Cu spectra and applicable Cu standards. Least squares linear combination fit for the corresponding spectra of the IN13 Copper Cliff tailings depth profile collected at APS beamline 20 ID. Gray vertical lines represent the energies of defining Cu features.

Table 3-2. Results of least squares linear combination fit for the corresponding Cu spectra from bulk tailings samples from different depths in the IN13 depth profile and goodness of fit parameters.

	1.3 m	1.7 m	1.8 m	1.9 m	2.3 m
Chalcopyrite	0.019	0.269	0.475	0.500	0.508
Covellite	0.023	0.122	0.270	0.271	0.284
Chalcocite	0.000	0.000	0.134	0.151	0.143
CuSO4	0.520	0.278	0.000	0.000	0.000
Cu(OH)2	0.441	0.315	0.119	0.069	0.068
Sum	1.003	0.983	0.999	0.991	1.002
Chi-square	0.05054	0.01694	0.03126	0.04392	0.06974

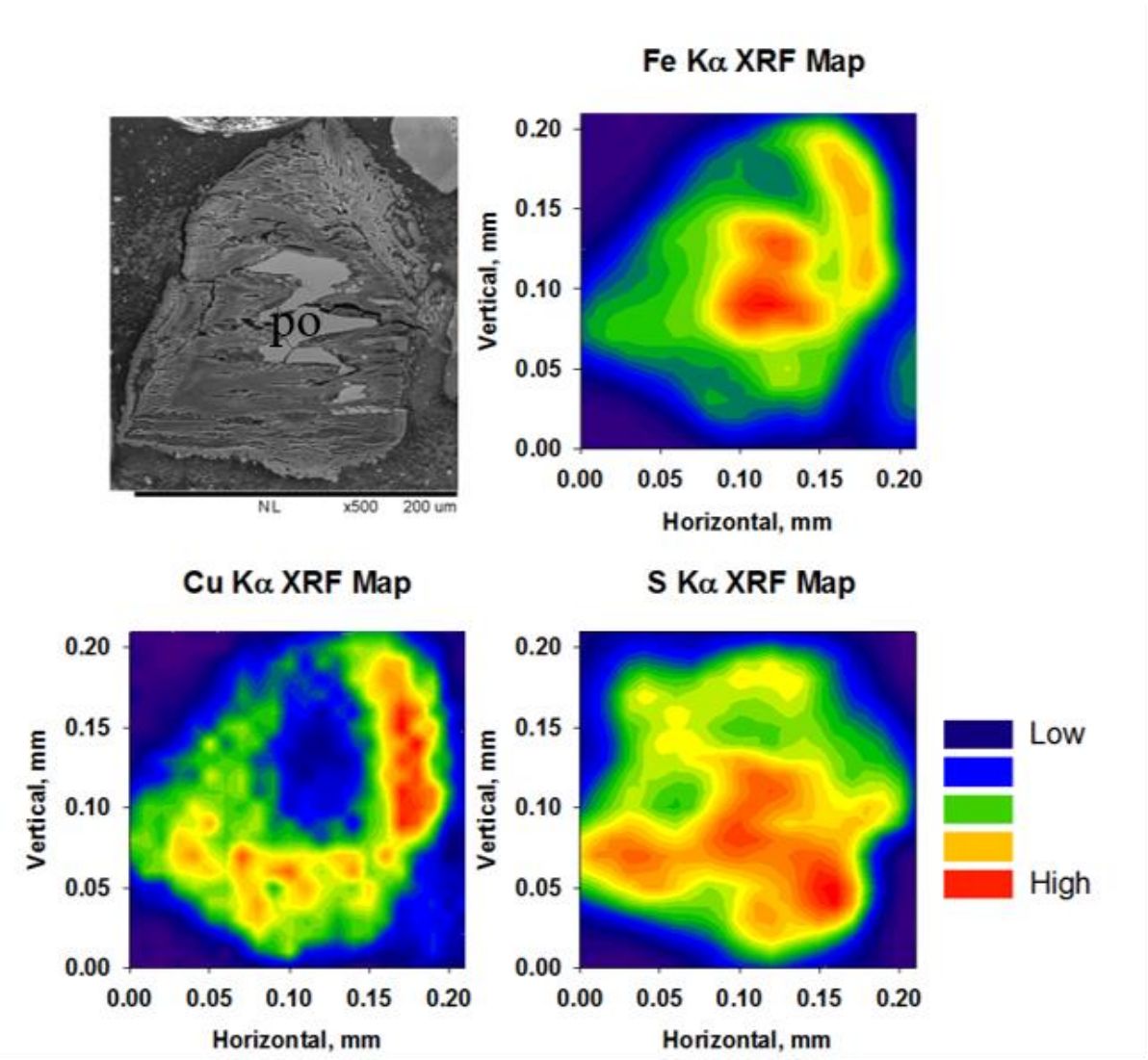

Figure 3-6. Scanning Electron Microscope images and Micro X-ray Fluoresence maps of Fe, Cu and S elemental distribution of pyrrhotite grains (depth: 1.7 m bgs) collected at CLS beamline SXRMB. Alteration rims consist of Fe(III) oxyhydroxide and Fe(III) oxysulfate.

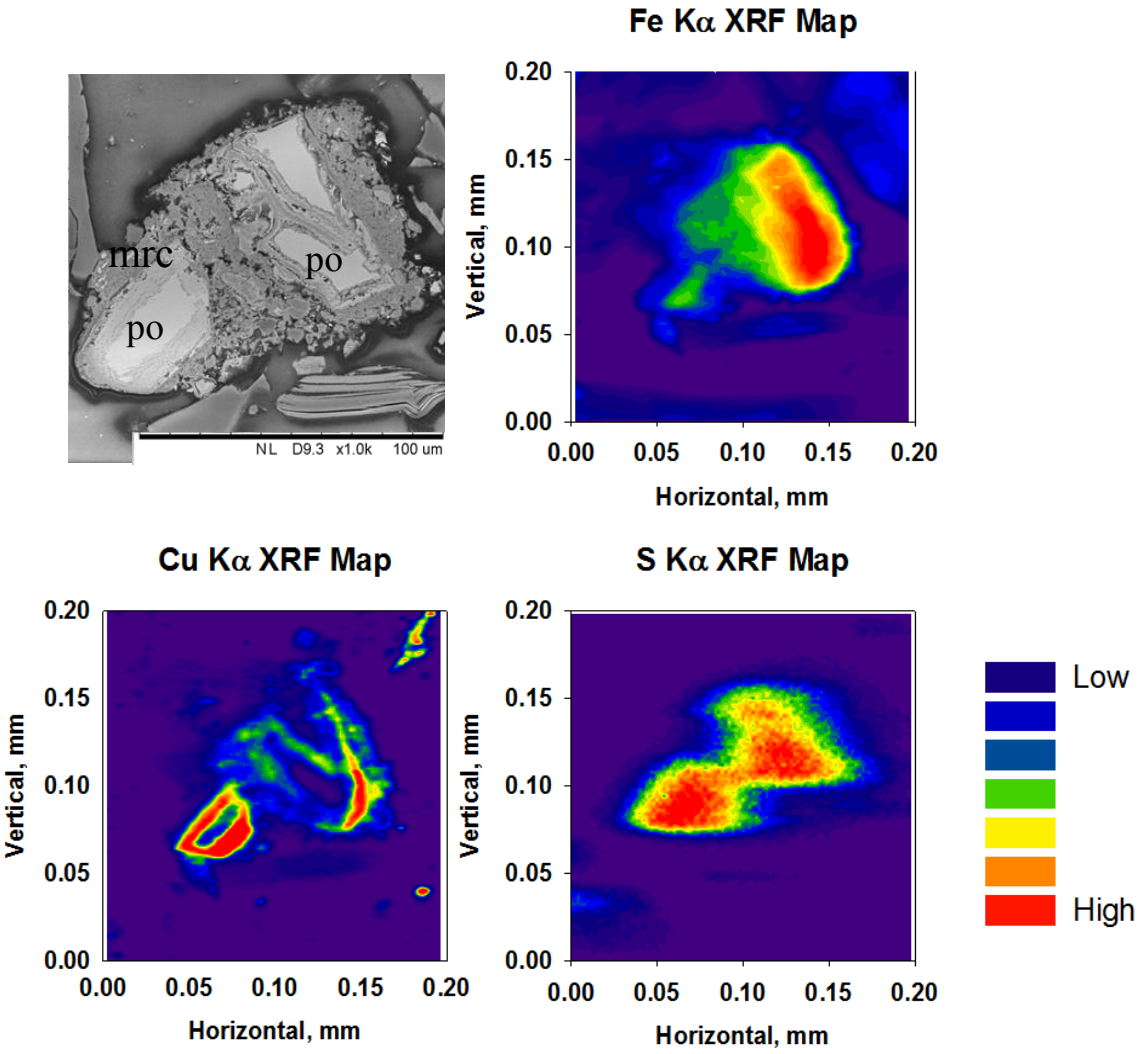

Figure 3-7. Scanning Electron Microscope images and Micro X-ray Fluoresence maps of Fe, Cu and S elemental distribution of pyrrhotite grains (depth: 2.0 m bgs) collected at APS beamline 13 ID-E. Note S map was collected at a different time using the same beamline. Alteration rims consist of marcasite, Fe(III) oxyhydroxide.

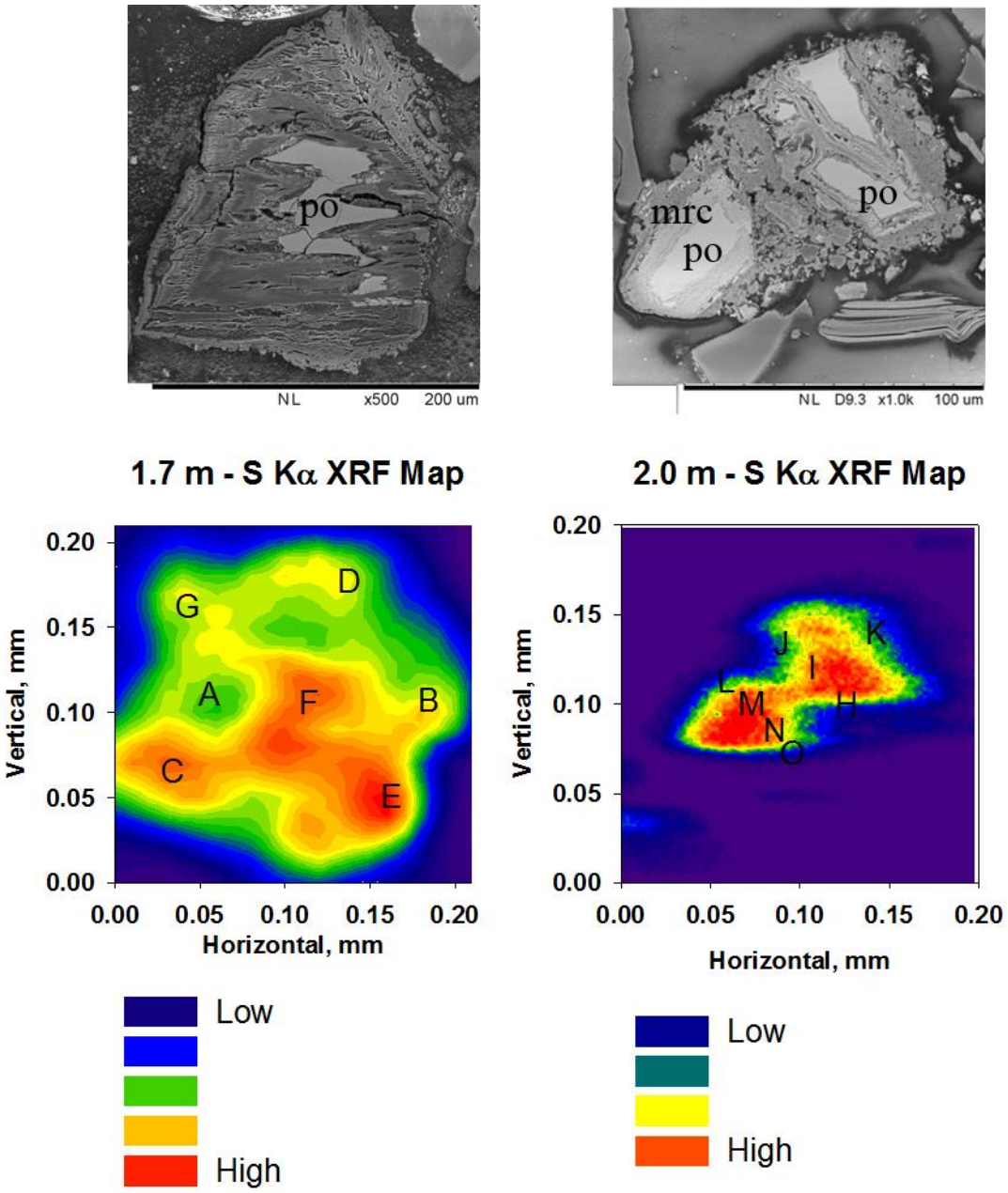

Figure 3-8. Sulfur µ-XRF maps and S XANES data collected on two pyrrhotite grains with Fe(III) oxyhydroxide alteration rims from depths of 1.7 m bgs (left) and 2.0 m bgs (right) collected at CLS beamline SXRMB and APS beamline 13 ID-E respectively. Spectra were collected at marked locations (A-O). Note the scales in the images on the right are different (Top: 120µm; Bottom: 200µm).

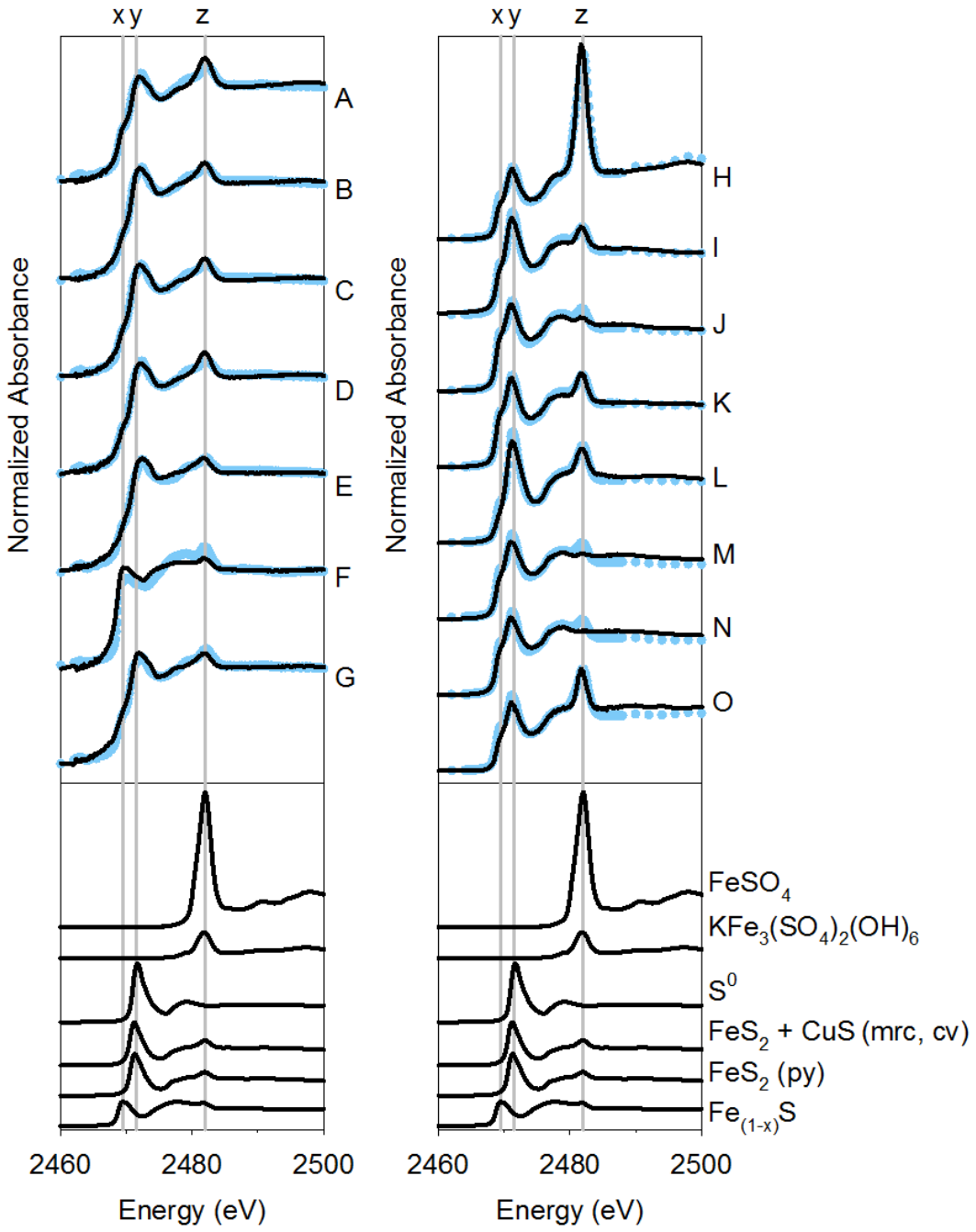

Figure 3-9. Sulfur K-edge spectra from spots (A-O) for two pyrrhotite grains (Figure 3-8) compared with sulfur standards used to fit spectra. Solid lines and circles represent experimental and fitted spectra respectively. Note the large Fe(II) sulfate peak in spectra H located on the outermost weathered rim is indicative of the secondary mineral melanterite ($FeSO_4 \cdot 7H_2O$). Vertical shaded areas represent measured S k-edge white line maxima for (x) pyrrhotite, (y) covellite, pyrite and/or marcasite, (z) jarosite and/or ferrous sulfate

Table 3-3. Results of least squares linear combination fit for the corresponding S spectra from the pyrrhotite grain at a depth of 1.7 m bgs in the IN13 depth profile and goodness of fit parameters.

	A	B	C	D	E	F	G
Pyrrhotite	0.22	0.15	0.15	0.15	0.14	0.53	0.17
Marcasite and Covellite	0.16	0.17	0.18	0.15	0.13	0.07	0.17
Pyrite	0.11	0.09	0.09	0.10	0.08	0.04	0.07
Elemental Sulfur	0.45	0.58	0.56	0.58	0.65	0.31	0.55
Jarosite	0.05	0.01	0.02	0.02	0.01	0.04	0.03
Ferrous Sulfate	-	-	-	-	-	-	-
Sum	0.98	1.001	1.001	1.002	1.014	0.985	0.997
Chi-square	0.26336	0.13465	0.14351	0.16251	0.17663	1.18852	0.26727

Table 3-4. Results of least squares linear combination fit for the corresponding S spectra from the pyrrhotite grain at a depth of 2.0 m bgs in the IN13 depth profile and goodness of fit parameters.

	H	I	J	K	L	M	N	O
Pyrrhotite	0.45	0.51	0.61	0.57	0.37	0.49	0.55	0.45
Marcasite and Covellite	0.21	0.38	0.28	0.32	0.49	0.29	0.26	0.28
Elemental Sulfur	0.09	0.09	0.08	0.07	0.09	0.07	0.08	0.05
Jarosite	-	-	-	-	-	0.02	-	-
Ferrous Sulfate	0.44	0.02	0.00	0.04	0.06	0.00	0.00	0.13
Sum	1.19	1.00	0.98	1.00	1.00	0.88	0.89	0.91
Chi-square	1.16958	0.34532	0.48984	0.19232	0.44849	0.89759	0.8592	0.90799

3.5.3. Copper Isotope Results

Copper isotope ratio measurements were conducted on pore-water extracted from two core samples. The δ^{65}Cu values ranged from -3.93±0.01‰ to 11.85±0.88‰ in profile A and -0.94±0.01‰ to 7.08±0.03‰ in profile B (Table 3-5, Figure 3-10). Profiles A and B showed similar δ^{65}Cu values near zero in the oxidized zone. In the oxidized zone the δ^{65}Cu ratio shows a slight enrichment in ^{65}Cu averaging 0.16±0.02‰. At the base of the oxidized zone at the oxidation front the average δ^{65}Cu ratio is isotopically light (-1.84±0.03‰). The largest depletion of ^{65}Cu (-3.93±0.01‰) was seen at the oxidation front in profile A. Below the oxidation front the δ^{65}Cu ratio is enriched in ^{65}Cu with an average value of 8.18±0.34‰. Samples from below the water table contained insufficient Cu relative to the concentration of Fe and attempts to extract and purify the Cu were not successful.

Table 3-5. Summary of average δ^{65}Cu values for the two core profiles (A, B) in the oxidized and unoxidized zones of the tailings profile.

	Oxidized Zone (0-1.6 m bgs)	**Unoxidized Zone (1.9-2.7m bgs)**
Profile A	0.34±0.04‰	11.85±0.88‰
Profile B	0.07±0.01‰	6.34±0.05‰

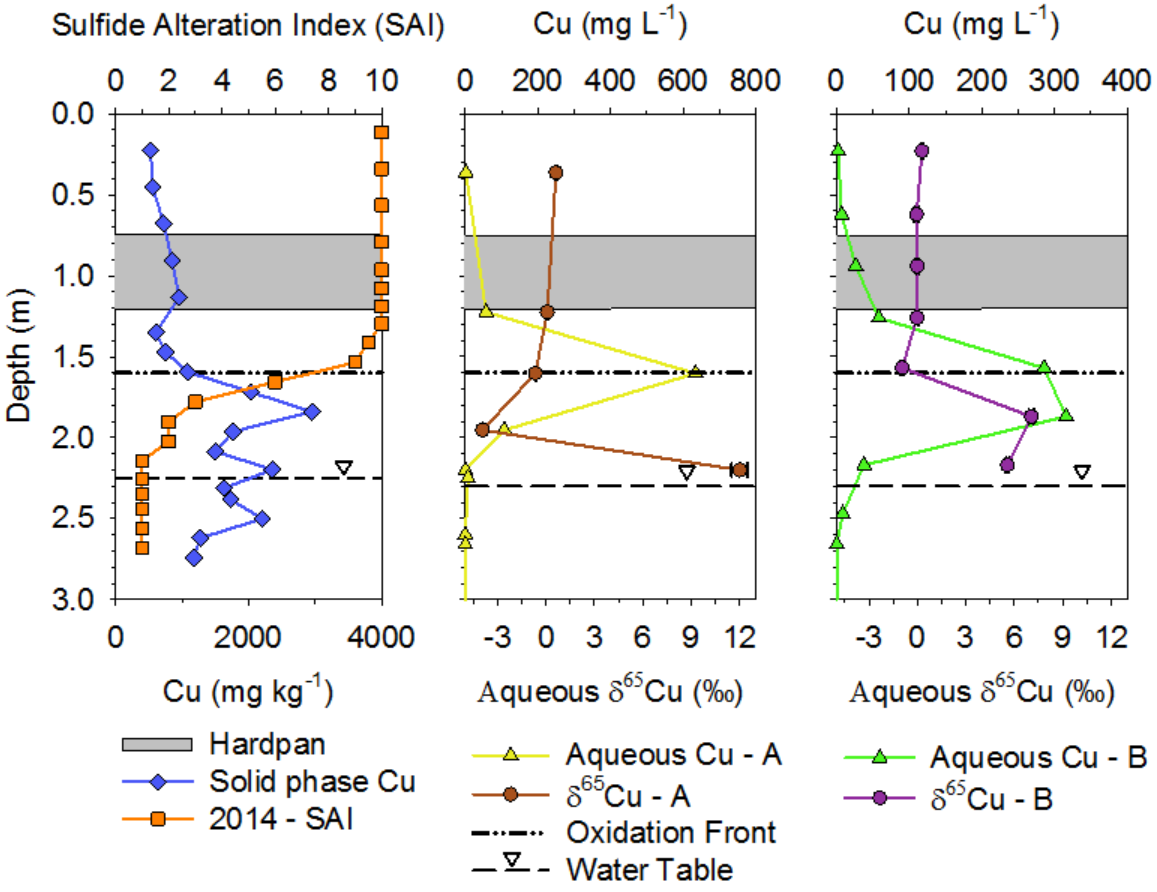

Figure 3-10. Geochemical and isotopic depth profiles of solid and aqueous Cu, sulfide alteration index and $\delta^{65}Cu$ values for both profiles (A,B). The shaded grey area represents the hardpan, the dashed dotted line represents the oxidation front and the dashed line indicates the water table. Error bars represent 2σ and are smaller than the symbol size.

3.6. Discussion

3.6.1. Metal and Sulfur accumulation

The oxidized zone of the tailings profile extends from the surface to a depth of 1.5 m bgs and was characterized using mineralogical observations of sulfide alteration (Figure 3-3). The sulfide minerals, pyrrhotite, pentlandite and pyrite were completely weathered and chalcopyrite grains showed significant weathering around grain boundaries and in fractures.

A 0.3 m thick hardpan layer, cemented by gypsum, goethite, ferrihydrite and jarosite was observed at a depth of 0.8 m in the oxidized zone (Chapter 2).

Two significant S peaks occur in the solid phase of the transition zone at 1.7 m bgs and 2.2 m bgs and these correlate well to a similar accumulation of the metals Fe, Cu, Ni and Zn in the solid phase (Chapter2; Figure 3-4). The two peak S contents could represent an accumulation of S in the transition between the oxidized and unoxidized zones of the tailings (Chapter 2).

The SAI in the transition zone (1.5 – 2.0 m bgs) was characterized by a sharp change in the degree of sulfide weathering. Pyrrhotite grains showed a wide range of weathering through the transition zone. From thick alteration rims and approximately 90% of pyrrhotite grains showing severe weathering to thin or non-existent rims and only 20% of pyrrhotite grains showing signs of weathering. The SAI was low for samples from below 2.0 m bgs in the unoxidized zone of the tailings.

Sulfur µ-XRF maps and µ-XANES were collected to further characterize the sulfide alteration. A comparison of two sulfide mineral samples from the depth profile, one specimen from a depth of 1.7 m and the other from a depth of 2.0 m provide insight into sulfur speciation in the oxidized and transition zone (Figure 3-6, Figure 3-8). Sulfur µ-XANES LCF on the

shallow sample suggest that pyrrhotite is depleted at this depth and the largest contribution to the S spectra was at the center of the sulfide grain, which is consistent with the advanced stage of weathering. Elemental sulfur is the predominant component of the LCF for the majority of the spectra and is present as an intermediary sulfur weathering product of partial oxidation or non-oxidative dissolution under acidic conditions of pyrrhotite and has been observed in previous studies of Copper Cliff mine tailings (McGregor et al., 1998). Elemental sulfur is also a product of the oxidation of covellite by Fe(III) (Córdoba et al., 2008):

$$(3.4) \quad CuS_{(s)} + Fe^{3+} \rightarrow Cu^{2+} + Fe^{2+} + S^0$$

The absence of SO_4^{2-} at this depth suggests that SO_4^{2-} may have been flushed from this depth by infiltrating recharge water or precipitated as a secondary sulfate mineral such as, jarosite ($KFe_3(OH)_6(SO_4)_2$), gypsum ($CaSO_4 \cdot 2H_2O$) or melanterite ($FeSO_4 \cdot 7H_2O$). Only the more crystalline secondary mineral jarosite was detected in the shallower sample, suggesting that precipitation and dissolution of jarosite may control the mobility of numerous elements at this depth including K, Fe, Cu, Ni, Zn and SO_4^{2-} . Attenuation of Cu, Ni and Zn by jarosite can be occur by the substitution at K or Fe sites of jarosite surfaces (Blowes et al., 1991).

The XAS spectra measured for the sample, from a depth of 2.0 m bgs exhibited an abundance of pyrrhotite and marcasite (FeS_2), both observed under reflected light microscopy. The pyrrhotite at a depth of 2.0 m bgs was less extensively weathered with alteration rims of varying thickness and a large percentage of unaltered cores. Marcasite is a secondary mineral frequently observed in alteration rims surrounding pyrrhotite grains and as individual grains (Moncur et al., 2005; Lindsay et al., 2015). Covellite and marcasite spectra are similar and could both be contributing to the fraction of marcasite observed in the LCF (Moncur et al., 2012). Ferrous

sulfate was present in spectra collected from the outermost weathered rim locations. Melanterite ($FeSO_4 \cdot 7H_2O$) precipitation could be a solid-phase control on Fe(II) and SO_4^{2-} in the vadose zone and below the zone of active oxidation (Blowes et al., 1991; Moncur et al., 2005):

$$(3.5) \quad Fe^{2+} + SO_4^{2+} + 7H_2O \rightarrow FeSO_4 \cdot 7H_2O$$

The dissolved Fe concentration peaked in the oxidized zone near the tailings surface, in the hardpan at the base of the oxidized zone and again at the water table (Figure 3-4). Iron is mainly found as (oxy) hydroxides, Fe(III) hydroxysulfates in the oxidized zone, Fe(II) sulfates and unaltered sulfide minerals in the unoxidized zone (Blowes et al., 1991; McGregor et al., 1998; Moncur et al., 2005; Lindsay et al., 2015).

The lowest pH value was observed at the same depth as the maximum concentrations of the metals Cu, Ni, and Zn. Pore-water pH is an important factor affecting the mobility of Cu in mine tailings (McGregor et al., 1998; Coggans et al., 1999; Dold and Fontboté, 2001; Gunsingeret al., 2006; Lindsay et al., 2015).

Covellite precipitation is the likely reaction leading to the attenuation of dissolved Cu in the Copper Cliff tailings impoundment. Covellite formation is favoured under anoxic conditions, a pH near 4.0 with dissolved H_2S present (Rickard, 1972). The pore-water at the bottom of the oxidized zone and at the water table is acidic and anoxic, indicating the presence of conditions suitable for the accumulation of covellite. A distinctive enrichment zone of solid-phase Cu is present at 1.8 m coinciding with the base of the oxidized zone and at 2.2 m, the depth of the water table (Figure 3-4). Covellite was first observed under reflected light microscopy at a depth of 1.8m.

Copper, and Fe µ-XRF maps were collected on two sulfide grains between the depths of 1.7 to 2.0 m bgs to investigate the spatial distribution of Cu and Fe. Copper was observed in the alteration rims surrounding pyrrhotite grains.

Copper XANES spectra were collected on bulk tailings samples to investigate changes in Cu speciation with depth. Bulk Cu XANES LCF analysis indicated the appearance of covellite in the depth interval between 1.7 m and 2.0 m with a peak contribution to the Cu spectra at 1.9 m (Figure 3-5). The Cu enrichment at 1.7 – 2.0 m bgs is distinct from the increase in solid Cu concentration observed deeper in the unoxidized zone, below 2.3 m. The small contribution of covellite to the Cu XAS spectra collected from the deepest sample at a depth of 2.3 m bgs indicated a low abundance covellite in this zone. Similar copper enrichment zones have been observed in other sulfide mine tailings impoundments (Blowes and Jambor, 1990; Holmstrom et al., 1999; Dold and Fontboté, 2001; M C Moncur et al., 2005; Gunsinger, et al., 2006; Pérez Rodríguez et al., 2013).

3.6.2. Copper Isotope Fractionation

In profiles A and B the $\delta^{65}Cu$ values of 0.015±0.14‰ measured in the oxidized zone are indicative of the oxidation of chalcopyrite (Kimball et al., 2009). Extensive weathering of sulfide minerals, including chalcopyrite was observed in the oxidized zone of the tailings.

Nearing the oxidation front and the transition zone the Cu isotope ratio in the pore-water becomes increasingly depleted in ^{65}Cu reaching a maximum depletion of -3.93±0.01. Immediately below the ^{65}Cu depletion analysis of the pore-water shows a dramatic enrichment in ^{65}Cu, 11.85±0.88‰ in profile A and 7.08±0.03‰ in profile B. Profile A had both higher concentrations of aqueous Cu and greater enrichment and depletion compared to the results from profile B (Figure 3-10). Samples from below the water table contained insufficient Cu relative to the concentration of Fe and attempts to extract and purify the Cu were not successful.

Dissolution and precipitation of covellite is the probable cause of the apparent depletion and enrichment of $\delta^{65}Cu$. Covellite formation preferentially incorporates ^{63}Cu into its structure acting as both a sink and source for ^{63}Cu depending on geochemical conditions (Ehrlich et al., 2004; Pérez Rodríguez et al., 2013; Sherman, 2013). Between the oxidation front and the water table the pore water is less oxic and the pH is approximately 4.0, conditions suitable for the formation of secondary Cu sulfides (Morse et al., 1987). A zone of solid Cu and S enrichment, observed in bulk Cu XAS, powder XRF and total S analysis was observed between the oxidation front and the water table suggesting that secondary Cu sulfides are accumulating in this region (Chapter 2).

Other reactions potentially impacting the observed isotope ratios include the adsorption of Cu onto ferrihydrite or goethite. Ferrihydrite and goethite are expected to be present in the tailings over the pH range 3.89 - 4.2 (Blowes et al., 1991; McGregor et al., 1998; Coggans et al.,

1999; Moncur et al., 2005). Adsorption of Cu onto Fe (oxy) hydroxides preferentially selects the heavier isotope leaving the solution enriched in the light isotope (Balistrieri et al., 2008).

A study of mine tailings and the associated Cu isotope ratios in the tailings solids was completed at the Laver mine in Northern Sweden (Pérez Rodríguez et al., 2013). Negative δ^{65}Cu values were observed in digests of solid samples from the interface between oxidized and unoxidized (Pérez Rodríguez et al., 2013). At the Laver mine, the Cu isotope ratio observed in the solid phase had contributions from different Cu species, including primary chalcopyrite and secondary covellite. The pore-water Cu isotope ratios measured in the current study indicate fractionation patterns that are consistent with the observations from the study at the Laver mine.

Results of this study are a good indication that analysis of Cu isotope ratios in tailings pore-water can be used to better understand and track the attenuation mechanisms of Cu across changing geochemical conditions. Analysis of the Cu isotope ratio can identify zones of secondary Cu accumulation and dissolution in sulfide mine tailings. Copper isotope ratios can potentially be used to track the migration of reaction fronts through Cu tailings systems by more precisely identifying the zones of active sulfide oxidation. There is also the potential to identify and isolate zones of secondary Cu enrichment for further extraction. Contamination from Cu mine tailings are an environmental concern and Cu isotopes provide an additional tool for proper management.

3.7. Conclusions

The investigation into the Cu isotope ratios at location IN13 within the Copper Cliff Central Tailings Impoundment focused on the nature and mobility of Cu and constituents while investigating δ^{65}Cu isotope fractionation in the pore-water. There is a pronounced difference between the Cu isotope ratios in the oxidized and unoxidized tailings. Oxidation of chalcopyrite in the oxidized zone and secondary covellite at the base of the oxidized zone are the dominant reactions affecting the Cu isotope ratio at that depth. The precipitation of covellite at a depth of 1.9 m can be reasonably linked to the observed enrichment of ^{65}Cu in the pore-water. Precipitation of covellite within the tailings leaves the pore-water enriched in ^{65}Cu. Dissolution of previously precipitated covellite is depleting the δ^{65}Cu ratio as more ^{63}Cu is released into the pore-water.

Ongoing sulfide oxidation has led to elevated concentrations of dissolved metals and sulfate. As the oxidation front progresses, the cycle of precipitation and dissolution of Cu as covellite limits the mobility of Cu and has led to an enrichment of ^{65}Cu in solution These findings demonstrate the potential application of analysis of dissolved Cu concentrations and Cu isotope ratios of field samples to monitor the progress of oxidation in Cu rich sulfide tailings.

Chapter 4. Conclusions

4.1. Research Summary and Recommendations

This investigation at the Sudbury Copper Cliff tailings impoundment focused on the advance of the sulfide oxidation front , the mobility and fate of metals with a specific focus on Cu and the fractionation of the Cu isotope ratio in a depth profile to better understand the prevailing reaction mechanisms and the relation to observed Cu isotope fractionation.

Sulfide minerals in the tailings have oxidized through exposure to atmospheric O_2 and Fe (III). The mechanisms controlling the release and attenuation of dissolved Cu and the associated stable isotope fractionation were investigated by collecting and analyzing a series of solid and aqueous samples from the field site. The stable Cu isotope ratio, $\delta^{65}Cu$ was measured in aqueous samples extracted from core samples of unsaturated tailings, providing measurements of the pore-water geochemistry from the ground surface to the water table. Solid tailings samples were analyzed using a wide range of analytical techniques including transmitted- and reflected-light optical microscopy, X-ray powder fluorescence, selective extractions and synchrotron based spectroscopy.

Modelling of O_2 diffusion and sulfide oxidation show that oxidation has been ongoing since 1990.Low pH pore-water has progressed to a depth of 6 m and large concentrations of dissolved metals and SO_4 were detected in 2014. Maximum dissolved concentrations of Fe (2,000 mg L^{-1}), Ni (500 mg L^{-1}), Cu (700 mg L^{-1}), Zn (30 mg L^{-1}) and SO_4 (20,000 mg L^{-1}) were observed at the modelled depth of oxidation, 1.6 m bgs. The water table was observed at a depth of 2.25 m below the ground surface in 2014 and represents a slight reducing barrier for dissolved Cu.

The total S content and the solid metal, Fe, Cu, Ni and Zn concentrations associated with sulfide minerals were depleted in the oxidized zone. Heavily altered sulfide minerals were observed in thin sections to a depth of 1.6 m. The degree of weathering was estimated based on the SAI and compared to observations made in previous studies (Coggans et al., 1999). Measurements of solid phase Cu were found to range between approximately 758 ppm in the oxidized zone, 2122 ppm in the transition zone and 1604 ppm in the unoxidized zone. These results show an accumulation of Cu in the transition zone between the base of the oxidized zone and the surface of the water table.

Results of selective extractions and geochemical modelling show that the Fe(III) oxyhydroxides and hydroxysulfates are saturated with respect to the pore-water and that the precipitation, dissolution of and adsorption onto these mineral phases play an important role in metal mobility. The extractions also show that there is an increase in the amount of easily oxidizable Cu in the transition zone where secondary covellite has been observed. With less significant amounts of Cu present in the weak acid extractable and exchangeable fractions in the hardpan and above the water table.

Micro-XRF elemental distribution maps of sulfide grains from the transition zone show Cu is present on grain boundaries, in the alteration rims and micro-fractures of pyrrhotite grains. The results of least squares linear combination fitting of bulk Cu XANES spectra show the appearance of covellite (CuS) as a main contributor to the Cu K-edge spectra in the transition zone (1.9 m bgs) of the tailings. Linear combination fitting of μ-XANES Cu spectra was completed on samples from a depth of 1.7 m bgs and 2.0 m bgs. The Cu spectra collect on the sample from 2.0 m bgs exhibited a 60% to 80% contribution from CuS to the Cu spectra while

the spectra collected from the shallower sample only had a 20% contribution from CuS to the Cu spectra.

Results from linear combination fitting of S μ-XANES show evidence of sulfide oxidation and that elemental sulfur is the main contributor to the S K-edge spectra at the base of the oxidized zone where sulfide oxidation is taking place. Whereas more reduced forms of S, marcasite and pyrrhotite are dominant in S spectra from the transition zone. Ferrous sulfate was detected on the outermost edge of a pyrrhotite grain and is the main form of oxidized S at this depth.

The Cu isotope ratios, δ^{65}Cu in the oxidation zone of tailings profiles A and B range between approximately 0.015 to -3.93‰ and could potentially represent the oxidation of primary and secondary Cu sulfides as well as the adsorption of Cu onto Fe (oxy) hydroxides.

A δ^{65}Cu value of 11.85±0.88‰ was recorded in profile A at the Copper Cliff location in the transition zone (1.9 - 2.0 m bgs). The enrichment of ^{65}Cu is reasonably linked to the formation of covellite at the base of the transition zone. Covellite precipitation removes ^{63}Cu from solution leaving the pore-water enriched in ^{65}Cu. The presence of covellite was confirmed by multiple methods including optical microscopy and Cu XAS. Covellite was observed as individual grains and in rims with other secondary precipitates goethite, marcasite and ferrihydrite around pyrrhotite grains. The precipitation of Cu as covellite (CuS) at the base of the transition zone is a control on the fate of Cu and has led to an enrichment of ^{65}Cu in solution as ^{63}Cu is more readily precipitated as CuS. These findings give an indication of how aqueous analysis and isotope measurements of field samples can be used to monitor the release of Cu through oxidation of chalcopyrite and attenuation of Cu through formation of secondary covellite in sulfide-rich mine waste.

The measurement of Cu isotope ratios can aid in understanding the evolution of sulfide alteration in mine waste and provide a potential tool for the environmental management of sulfide tailings. Significant Cu isotope fractionation has been observed in the field in both solid-phase and aqueous samples. Digested solid tailings from Laver Mine in Sweden indicated the solid tailings were depleted in ^{65}Cu in a zone of solid Cu enrichment in the transition zone of the tailings (Pérez Rodríguez et al., 2013). Due to the relatively low cost of sampling and processing samples from mine sites the measurement of copper isotope ratios in the aqueous phase can be utilized to identify prevailing reaction mechanisms and provide information on the extent of sulfide alteration. Recommendations for future work include analysis of Cu isotope ratios in the solid phase to be paired with the aqueous Cu isotope ratios along the same depth profile. Additional measurements of field samples from different field sites in an effort to better understand the effects of varying reaction mechanisms on the fractionation of isotope ratios in different geochemical environments. Modelling of the Cu isotope ratio fractionation with time on a field site would be advantageous in that it could provide a long term environmental management tool for mine waste.

References

Archer C. and Vance D. (2004) Mass discrimination correction in multiple-collector plasma source mass spectrometry: an example using Cu and Zn isotopes. *J. Anal. At. Spectrom.* **19**, 656–665.

Asael D., Matthews A., Bar-Matthews M. and Halicz L. (2007) Copper isotope fractionation in sedimentary copper mineralization (Timna Valley, Israel). *Chem. Geol.* **243**, 238–254.

Balistrieri L. S., Borrok D. M., Wanty R. B. and Ridley W. I. (2008) Fractionation of Cu and Zn isotopes during adsorption onto amorphous Fe (III) oxyhydroxide: experimental mixing of acid rock drainage and ambient river water. *Geochim. Cosmochim. Acta* **72**, 311–328.

Blowes D. D. W., Ptacek C. C. J. and Jambor J. L. (2013) *Mineralogy of mine wastes and strategies for remediation*. eds. D. J. Vaughan and R. A. Wogelius, The Mineralogical Society of Great Britain and Ireland.

Blowes D. W. and Jambor J. L. (1990) The pore-water geochemistry and the mineralogy of the vadose zone of sulfide tailings, Waite Amulet, Quebec, Canada. *Appl. Geochemistry* **5**, 327–346.

Blowes D. W., Ptacek C. J., Jambor J. L., Weisener C. G., Paktunc D., Gould W. D. and Johnson D. B. (2014) *The Geochemistry of Acid Mine Drainage*., Elsevier.

Blowes D. W., Ptacek C. J. and Jurjovec J. (2003) Mill tailings: hydrogeology and geochemistry. *Environ. Asp. mine wastes* **31**, 95–116.

Blowes D. W., Reardon E. J., Jambor J. L. and Cherry J. A. (1990) The formation and potential importance of cemented layers in inactive sulfide mine tailings. *Geochim. Cosmochim. Acta* **55**, 965–978.

Blowes D. W., Reardon E. J., Jambor J. L. and Cherry J. A. (1991) The formation and potential importance of cemented layers in inactive sulfide mine tailings. *Geochim. Cosmochim. Acta* **55**, 965–978.

Boorman R. and Watson D. (1976) Chemical processes in abandoned sulphide tailings dumps and environmental implication for northeastern New Brunswick. *Can. Min. Metall. Bull.*

Boorman R. and Watson D. (1975) Mineralogical review of lead-zinc-copper sulphide deposits, Bathurst-Newcastle area, New Brunswick, New Brunswick Research and Productivity Council.

Brookfield A. E., Blowes D. W. and Mayer K. U. (2006) Integration of field measurements and reactive transport modelling to evaluate contaminant transport at a sulfide mine tailings impoundment. *J. Contam. Hydrol.* **88**, 1–22.

Chiriţă P. and Rimstidt J. D. (2014) Pyrrhotite dissolution in acidic media. *Appl. Geochemistry* **41**, 1–10.

Coggans C. J. (1992) Hydrogeology and Geochemistry of the Inco Ltd., Copper Cliff, Ontario, Mine Tailings Impoundments. University of Waterloo, Waterloo, ON.

Coggans C. J., Blowes D. W., Robertson W. D. and Jambor J. L. (1999) The hydrogeochemistry of a nickel-mine tailings impoundment, Copper Cliff, Ontario. *Rev. Econ. Geol. B* **6**, 447–465.

Córdoba E. M., Muñoz J. A., Blázquez M. L., González F. and Ballester A. (2008) Leaching of chalcopyrite with ferric ion. Part II: Effect of redox potential. *Hydrometallurgy* **93**, 88–96.

Davis G. B. and Ritchie A. I. M. (1986) A model of oxidation in pyritic mine wastes: part 1 equations and approximate solution. *Appl. Math. Model.* **10**, 314–322.

Dold B. (2003) Speciation of the most soluble phases in a sequential extraction procedure adapted for geochemical studies of copper sulfide mine waste. *J. Geochemical Explor.* **80**, 55–68.

Dold B. and Fontboté L. (2001) Element cycling and secondary mineralogy in porphyry copper tailings as a function of climate, primary mineralogy, and mineral processing. *J. Geochemical Explor.* **74**, 3–55.

Ehrlich S., Butler I., Halicz L., Rickard D., Oldroyd A. and Matthews A. (2004) Experimental study of the copper isotope fractionation between aqueous Cu(II) and covellite, CuS. *Chem. Geol.* **209**, 259–269.

Ehrlich S., Butler I., Halicz L., Rickard D., Oldroyd A. and Matthews A. (2004) Experimental study of the copper isotope fractionation between aqueous Cu (II) and covellite, CuS. *Chem. Geol.* **209**, 259–269.

Elliott H. (1990) Content and fractionation of heavy metals in water treatment sludges. *J. Environ. …*.

Fellin S. C. (2013) Geochemical Characterization of Weathered Sulfidic Tailings from Copper Cliff Mine - Ontario, Canada. University of Waterloo.

Gibbs R. J. (1977) Transport phases of transition metals in the Amazon and Yukon Rivers. *Geol. Soc. Am. Bull.* **88**, 829–843.

Gómez Ariza J. L., Giráldez I., Sánchez-Rodas D. and Morales E. (2000) Metal sequential extraction procedure optimized for heavily polluted and iron oxide rich sediments. *Anal. Chim. Acta* **414**, 151–164.

Graham S., Pearson N., Jackson S., Griffin W. and O'reilly S. Y. (2004) Tracing Cu and Fe from source to porphyry: in situ determination of Cu and Fe isotope ratios in sulfides from the Grasberg Cu--Au deposit. *Chem. Geol.* **207**, 147–169.

Gunsinger M. R., Ptacek C. J., Blowes D. W. and Jambor J. L. (2006) Evaluation of long-term sulfide oxidation processes within pyrrhotite-rich tailings, Lynn Lake, Manitoba. *J. Contam. Hydrol.* **83**, 149–170.

Gunsinger M. R., Ptacek C. J., Blowes D. W., Jambor J. L. and Moncur M. C. (2006) Mechanisms controlling acid neutralization and metal mobility within a Ni-rich tailings impoundment. *Appl. Geochemistry* **21**, 1301–1321.

Hayes S. M., Root R. a., Perdrial N., Maier R. M. and Chorover J. (2014) Surficial weathering of iron sulfide mine tailings under semi-arid climate. *Geochim. Cosmochim. Acta* **141**, 240–257.

Heron G. and Crouzet C. (1994) Speciation of Fe (II) and Fe (III) in contaminated aquifer sediments using chemical extraction techniques. *… Sci. Technol.* **28**, 1698–1705.

Holmstrom H., Ljungberg J., Ekstrom M. and Ohlander B. (1999) Secondary copper enrichment in tailings at the Laver mine, northern Sweden. *Environ. Geol.* **38**, 327–342.

Jambor J. L. (1987) Character and Depth of Oxidation of the Reactive Acid Tailings at the Waite Amulet Minesite, Noranda, Quebec.

Jambor J. L. (1994) *Mineralogical study of tailings from the Copper Cliff impoundments*., Sudbury, ON.

Jambor J. L. (2003) Mine-waste mineralogy and mineralogical perspectives of acid-base accounting. *Environ. Asp. mine wastes* **31**, 117–145.

Janzen M. P., Nicholson R. V and Scharer J. M. (2000) Pyrrhotite reaction kinetics: reaction rates for oxidation by oxygen, ferric iron, and for nonoxidative dissolution. *Geochim. Cosmochim. Acta* **64**, 1511–1522.

Johnson R. H., Blowes D. W., Robertson W. D. and Jambor J. L. (2000) The hydrogeochemistry of the Nickel Rim mine tailings impoundment, Sudbury, Ontario. *J. Contam. Hydrol.* **41**, 49–80.

Kimball B. E., Mathur R., Dohnalkova A. C., Wall A. J., Runkel R. L. and Brantley S. L. (2009) Copper isotope fractionation in acid mine drainage. *Geochim. Cosmochim. Acta* **73**, 1247–1263.

de Laeter J. R., Böhlke J. K., De Bièvre P., Hidaka H., Peiser H. S., Rosman K. J. R. and Taylor P. D. P. (2003) Atomic weights of the elements. Review 2000 (IUPAC Technical Report). *Pure Appl. Chem.* **75**, 785. Available at: http://www.degruyter.com/view/j/pac.2003.75.issue-6/pac200375060683/pac200375060683.xml [Accessed September 16, 2015].

Langman J. B., Blowes D. W., Veeramani H., Wilson D., Smith L., Sego D. C. and Paktunc D. (2015) The Mineral and Aqueous Phase Evolution of Sulfur and Nickel with Weathering of Pyrrhotite in a Low Sulfide, Granitic Waste Rock. *Chem. Geol.* **401**, 169–179.

Larson P. B., Maher K., Ramos F. C., Chang Z., Gaspar M. and Meinert L. D. (2003) Copper isotope ratios in magmatic and hydrothermal ore-forming environments. *Chem. Geol.* **201**, 337–350.

Light T. S. (1972) Standard solution for redox potential measurements. *Anal. Chem.* **44**, 1038–1039.

Lindsay M. B. J., Condon P. D., Jambor J. L., Lear K. G., Blowes D. W. and Ptacek C. J. (2009) Mineralogical, geochemical, and microbial investigation of a sulfide-rich tailings deposit characterized by neutral drainage. *Appl. Geochemistry* **24**, 2212–2221.

Lindsay M. B. J. J., Moncur M. C., Bain J. G., Jambor J. L., Ptacek C. J. and Blowes D. W. (2015) Geochemical and mineralogical aspects of sulfide mine tailings. *Appl. Geochemistry* **57**, 157–177.

Liu S.-A., Li D., Li S., Teng F.-Z., Ke S., He Y. and Lu Y. (2014) High-precision copper and iron isotope analysis of igneous rock standards by MC-ICP-MS. *J. Anal. At. Spectrom.* **29**, 122–133.

Luther G. W., Theberge S. M., Rozan T. F., Rickard D., Rowlands C. C. and Oldroyd A. (2002) Aqueous copper sulfide clusters as intermediates during copper sulfide formation. *Environ. Sci. Technol.* **36**, 394–402.

Maréchal C. N., Télouk P. and Albarède F. (1999) Precise analysis of copper and zinc isotopic compositions by plasma-source mass spectrometry. *Chem. Geol.* **156**, 251–273.

Markl G., Lahaye Y. and Schwinn G. (2006) Copper isotopes as monitors of redox processes in hydrothermal mineralization. *Geochim. Cosmochim. Acta* **70**, 4215–4228.

Mason T. F. D., Weiss D. J., Chapman J. B., Wilkinson J. J., Tessalina S. G., Spiro B., Horstwood M. S. A., Spratt J. and Coles B. J. (2005) Zn and Cu isotopic variability in the Alexandrinka volcanic-hosted massive sulphide (VHMS) ore deposit, Urals, Russia. *Chem. Geol.* **221**, 170–187.

Mathur R., Ruiz J., Titley S., Liermann L., Buss H. and Brantley S. (2005) Cu isotopic fractionation in the supergene environment with and without bacteria. *Geochim. Cosmochim. Acta* **69**, 5233–5246.

McGregor R. G. (1994) The solid phase controls on the mobility of metals at the Copper Cliff tailings area, near Sudbury, Ontario. M.Sc., University of Waterloo.

McGregor R. G. and Blowes D. W. (2002) The physical, chemical and mineralogical properties of three cemented layers within sulfide-bearing mine tailings. *J. geochemical Explor.* **76**, 195–207.

McGregor R. G., Blowes D. W., Jambor J. L. and Robertson W. D. (1998) The solid-phase controls on the mobility of heavy metals at the Copper Cliff tailings area, Sudbury, Ontario, Canada. *J. Contam. Hydrol.* **33**, 247–271.

McGregor R. G., Blowes D. W. and Robertson W. D. (1995) The application of chemical extractions to sulfide tailings at the Copper Cliff tailings area, Sudbury, Ontario. In *Sudbury* pp. 1133–1142.

Moncur M. C., Blowes D. W. and Ptacek C. J. (2013) Pore-water extraction from the unsaturated and saturated zones. *Can. J. Earth Sci.* **50**, 1051–1058.

Moncur M. C., Jambor J. L., Ptacek C. J. and Blowes D. W. (2009) Mine drainage from the weathering of sulfide minerals and magnetite. *Appl. Geochemistry* **24**, 2362–2373.

Moncur M. C., Ptacek C. J., Blowes D. W. and Jambor J. L. (2005) Release, transport and attenuation of metals from an old tailings impoundment. *Appl. Geochemistry* **20**, 639–659.

Moncur M. C., Ptacek C. J., Blowes D. W. and Jambor J. L. (2005) Release, transport and attenuation of metals from an old tailings impoundment. *Appl. Geochemistry* **20**, 639–659.

Moncur M. C., Ptacek C. J., Blowes D. W., Lindsay M. B. J. and Jambor J. L. (2012) Long-term Storage of Sulfide-rich Tailings under a Shallow Water Cover. *9th Int. Conf. Acid Rock Drain.*, 1–12.

Moncur M. C., Ptacek C. J., Lindsay M. B. J., Blowes D. W. and Jambor J. L. (2015) Long-term mineralogical and geochemical evolution of sulfide mine tailings under a shallow water cover. *Appl. Geochemistry* **57**, 178–193.

Morse J., Millero F., Cornwell J. and Rickard D. (1987) The chemistry of the hydrogen sulfide and iron sulfide systems in natural waters. *Earth-Science Rev.* **24**, 1–42.

Naldrett A. J. (1984) Mineralogy and composition of the Sudbury ores. *Geol. ore Depos. Sudbury Struct.* **1**, 309–325.

Nicholson R. V and Scharer J. M. (1994) Laboratory studies of pyrrhotite oxidation kinetics. In *ACS Symposium Series* pp. 14–30.

Nordstrom D. K. (1977) Thermochemical redox equilibria of ZoBell's solution. *Geochim. Cosmochim. Acta* **41**, 1835–1841.

Nordstrom D. K. and others (1982) Aqueous pyrite oxidation and the consequent formation of secondary iron minerals. *Acid sulfate Weather.*, 37–56.

Parkhurst D. and Appelo C. (2013) Description of Input and Examples for PHREEQC Version 3—A Computer Program for Speciation, Batch-Reaction, One-Dimensional Transport, and Inverse Geochemical Calculations.

Parviainen A. (2009) Tailings mineralogy and geochemistry at the abandoned Haveri Au-Cu mine, SW Finland. *Mine Water Environ.* **28**, 291–304.

Pattrick R. a. D., Mosselmans J. F. W., Charnock J. M., England K. E. R., Helz G. R., Garner C. D. and Vaughan D. J. (1997) The structure of amorphous copper sulfide precipitates: An X-ray absorption study. *Geochim. Cosmochim. Acta* **61**, 2023–2036.

Pattrick R. a. D., Mosselmans J. F. W., Charnock J. M. M., England K. E. R., Helz G. R., Garner C. D. and Vaughan D. J. (1997) The structure of amorphous copper sulfide precipitates: An X-ray absorption study. *Geochim. Cosmochim. Acta* **61**, 2023–2036.

Peacock C. L. and Sherman D. M. (2004) Copper(II) sorption onto goethite, hematite and lepidocrocite: A surface complexation model based on ab initio molecular geometries and EXAFS spectroscopy. *Geochim. Cosmochim. Acta* **68**, 2623–2637.

Pérez Rodríguez N., Engström E., Rodushkin I., Nason P., Alakangas L. and Öhlander B. (2013) Copper and iron isotope fractionation in mine tailings at the Laver and Kristineberg mines, northern Sweden. *Appl. Geochemistry* **32**, 204–215.

Peters T. H. (1995) *Revegetation of the Copper Cliff Tailings Areas*., Springer New York.

Pokrovsky O. S., Viers J., Emnova E. E., Kompantseva E. I. and Freydier R. (2008) Copper isotope fractionation during its interaction with soil and aquatic microorganisms and metal oxy (hydr) oxides: Possible structural control. *Geochim. Cosmochim. Acta* **72**, 1742–1757.

Pye E. G., Giblin P. E. and Naldrett A. J. (1984) *The geology and ore deposits of the Sudbury structure*., Ontario Ministry of Natural Resources.

Rauret G., López-Sánchez J. F., Sahuquillo a, Rubio R., Davidson C., Ure a and Quevauviller P. (1999) Improvement of the BCR three step sequential extraction procedure prior to the certification of new sediment and soil reference materials. *J. Environ. Monit.* **1**, 57–61.

Ravel B. and Newville M. (2005) ATHENA, ARTEMIS, HEPHAESTUS: data analysis for X-ray absorption spectroscopy using IFEFFIT. *J. Synchrotron Radiat.* **12**, 537–41.

Ribeta I., Ptacek C. J., Blowes D. W. and Jambor J. L. (1995) The potential for metal release by reductive dissolution of weathered mine tailings. *J. Contam. Hydrol.* **17**, 239–273.

Rickard D. T. (1973) Copper sulphide formation chemistry at low temperatures. *TMPM Tschermaks Mineral. und Petrogr. Mitteilungen* **19**, 60–76.

Rickard D. T. (1972) Covellite Formation in Low Temperature Aqueous Solutions. **188**, 180–188.

Rickard J. H. and Watkinson D. H. (2001) Cu-Ni-PGE mineralization within the Copper Cliff offset dike, Copper Cliff North mine, Sudbury, Ontario: Evidence for multiple stages of emplacement. *Explor. Min. Geol.* **10**, 111–124.

Rimstidt J. D., Chermak J. A. and Gagen P. M. (1994) Rates of reaction of galena, sphalerite, chalcopyrite, and arsenopyrite with Fe (III) in acidic solutions. In *ACS symposium series* p. 2.

Rouxel O. J., Bekker A. and Edwards K. J. (2005) Iron isotope constraints on the Archean and Paleoproterozoic ocean redox state. *Science* **307**, 1088–91.

Sherman D. M. (2013) Equilibrium isotopic fractionation of copper during oxidation/reduction, aqueous complexation and ore-forming processes: Predictions from hybrid density functional theory. *Geochim. Cosmochim. Acta* **118**, 85–97.

Sidenko N. V. and Sherriff B. L. (2005) The attenuation of Ni, Zn and Cu, by secondary Fe phases of different crystallinity from surface and ground water of two sulfide mine tailings in Manitoba, Canada. *Appl. Geochemistry* **20**, 1180–1194.

Silveira M. L., Alleoni L. R. F., O'Connor G. a. and Chang a. C. (2006) Heavy metal sequential extraction methods-A modification for tropical soils. *Chemosphere* **64**, 1929–1938.

Stumm W. (1992) *Chemistry of the solid-water interface: processes at the mineral-water and particle-water interface in natural systems*.,

Swedlund P. J. and Webster J. G. (2001) Cu and Zn ternary surface complex formation with SO4 on ferrihydrite and schwertmannite. *Appl. Geochemistry* **16**, 503–511.

Tessier a, Campbell P. G. C. and Bisson M. (1979) Sequential Extraction Procedure for the Speciation of Particulate Trace Metals. *Anal. Chem.* **51**, 844–851.

Thomas J. E., Jones C. F., Skinner W. M. and Smart R. S. C. (1998) The role of surface sulfur species in the inhibition of pyrrhotite dissolution in acid conditions. *Geochim. Cosmochim. Acta* **62**, 1555–1565.

Wang X., Forssberg E. and Bolin N. J. (1989) Pyrrhotite activation by Cu(II) in acidic to neutral pH media. *Scand. J. Metall.*

Webster J. G., Swedlund P. J. and Webster K. S. (1998) Trace metal adsorption onto an acid mine drainage iron(III) oxyhydroxy sulfate. *Environ. Sci. Technol.* **32**, 1361–1368.

Wunderly M. D., Blowes D. W., Frind E. O. and Ptacek C. J. (1996) Sulfide mineral oxidation and subsequent reactive transport of oxidation products in mine tailings impoundments: A numerical model. **32**, 3173–3187.

Zeien H. and Bruemmer G. (1991) Chemical extraction in the determination of the binding forms of heavy metals in soils. *Berichte aus der Oekologischen Forsch.*

Zhu X. K., O'nions R. K., Guo Y., Belshaw N. S. and Rickard D. (2000) Determination of natural Cu-isotope variation by plasma-source mass spectrometry: implications for use as geochemical tracers. *Chem. Geol.* **163**, 139–149.

ZoBell C. E. (1946) Studies on redox potential of marine sediments. *Am. Assoc. Pet. Geol. Bull.* **30**, 477–513.

Appendices

A. Aqueous Geochemistry

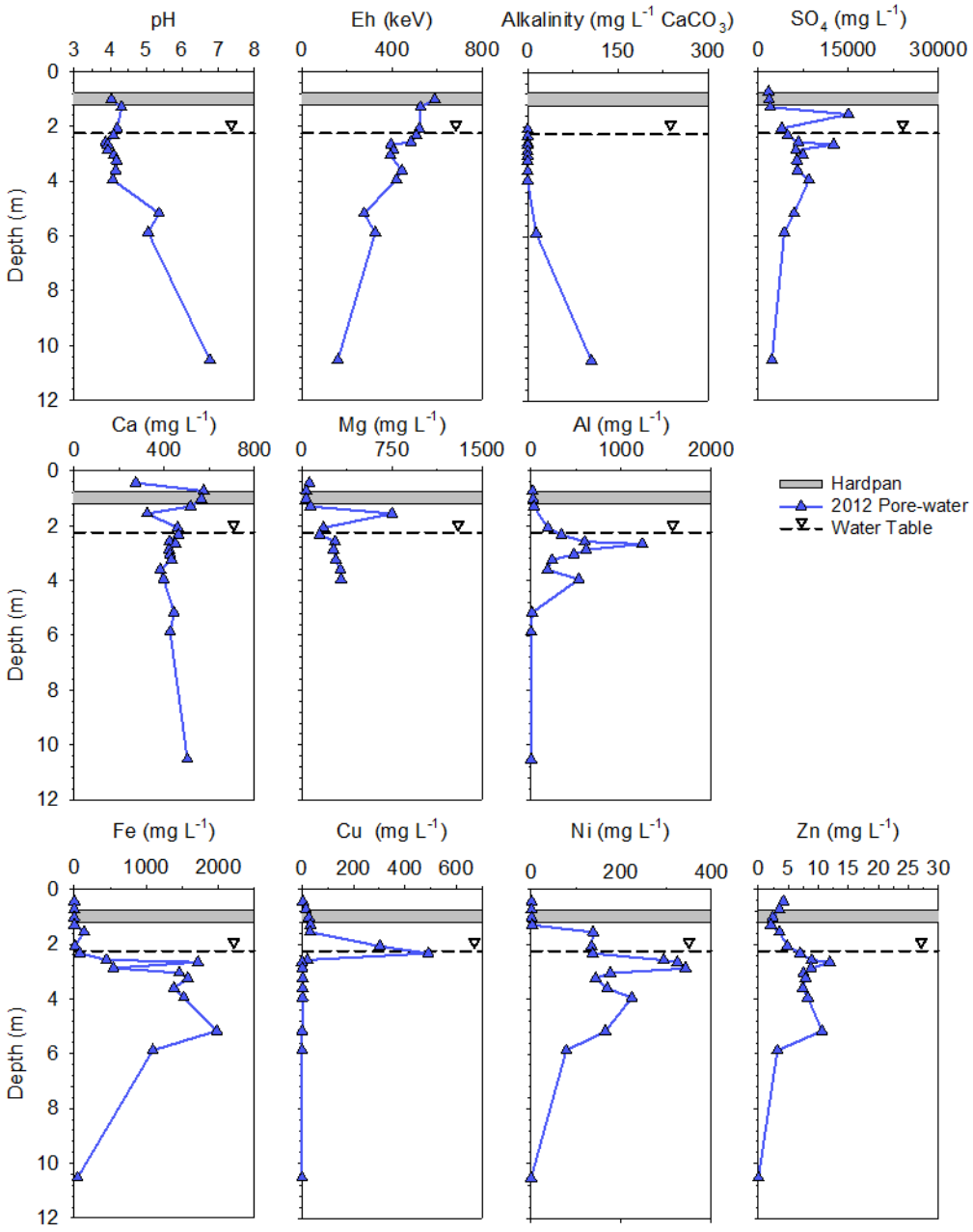

Figure 0-1. Geochemistry of the pore-water in 2012 at IN13 from piezometers and pore-water extracted from cores.

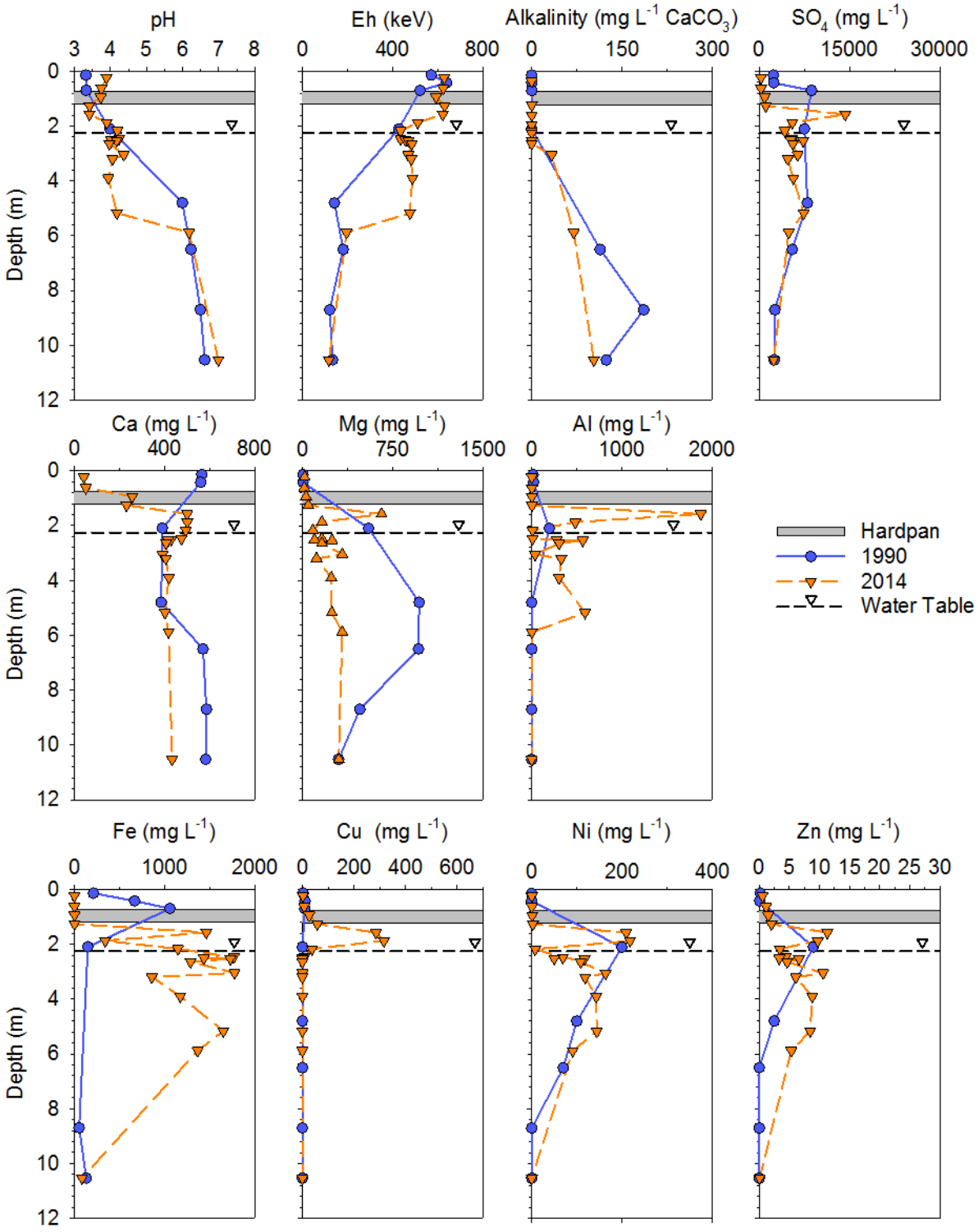

Figure 0-2. Geochemistry of the pore-water in profile B collected in 2014 at IN13 from piezometers and pore-water extracted from cores.

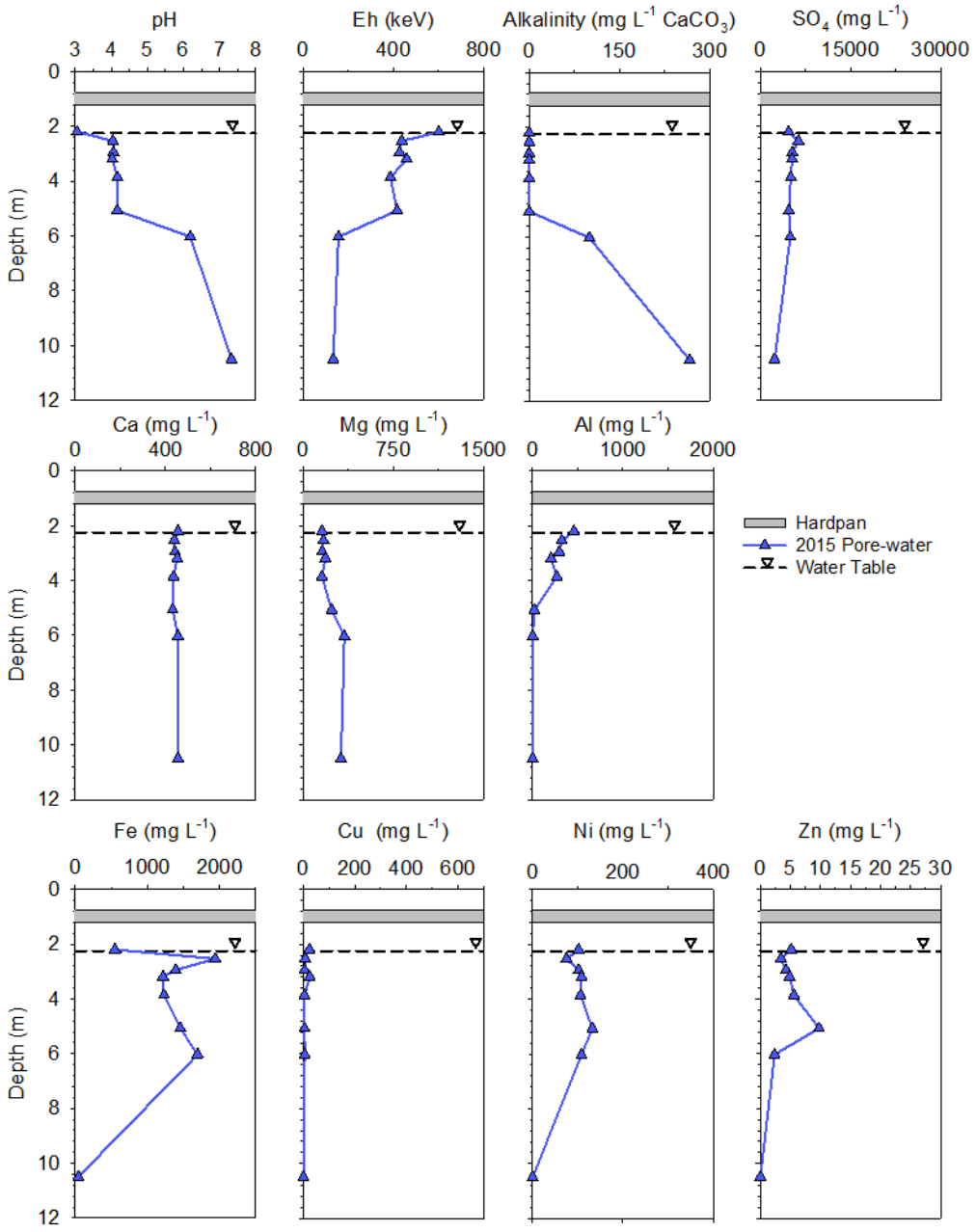

Figure 0-3. Geochemistry of the pore-water in 2015 at IN13 from piezometers only.

B. Solid Geochemistry

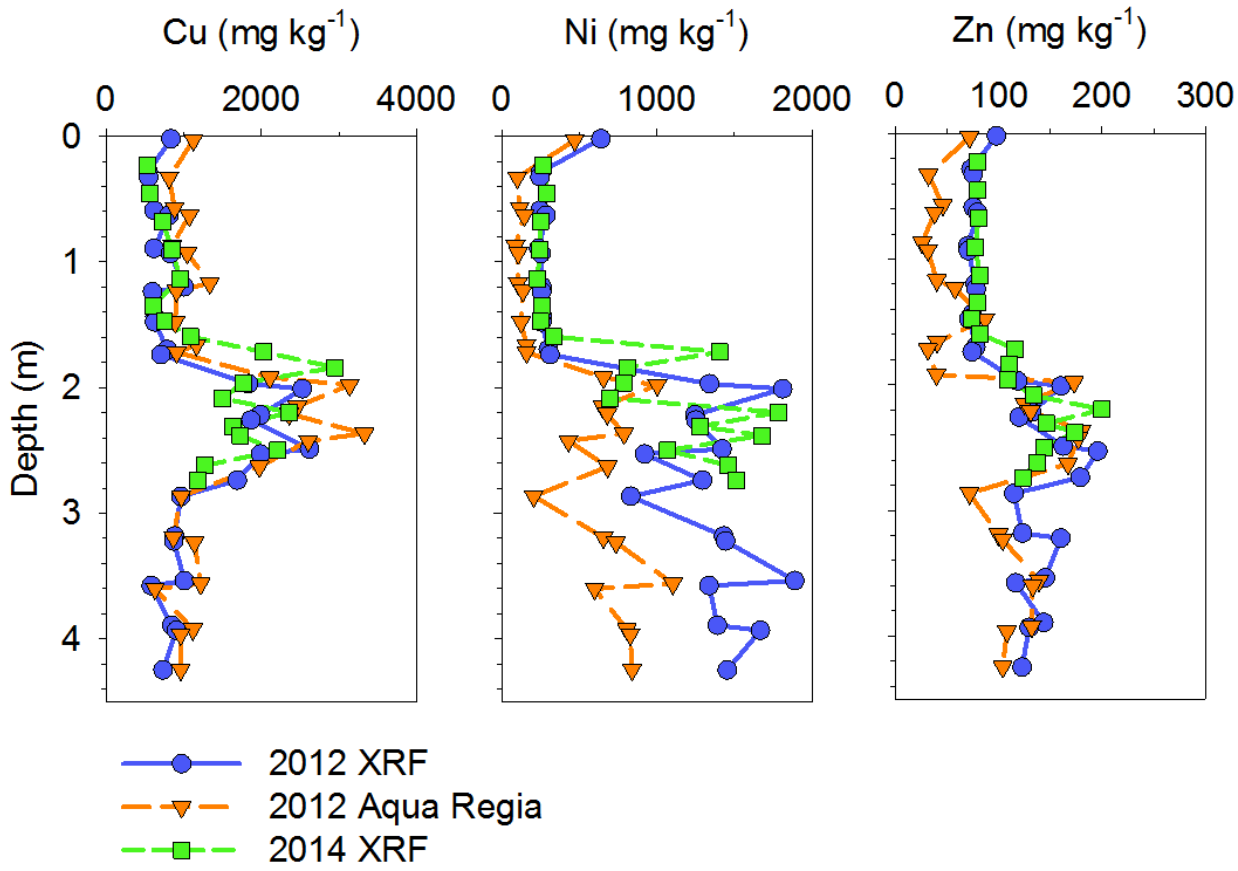

Figure 0-4. A comparison of powder XRF data on samples collected in 2012 and 2014 to aqua reiga performed on the samples from 2012.

Table 0-1. XRF elemental averages and error of reported elements.

Element	Oxidized Zone (0-1.72 m bgs)			Transition Zone (1.72-2.14 m bgs)			Unoxidized Zone (2.14-2.68mbgs)		
Al_2O_3 (%)	12.75	±	0.73	13.77	±	0.72	13.50	±	0.44
SiO_2 (%)	56.70	±	1.07	53.59	±	3.37	52.50	±	1.53
CaO (%)	5.65	±	0.46	5.31	±	0.46	4.84	±	0.27
TiO_2 (%)	0.77	±	0.08	0.71	±	0.11	0.61	±	0.03
MnO (%)	0.14	±	0.01	0.13	±	0.01	0.12	±	0.01
Fe_2O_3 (%)	16.45	±	2.33	14.43	±	2.57	15.73	±	1.19
Na_2O (%)	1.11	±	0.20	1.34	±	0.12	0.72	±	0.82
MgO (%)	7.43	±	0.40	7.83	±	0.57	7.55	±	0.39
K_2O (%)	1.02	±	0.05	0.90	±	0.09	0.87	±	0.05
Sr (ppm)	206.1	±	15.0	170.1	±	14.5	160.6	±	11.2
Ba (ppm)	291.0	±	150.4	573.2	±	229.8	692.8	±	82.6
Ni (ppm)	266.9	±	32.4	1095.8	±	477.1	1400.1	±	232.8
Rb (ppm)	35.6	±	2.0	33.8	±	4.5	32.2	±	2.2
Pb (ppm)	23.0	±	1.4	21.2	±	1.0	21.1	±	0.6
Cu (ppm)	758.4	±	196.6	2122.7	±	562.8	1604.7	±	409.7
S (ppm)	15673.8	±	2250.6	31049.8	±	11190.2	37916.1	±	37916.1
Cr (ppm)	377.6	±	21.8	307.1	±	22.7	300.5	±	15.8
Co (ppm)	71.1	±	11.0	64.6	±	11.8	69.4	±	6.2
Zn (ppm)	79.3	±	2.6	133.6	±	38.4	144.9	±	18.6
As (ppm)	9.6	±	2.1	5.0	±	2.0	5.2	±	1.3
V (ppm)	111.1	±	5.7	102.3	±	9.1	92.1	±	2.3

C. Sulfide Oxidation Modelling

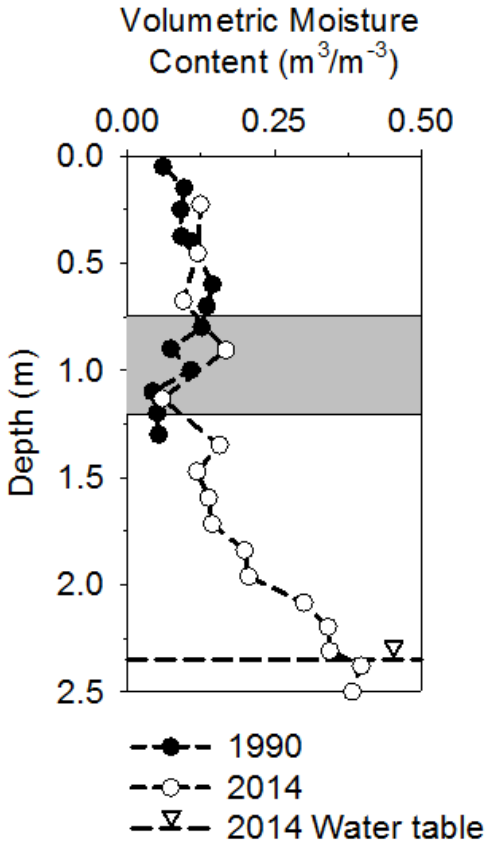

Figure 0-5. Volumetric moisture content values for 1990 and October 2014.

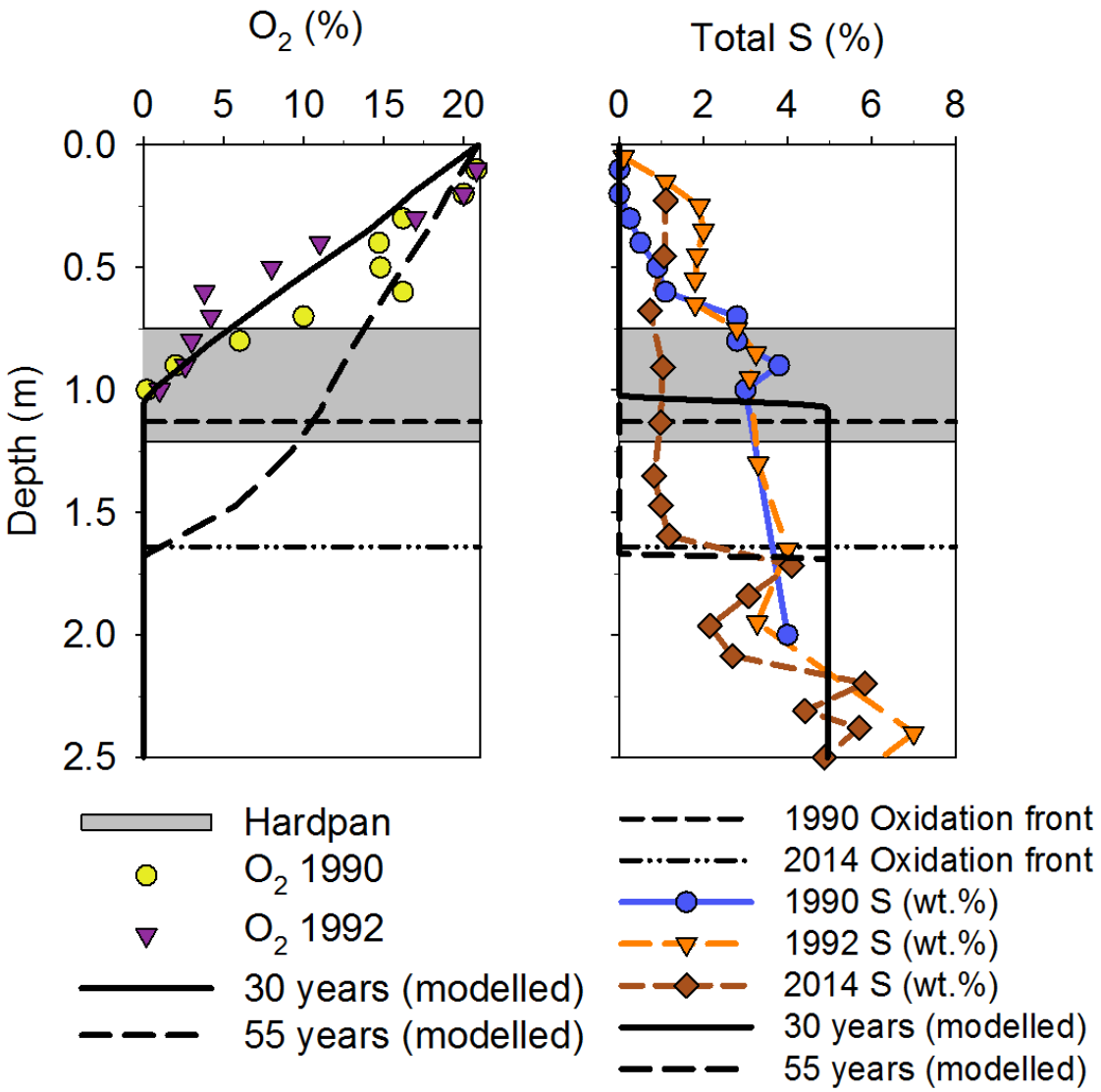

Figure 0-6. Left: Measured concentrations of gas-phase O_2 for 1990, 1992 and 2015. O_2 depletion was modelled for 1990 (30 years) and 2015 (55 years) using PYROX and the parameters in McGregor, 1994. Right: Total sulfur content of samples collected in 1990, 1992 and 2014. The amount of sulfides remaining was modelled for 1990 (30 years) and 2015 (55 years) using PYROX. The oxidation fronts are based on the PYROX model output.

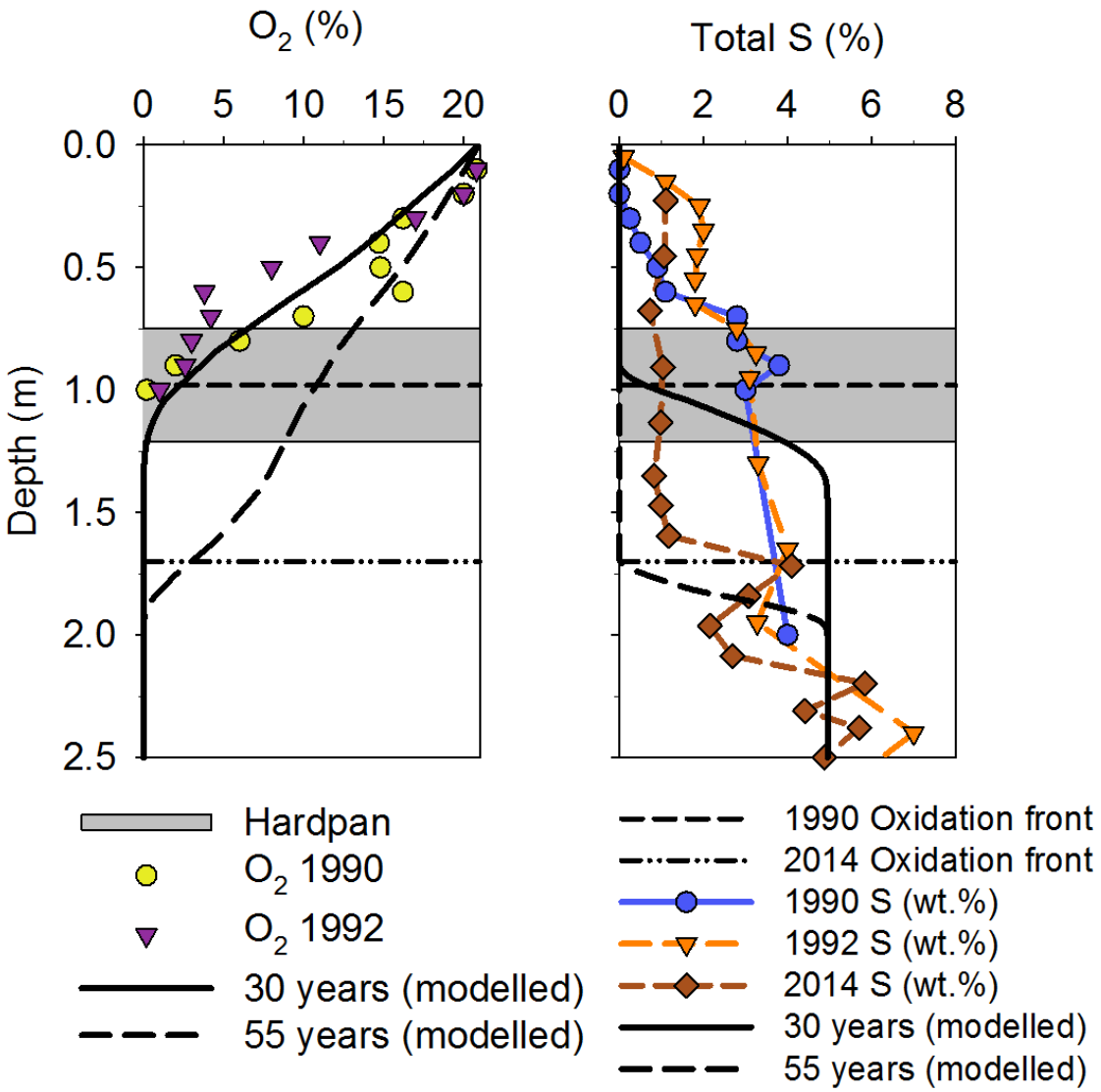

Figure 0-7. Left: Measured concentrations of gas-phase O_2 for 1990, 1992 and 2015. O_2 depletion was modelled for 1990 (30 years) and 2015 (55 years) using PYROX and the parameters in (Coggans et al., 1999). Right: Total sulfur content of samples collected in 1990, 1992 and 2014. The amount of sulfides remaining was modelled for 1990 (30 years) and 2015 (55 years) using PYROX. The oxidation fronts are based on the PYROX model output.